



MARTIN-LUTHER-UNIVERSITÄT, HALLE-WITTENBERG

NANOMEDICINES BASED ON MODIFIED HYDROXYETHYL STARCH

From synthesis to in vivo evaluation

Dissertation

Zur Erlangung des akademischen Grades
Doctor rerum naturalium (Dr. rer. nat.)

Vorgelegt der
Naturwissenschaftlichen Fakultät I
Biowissenschaften
der Martin-Luther-Universität Halle-Wittenberg
von

Ahmed Ibrahim Hamed Besheer

geboren am 14. Oktober 1976 in Kairo, Ägypten

Gutachter:

1. Prof. Dr. rer. nat. Habil. Karsten Mäder
2. Prof. Dr. rer. nat. Habil. Jörg Kressler
3. Prof. Dr. rer. nat. Habil. Alfred Fahr

Halle (Saale), den 29.09.08

To

My father, mother and brother.

This work is the fruit of their unconditional love, sacrifice and support.

ACKNOWLEDGMENTS

I feel indebted to the many people whom, without their help, cooperation or guidance, this work would have never been completed in its present form.

First of all, I have to express my deep gratitude and heartily appreciation to my supervisors, Prof. Karsten Mäder and Prof. Jörg Kressler for their continuous support, advice and inspiration, not only during this thesis work, but also throughout all my master's and Ph.D. studies.

My thanks go also to Dr. Metz for the useful discussions and instructions regarding ESR simulation and MRI instrumentation, and to Dr. Kuntsche for the assistance with field flow fractionation.

I have also to thank Prof. Thomas Groth and the coworkers in his group, namely Dr. Vogel, Dr. Sarun, Dr. Lee and Dieter Peschle for the very useful discussions, guidance and support with the cell culture and phagocytosis experiments. I am also grateful to Prof. Markus Pietzsch and his group, namely Dr. Hertel, Dr. Marx and Hany Hassounah for their constructive suggestions and cooperation regarding the enzymatically-catalyzed HESylation.

I have to express my gratitude to the late Prof. Siegfried Wartewig for his invaluable help with Raman spectroscopy, to Dr. Hause for the electron microscopy, to Dr. Glanz for the confocal laser scanning microscopy, and to Dr. Müller for the i.v. injections to the mice.

I have also to thank all my colleagues in the groups of Prof. Mäder and Prof. Kressler as well as the technical assistants for providing a quite friendly and helpful working environment and solving my day to day problems. I should specially acknowledge Hagen Nitzsche for providing the *in vitro* MRI images, Henrike Caysa

for her valuable help with the *in vivo* experiments, Samuel Kyeremateng for his assistance with the synthesis of HM-HES.

Special thanks go to Ahmed Abdalla, his wife Marwa and his son Khaled. They were certainly the best friends, family and companions throughout the last 4 years.

Without my parents' and my brother's love and support, this work would have never been finished. Simply, no words can express my gratitude to them.

Last, but by no means least, I thank God.

Ahmed Besheer

Halle, September 2008

NANOMEDICINES BASED ON MODIFIED HYDROXYETHYL STARCH (HES)

From Synthesis to In Vivo Evaluation

TABLE OF CONTENTS

Synopsis	III
Part I – General introduction and characterization of hydroxyethyl starch (HES)	1
Chapter 1 – General Introduction	2
1.1 Nanomedicine	2
1.1.1 The nanosized polymeric toolbox	3
1.2 Thesis objectives	7
Chapter 2 – Characterization of hydroxyethyl starch (HES)	9
2.1 Hydroxyethyl starch (HES)	9
2.2 Experimental	12
2.2.1 Materials	12
2.2.2 Asymmetric flow field flow fractionation (AF4)	12
2.2.3 Dynamic light scattering (DLS)	13
2.2.4 ¹ H NMR	13
2.3 Results and discussion	
2.3.1 Asymmetric flow field flow fractionation (AF4)	14
2.3.1.1 Theory	14
2.3.1.2 Results	17
2.3.2 Dynamic light scattering	21
2.3.3 ¹ H NMR	21
2.4 Conclusions and outlook	24
2.5 References	25
Part II – Hydrophobically modified hydroxyethyl starch (HM-HES)	32
Chapter 3- Synthesis, characterization and self assembly of HM-HES	33
3.1 Hydrophobically-modified polysaccharides	33
3.2 Experimental	35
3.2.1 Materials	35
3.2.2 Synthesis	35
3.2.3 ¹ H NMR spectroscopy	36
3.2.4 Raman spectroscopy	36
3.2.5 Asymmetric flow field flow fractionation (AF4)	36
3.2.6 Preparation of nanodispersions	36
3.2.7 Transmission electron microscopy	37
3.3 Results and discussion	37
3.3.1 Synthesis and ¹ H NMR	37
3.3.2 Raman spectroscopy	44
3.3.3. Self assembly of the water soluble HM-HES	48
3.3.3.1 Asymmetric flow field flow fractionation (AF4)	48
3.3.3.2 TEM	50
3.4 Conclusions and outlook	53

Chapter 4 – Application of HM-HES for the surface modification of PLGA nanospheres	55
4.1 Introduction	55
4.2 Experimental	57
4.2.1 Materials	57
4.2.2 Nanosphere preparation	57
4.2.3 Physicochemical characterization	58
4.2.4 Protein adsorption	59
4.2.5 Phagocytosis of the nanospheres	59
4.2.6 Confocal laser scanning microscopy (CLSM)	60
4.3 Results and discussion	61
4.3.1 Physicochemical characterization	62
4.3.2 Protein adsorption	65
4.3.3 Phagocytosis of nanospheres	68
4.4 Conclusions and outlook	71
4.5 References	73
Part III – Gd-HES: A macromolecular MRI contrast agent	81
Chapter 5 – Synthesis, characterization and <i>in vivo</i> evaluation of Gd-HES	82
5.1 Introduction	82
5.1.1 Magnetic resonance imaging	83
5.1.2 MRI contrast agents	89
5.2 Experimental	91
5.2.1 Materials	91
5.2.2 Synthesis of the Gd-HES chelates	91
5.2.3 ¹ H NMR spectroscopy	92
5.2.4 Conductometric analysis	92
5.2.5 Asymmetric flow field flow fractionation (AF4)	92
5.2.6 Determination of relaxivity	93
5.2.7 <i>In vitro</i> imaging	94
5.2.8 <i>In vivo</i> imaging	94
5.3 Results and discussion	96
5.3.1 ¹ H NMR and conductometric titration	96
5.3.2 Asymmetric flow field flow fractionation (AF4)	99
5.3.3 Relaxivity	103
5.3.4 <i>In vitro</i> imaging	105
5.3.5 <i>In vivo</i> imaging	106
5.4 Conclusions and outlook	115
5.5 References	116
Part IV – Enzymatically-catalyzed HESylation	120
Chapter 6 – Enzymatically-catalyzed HESylation using microbial transglutaminase:	
Proof of feasibility	121
6.1 Introduction	121
6.2 Experimental	123
6.2.1 Materials	123
6.2.2 HES carrying a lysine component	123
6.2.3 HES carrying a glutaminyl component	124
6.2.4 ¹ H NMR	125
6.2.5 Preparation of rMTG	125

6.2.6 Reaction of HES 70-GQ-Z with monodansyl cadaverine (MDC)	125
6.2.7 Reaction of HES 70-Amine with dimethyl casein (DMC)	126
6.3 Results and discussion	126
6.4 Conclusions and outlook	131
6.5 References	132
Part V – Summary	136
Chapter 7 – Summary	137
6.1 English version	137
6.2 German version	138

Synopsis

The term nanomedicine was introduced around the turn of the century to describe the use of nanotechnology in medicine. Nanosized polymeric structures are among the most widely researched nanotechnology platforms for application in drug delivery and diagnosis due to their versatility and biocompatibility. This thesis includes three projects describing the modification of the biodegradable polymer hydroxyethyl starch (HES) for the production of polymeric nanomedicines as drug and contrast agent carriers.

The first project involves the esterification of HES using different fatty acids to give amphiphilic polymers with varying degrees of modification. This hydrophobically-modified HES (HM-HES) was characterized using $^1\text{H-NMR}$ and Raman spectroscopy. The former was used to determine the molar substitution, which ranged between 2 to 23.3 mol%, while the latter confirmed the amorphous state of the alkyl chains in the amphiphilic polymers. Field flow fractionation (FFF) was used to determine the molar mass and size of the water soluble polymers. It showed the formation of self-assembled aggregates ranging in size between 100-200 nm. These were confirmed to be polymersomes using cryo-TEM. This is one of the first reports on polymersomes from hydrophobically-modified branched polymers.

As an application for HM-HES, it was used to modify the surface of PLGA nanospheres, and compared to nanospheres coated with pluronic F68 and F127. The thickness of the adsorbed polymer layer was measured using dynamic light scattering (DLS) and zeta-potential measurements as a function of electrolyte concentration. The thickness of the polymer layer was found to be in the range of 3-15 nm. The ability of the surface coats to prevent the adsorption of proteins was evaluated, where the HM-HES as well as pluronic F68 and F127 succeeded in preventing the adsorption of human serum albumin, while only F68 failed in preventing the adsorption of the more hydrophobic protein fibrinogen. The

phagocytosis of the surface-modified nanospheres by the murine monocyte-macrophage cell line J 774.2 was evaluated qualitatively using confocal laser scanning microscopy (CLSM) and quantitatively using fluorescence spectroscopy. Results show that HM-HES having the largest molar mass could reduce phagocytosis as good as pluronic F127. These results suggest that the fully biodegradable HM-HES might be used as a substitute for pluronics in stabilizing polymeric nanospheres, but the *in vivo* behaviour remains to be studied.

The second project describes the preparation of Gd-HES chelates for MRI imaging. These were prepared by esterification of HES with diethylenetriaminepentaacetic acid (DTPA), then chelation of Gd³⁺ ions. Molar substitution was determined using ¹H-NMR and conductometry, and was found to range between 18 and 25 mol%. FFF measurements showed the formation of crosslinked aggregates due to the fact that DTPA is multivalent. The longitudinal and transverse relaxivities of the macromolecular chelates were 2-3 times those of Gd-DTPA, showing a higher efficiency as an MRI contrast agent. Finally, Gd-HES was tested *in vivo* for angiography and as a tumor contrast agent using a novel benchtop MRI instrument. The images showed that Gd-HES circulated in the blood more than 2.5 h and was mainly eliminated through the kidneys, while the small contrast agent Gd-BOPTA (Multihance[®]) was eliminated within 20 min. Moreover, Gd-HES showed a significant rim enhancement in subcutaneously-injected colon carcinoma tumor models that persisted for approximately 4 h, while with Gd-BOPTA, it is known that such enhancement disappears after 2 min from injection (E. A. Morris, *Radiologic Clinics of North America*, 40 (2002) 43-466).

The third project describes an approach for enzymatically catalyzed HESylation of model proteins and small molecules using the enzyme microbial transglutaminase (MTG). The later catalyses the acyl transfer between the γ -carboxamide group of a glutaminy residue (acyl donors) and a variety of primary amines (acyl acceptors), including the amino group of lysine. In order to act as a substrate for MTG, HES was modified HES with N-carbobenzyloxy glutaminy glycine (Z-QG) and hexamethylenediamine (HMDA) to act as acyl donor and acyl acceptor, respectively. Using ¹H-NMR, the degree of modification with Z-QG and HMDA was found to be 4.6 and 3.9 mol% respectively. Using SDS-PAGE, it was possible to show that the modified HES successfully coupled to dimethyl casein (DMC), a model protein, and

monodansyl cadaverine (MDC), a fluorescent probe, proving that the modified HES was accepted as a substrate by MTG. This process is a simple and mild approach to produce fully biodegradable polymer-drug and polymer-protein conjugates.

PART I

General introduction and characterization of hydroxyethyl starch

Chapter 1

General introduction

1.1 Nanomedicine

The term nanomedicine was introduced around the turn of the century to describe the integration of nanotechnology and medicine [1]. Nanotechnology comes from the Greek word *nano* for dwarf. It encompasses a wide range of enabling technologies, and can be defined as the design, production and application of structures at the molecular or sub-micrometer scale [2]. Historically speaking, nanosized structures were produced and studied under other terminologies, like colloids or ultrafine particles. For instance, the purple of Cassius, a pigment used in chinaware that owes its color to a coated gold colloid, was discovered in the 17th century, while Michael Faraday was able to elucidate the mechanism of formation of colloidal metals as early as 1857 [3]. Similarly, nanomedicine-related research was conducted long before the term was coined, where the first reported lipid vesicles (liposomes) date back to 1965 [1]. However, the term nanomedicine crystallized lately as a culmination to the rapid and significant advancements in the field of nanotechnology and its biomedical applications over the last 2 decades. Today, nanomedicine covers a wide field of applications, involving the use of nanotechnology for the treatment, diagnosis, monitoring and control of biological systems [4, 5].

Operating at the nanoscale provides a lot of opportunities to overcome problems associated with drug delivery and diagnosis. For example, it can be used to enhance the solubility of poorly soluble drugs [6], or to protect sensitive macromolecules, such as nucleic acids, from degradation and promote their intracellular penetration and

distribution [7, 8]. Specially-engineered nanoparticles, which are smaller than 200 nm, can alter the drug pharmacokinetics and tissue biodistribution by persisting in the circulation for a long period of time [9]. Furthermore, nanocarriers can hold a large payload, and allow the specific active or passive targeting of their payloads to certain organs or tissues, or even particular cell organelles [5]. All these issues are being addressed, with eventual successes reaching the market. However, being in its infancy, nanomedicine is expected to contribute more. As the Nobel physics laureate Richard Feynman mentioned in a visionary lecture at Caltech in 1959, there is still “plenty of room at the bottom” [10, 11].

1.1.1 The nanosized polymeric toolbox

To achieve effective treatment, diagnosis and control of biological systems, researches have used polymers, lipids, inorganic metals and metal oxides, or composites combining 2 or more of these materials. Among these, polymers have played an important role due to their biocompatibility and great versatility. Today, the nanosized polymeric toolbox for nanomedicines includes conjugates of drugs or proteins to soluble polymers, micelles, dendrimers, polyplexes, polymersomes and nanoparticles [12-14]. Some of these systems will be briefly described below, with an emphasis on the applications and clinical use (see Figure 1.1 and Table 1.1).

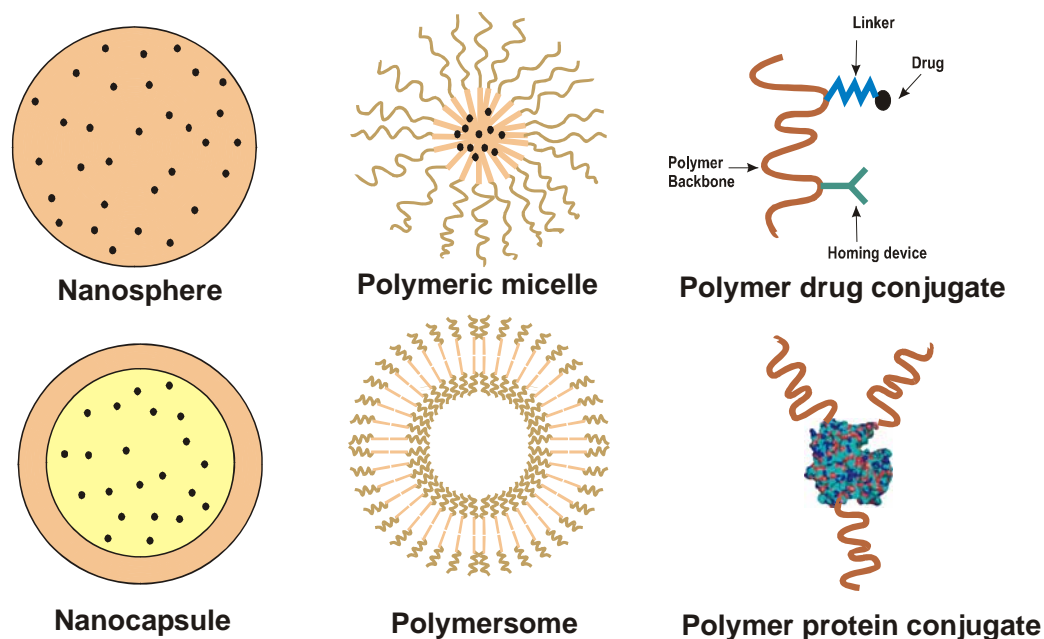


Figure 1.1. Different nanosized polymeric platforms for nanomedicine.

Table 1.1. Some nanosized polymeric drug delivery systems under clinical use or investigation.

System	Name	Status	Indication	Ref.
Polymer drug conjugates				
HPMA-doxorubicin	PK1	Phase II	Various cancers, particularly lung and breast cancer	[15]
HPMA-doxorubicin-galactosamine (PK2)	PK2	Phase I/II	Hepatocellular carcinoma	[16]
HPMA-carboplatin platinatate	AP5280	Phase I/II	Various cancers	[17]
HPMA copolymer-DACH-platinae	ProLindac	Phase I/II	Various cancers	[18]
Poly(glutamate)-paclitaxel	Opaxio (Xyotax)	Phase III	Various cancers, particularly non small cell lung cancer and ovarian cancer	[18]
Polymer protein conjugates				
Styrene-co-maleic acid neocarzinostatin (SMANCS)	Zinostatin Stimalmer	Market	Hepatocellular carcinoma	[19]
PEG-L-asparaginase	Oncaspar	Market	Acute lymphoblastic leukaemia	[18]
PEG-GCSF	Neulasta	Market	Prevention of neutropaenia associated with cancer chemotherapy	[18]
PEG-IFN α 2a	PEG-asys	Market	Hepatitis C	[18]
PEG-IFN α 2b	PEG-Intron	Market	Hepatitis C	[18]
PEG-arginine deiminase	ADI-PEG20	Phase I	Hepatocellular carcinoma	[18]
Polymeric micelles				
PEG-poly(aspartic acid) micelles with conjugated doxorubicin	NK911	Phase I	Different advanced cancer conditions	[20]
Pluronic [®] L61 and F127 micelles encapsulating doxorubicin	SP1049C	Phase I	Different advanced cancer conditions	[21]
Nanoparticles				
Albumin nanoparticles	Abraxane	Market	Breast cancer, Squamous cell carcinoma of head and neck	[22]

The conjugates of soluble polymers to small drug molecules or proteins are among the most promising nanosized polymeric drugs [23]. They confer a number of advantages, including increase in solubility, reduction of side effects/toxicity, and alteration of the pharmacokinetics and biodistribution of drugs. The most widely studied polymers for this purpose are poly(ethylene glycol) (PEG), poly(hydroxypropyl methacrylamide) (HPMA) and poly(L-glutamic acid) (PGA). Among these, only PGA is biodegradable, thus dictating a size limit of 40 kDa for the other non-biodegradable polymers to facilitate their renal elimination [24]. These polymer drug conjugates are particularly interesting for cancer treatment. This is because they can selectively penetrate the leaky vasculature of solid tumors, while their elimination from the tumor site is hindered due to the lack of lymphatic drainage in the inherently-disorganized tumors. This phenomenon was termed “enhanced permeation and retention effect”, or EPR effect [25]. Currently, this concept is the gold standard in macromolecular anticancer drugs [18]. While a number of these conjugates are in clinical studies, OPAXIO[®] (formerly branded as XYOTAX[®]), a conjugate of paclitaxel to PGA, has finished phase III clinical trials and is awaiting approval in the EU.

Polymer-protein conjugates have shown more success, with a number of successful candidates in the market (see Table 1.1). The conjugate of polymers to polypeptides and proteins extends their half-life, protects them from degradation by proteolytic enzymes and reduces their immunogenicity [26]. The most widely used polymer for this approach is PEG, and the PEGylation technology is now an established approach to bring to the market the new drug molecules coming from the biotech revolution. A number of reports review the chemistry of PEGylation as well as the effect on the stability and bioavailability of the proteins [26-30].

Another delivery platform is polymeric micelles. Micelles are formed by the self-assembly of low molar mass amphiphilic molecules (surfactants) above the critical micellar concentration (CMC). They have a hydrophilic shell and a hydrophobic core, where the latter can accommodate hydrophobic molecules, such as drugs with low water solubility, thus increasing their apparent solubility. This is an important achievement, since dissolution is an important prerequisite for the absorption and biodistribution of drugs. However, since these micelles are in a state of

thermodynamic equilibrium, they instantly disassemble upon dilution or changes in the temperature, leading to precipitation of their payloads.

Amphiphilic block- and graft-copolymers form micelles which can overcome these problems. Compared to surfactant micelles, polymeric micelles have a very low CMC, and a slower rate of dissociation, releasing their payloads over a long time upon dilution [31]. Moreover, they are not rapidly eliminated by the kidneys, since their size is usually several tens of nanometers [32]. Their hydrophilic shells and small size allow them to evade the mononuclear phagocytic system, and thus have long circulation times. They can also accumulate in solid tumors by the EPR effect, leading to a physical targeting of cancer [33]. An illustration for this application was provided by the group of Kataoka, where micelles from diblock copolymers of poly(ethylene glycol)-poly(β -benzyl-L-aspartate) were loaded with doxorubicin (DOX). The release of DOX was biphasic, taking place over more than 80 h. *In vivo*, the micellar formulation showed a dramatic increase in circulation time as compared to free DOX, and a higher efficiency against subcutaneously injected tumor models [34].

Nanoparticles represent another example of the nanotechnology tools. Their definition depends on the discipline. While in physics and colloid chemistry, nanoparticles are considered to be < 100 nm, in drug delivery they are defined as having a size smaller than 1 μm [35, 36]. They may be produced from natural or synthetic polymers, organic drug crystals, or inorganic metals and metal oxides. The polymeric nanoparticles have been extensively studied as drug carriers [13, 37]. They can be classified into the widely investigated nanospheres and the less common nanocapsules [13]. The former are formed of a monolithic matrix that entraps a molecularly dispersed drug, while the latter consist of a small polymeric shell encapsulating an oil reservoir [13]. For the preparation of nanospheres, many polymers have been investigated, including natural polymers (such as chitosan and albumin), synthetic non-degradable polymers (such as poly(methyl methacrylates) and poly(alkyl cyanoacrylates)), or synthetic biodegradable polymers (such as poly(lactic acid) and poly(lactic-co-glycolic acid)). Despite the fact that these systems have been investigated for more than 30 years [38], only 1 product reached the market in 2005 [13]. This was Abraxane[®], an albumin nanoparticle system carrying paclitaxel for cancer therapy.

Another approach is to prepare nanoparticles from the drug itself, in order to influence its dissolution [38]. For example, Elan Corporation uses a wet milling approach to prepare drug crystals smaller than 400 nm (NanoCrystal[®]). The know-how depends in this case on the successful use of the appropriate surfactants. This method increases the solubility and bioavailability of poorly soluble drugs, and is now used for 4 commercially available products, namely; Rapamune[®] (sirolimus, Wyeth), Emend[®] (aprepitant, MK 869, Merck), TriCor[®] (fenofibrate, Abbott), and Megace[®] ES (megestrol acetate, Par Pharmaceutical, Inc.). Pharmasol GmbH, Berlin, uses a modified high pressure homogenization method to produce the nanocrystals in molten PEG. They can be immediately filled into capsules, or pelletized after solidification. The inclusion into PEG matrix prevents aggregation and insures rapid dissolution of the drug [39].

Polymeric vesicles are a new addition to the toolbox of nanosized polymeric platforms. In general, vesicles are globular compartments formed when a membrane encloses aqueous medium. Phospholipids self-assemble in water to form vesicles, which are known as “liposomes”. Recently, it was found that polymers can also form vesicular structures. These were given the name “polymersomes” [40, 41]. The basic principles underlying this vesicular self-assembly were reviewed by Antonietti and Förster [42]. Compared to liposomes, polymersomes have a larger membrane thickness, higher mechanical strength and lower transport rates across their membranes [40]. Since these properties are attractive for producing a drug vehicle, the group of Discher produced biodegradable polymersomes from PEG-PLGA and found that they encapsulated anticancer drugs and successfully delivered them to solid tumors [43, 44].

1.2 Thesis objectives

In the present thesis, three projects were designed to modify hydroxyethyl starch (HES) in order to formulate different nanosized drug and contrast agent carriers. In the first project, an amphiphilic HES was synthesized by esterification with different fatty acids, with the aim of producing a fully biodegradable polymeric surfactant that can modify the surface of polymeric nanospheres as an alternative for non-biodegradable surfactants such as Pluronic[®]. In the second project, a macromolecular MRI contrast agent based on HES was synthesized, with the aim of

producing a long circulating contrast agent that can be used for angiogenesis and tumor imaging. In the third project, HESylation of model proteins and low molar mass compounds was attempted. A new enzymatic approach for the coupling of HES was developed and tested, which can be a mild alternative to the many chemical coupling methods reported in the patent literature.

Chapter 2

Characterization of hydroxyethyl starch (HES)

2.1 Hydroxyethyl Starch (HES)

Hydroxyethyl starch (HES) is one of the first line colloidal plasma volume expanders* (PVEs) in Europe, particularly in Germany [45]. It offers a number of advantages over other (PVEs) such as albumin and dextran. These include lack of bacterial or viral contamination hazards, a clearly lower incidence of hypersensitivity [46] and no drug interactions (for instance albumin interacts with ACE inhibitors) as well as a higher cost effectiveness [47].

HES is usually produced from waxy maize starch - and less frequently from potato starch - by alkaline derivatization with ethylene oxide. Starch consists of two types of polyglucans; amylose, a non-branched polymer of glucose units attached through α -(1,4) glycosidic bonds, and amylopectin, which contains branch points with α -(1,6) glycosidic bonds. Waxy maize starch consists mainly of amylopectin which is structurally similar to glycogen, the branched glucose storage polymer in humans. This close similarity is believed to be one reason why HES lacks immunogenicity [46]. Furthermore, amylose is responsible for retrogradation and syneresis, which makes amylopectin more favourable [48].

* PVE are classified as colloidal (which use polymers for plasma substitution) and crystalloid (which use electrolyte solutions from salts and/or sugars). The colloidal ones have the advantage of smaller volume, but may have unwanted side effects. The crystalloids are safer, but due to the very short half lives, large volumes are needed. Upon infusion of PVE, the colloid osmotic pressure causes a flux of tissue fluid, hence the name plasma volume expander. They are used in cases of blood and fluid loss that can lead to circulatory failure, such as hypovolemia, hypoalbuminemia and burns [45].

To characterize the substitution of starch with hydroxyethyl units, two terms are used in the literature, namely degree of substitution (DS) and molar substitution (MS). The definition of these terms in the literature is not unequivocal, and are often interchanged leading to confusion [49-51]. In this manuscript, DS is defined as the average number of hydroxyethyl groups per anhydroglucose unit (AGU), while MS represents the fraction of substituted AGU. Accordingly, DS can have a maximum value of 3, while MS can have a maximum of 1.

During hydroxyethylation, the ethylene oxide units can add to the hydroxyl groups of the AGU, or to that of an already attached hydroxyethyl group, leading to the formation of short poly(ethylene glycol) chains [48]. Furthermore, the acidity of the three hydroxyl groups of the AGU is different leading to a preferred attachment to C2, followed by C6 then C3 [48].

After hydroxyethylation, HES is hydrolysed to the desired molecular weight either by acid hydrolysis or by enzymatic hydrolysis. Sommermeyer and coworkers used GC/MS to investigate the homogeneity of substitution throughout the polymer chain as well as the effect of the different methods of hydrolysis. They found that the non-reducing chain end has a higher substitution followed by the normal α 1,4 AGU then the branch point AGU. Additionally, the α -amylase-hydrolysed polymer turned out to be more branched, and thus more hydrodynamically compact, in comparison to the acid hydrolysed polymer with the same molecular weight. They presume that this can have an effect on the in vivo performance, where the enzymatic hydrolysis reduces the possible attack points for serum α -amylase decreasing the in vivo hydrolysis [49].

Hydroxyethylation of starch is carried out to achieve a number of objectives, namely, increasing the solubility and solution stability of starch, reducing the viscosity of starch solution, and more importantly, to decrease its in vivo hydrolysis [46, 51]. The half life of soluble starch is of the order of few minutes due to the rapid hydrolysis by serum α -amylase. Hydroxyethylation hinders this enzymatic degradation leading to complete elimination after few weeks [46]. Contrary to dextran, HES is not metabolized to CO₂ but to oligomers that are predominantly filtered through the kidneys and excreted in urine. The in vivo degradation of HES depends on a number of factors, including the MS and the so called pattern of substitution (PS), which is the ratio of C2/C6 substitution. In contrast, the molecular weight has little effect on elimination, provided that the molecular weight is greater than the renal threshold

which is approximately 70,000 g/mol [52]. Meanwhile, and as a rule of thumb, an increase of MS by 0.1 leads to a doubling of the half life [50]. The ratio of C2 to C6 substitution plays also an important role, since a substitution at C2 slows down the hydrolysis by α -amylase [53, 54].

Adverse effects to HES are generally regarded as mild and clinically insignificant [47]. Nevertheless, HES can cause an increase in bleeding time due to interference with the action of blood clotting factors and blood platelets [55]. Such effects can be minimized by using moderately or rapidly degrading starches [46]. Furthermore, cases of acute pruritis that do not respond to medication have been reported. It is postulated that this severe itching is due to tissue storage in cutaneous nerves after high cumulative dosage administration [56].

It is worth noting that, contrary to many synthetic polymers, the molecular structure of HES is very complicated, and a comparison of results through the literature regarding structural properties is not easy. For instance, the branching of amylopectin differs whether the source is waxy maize starch or potato starch, as well as if the molecule was hydrolysed enzymatically or by an acid. The differences in the MS, DS and PS were found to affect the in vivo performance and side effects. Even the molecular weight distribution may vary a lot, despite the same nominal average molecular weight [47]. In general, a valid structure-property relationship for HES is still lacking [47].

In addition to its use as PVE, HES is also used as a cryopreservative of biological cells [57]. There are only few attempts to use HES for drug delivery purposes. On the one hand, some labs tried the conjugation of drug molecules, particularly proteins, to HES, in an attempt to replace poly(ethylene glycol) (PEG) with a biodegradable polymer [58], and there is a number of patents on the HESylation of proteins. The group of DeLuca derivatized HES with acryloyl chloride then crosslinked the product to form hydrogel microspheres that were capable of swelling in water and entrapping hydrophilic protein molecules [59]. In another study, they incorporated insulin-loaded hydrogels into PLGA microspheres to achieve a sustained drug release and to avoid the initial burst effect [60]. Devy *et al.* produced protein loaded HES microcapsules (MC) produced by interfacial cross linking of emulsified HES solution [61]. They showed that a substantial part of the loaded albumin is released only after the

biodegradation of the MC, and that α -amylase and not esterase can degrade the MC in vitro.

In the present thesis, HES was chosen as a raw material for the production of derivatives suitable for biomedical applications. This is because it possess a number of advantages, including

1. It is highly water soluble (contrary to starch which only swells in water).
2. It is biodegradable.
3. It is pharmaceutically acceptable (as it is already clinically used as a plasma expander under the trade name VitaHES[®] and Infukoll[®] HES by Serumwerk Bernburg, Germany, Voluven[®] by Fresenius Kabi, Bad Homburg, Germany and Hespan[®] by the US branch of B. Braun)
4. It is commercially available with different molecular weights and different degrees of substitution (the latter affects the in-vivo degradation rate [52])
5. It is readily modified (due to the abundance of hydroxyl groups)

In this chapter, the characterization of the raw HES using asymmetric flow field flow fractionation (AF4), dynamic light scattering (DLS) and ¹H NMR spectroscopy is briefly described.

2.2 Experimental

2.2.1 Materials

HES with M_w 70 000, 200 000 and 450 000 g/mol and MS 0.5 was a kind gift from Serumwerk Bernburg, Germany. The samples are named HES70, HES200, HES450, respectively.

2.2.2 Asymmetric flow field flow fractionation (AF4)

For AF4 separation, the Eclipse FFF system (Wyatt Technology Corp., California, USA) was used. It was coupled to an 18 angle MALS detector (DAWN EOS MALS, Wyatt Technology Corp., California, USA) having a 690 nm GaAs laser, and an RI detector Shodex 101 (Shoko America, Colorado, USA). Samples were prepared with a concentration of 5 mg/ml in 50 mM NaCl solution in bidistilled water, filtered through 0.1 μ m filter and preserved with 0.02 % w/v NaN₃. 100 μ l of the solution were injected into a channel having a 350 μ m spacer and a 5,000 g/mole regenerated cellulose

ultrafiltration membrane (Nadir C010F, Microdyn-Nadir GmbH). A channel flow of 2 ml/min was maintained using the same NaCl solution, and a linearly decreasing cross flow from 2 ml/min to 0 ml/min over 30 min was used for separation (see Table 2.1). Data were evaluated using ASTRA software v.4.90.08 (Wyatt Technology Corp., California, USA).

The refractive index increment (dn/dc) was determined for each sample at 30 °C by measuring 3 concentrations, each in triplicates.

Table 2.1. Cross-flow program used for AF4 sample separation.

	Duration (min)	Cross flow (ml/min)		Focus flow (ml/min)
		Start	End	
Elution	2	2	2	–
Focus	1	–	–	2
Focus+inj	2	–	–	2
Focus	1	–	–	2
Elution	30	2	0	–
Elution	10	0	0	–
Elution+inj	10	0	0	–

2.2.3 Dynamic light scattering (DLS)

HES samples were dissolved in 50 mM NaCl solution preserved with 0.02 % w/v NaN_3 to give a concentration of 5 mg/ml. Samples were diluted 1:10, and the hydrodynamic diameter (d_h) of the HES molecules in solution was determined by dynamic light scattering (DLS) at 25 °C, using the back scattering mode at 173° (HPPS, Malvern Instruments, UK). The hydrodynamic radius (r_h) was obtained by dividing the hydrodynamic diameter by 2.

2.2.4 ^1H NMR

For ^1H NMR measurements, 60 mg polymer samples were dissolved in 700 μl DMSO-d_6 , or D_2O and measured at 400 MHz (Gemini 2000, Varian Inc.)

2.3 Results and discussion

2.3.1 Asymmetric flow field flow fractionation (AF4)

2.3.1.1 Theory

FFF is a flow-based separation technology that can be considered a hybrid of chromatography and field-based separation methods like electrophoresis [62]. In chromatography, molecules are separated by differential retention between a solid stationary phase (column) and a fluid mobile phase. In FFF, fractionation is performed in a channel through which a liquid is pumped giving a laminar flow with a parabolic velocity profile [63, 64]. Separation takes place by applying an external field perpendicular to the flow in the channel. The most commonly used fields are the sedimentation field (using gravitational or centrifugal forces), thermal field (using a thermal gradient) and cross flow (using a perpendicular flow field) [63]. The use of an external field leads to great versatility for the FFF technique; because the strength of the field can be precisely controlled and rapidly varied, leading to an enhanced separation. This versatility, however, does not come without a cost, since it adds to the complexity of the method, making a universal approach for separation not feasible [65].

In the flow FFF, the field is a second independent flow stream (cross-flow) passing perpendicular to the primary flow from the porous upper wall (depletion wall) to the lower frit covered by an ultrafiltration membrane (accumulation wall). In the asymmetric flow field flow fractionation (AF4), there is no second independent flow, and the depletion wall is a nonporous transparent glass or plastic plate. Accordingly, the cross flow originates from within the channel itself, where the cross flow rate corresponds to the loss of axial flow that occurs as the carrier fluid moves downstream [66]. Figure 2.1 shows a schematic representation of the flow channel and separation principle.

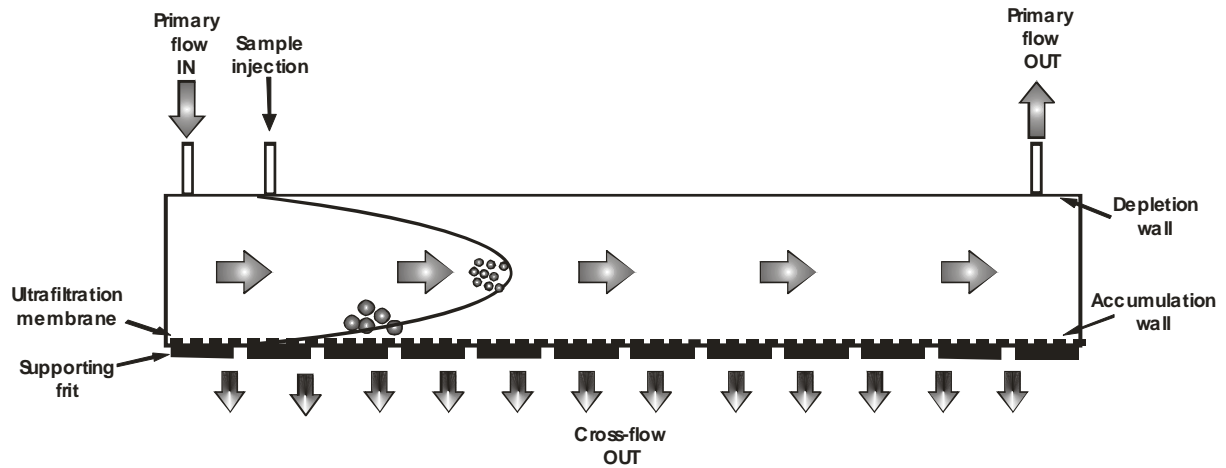


Figure 2.1. Schematic representation for AF4 separation channel.

Generally, the external field forces the different particles or molecules against the accumulation wall. Brownian motion of the analytes will counteract the field-induced forces, pushing them towards the depletion wall. At equilibrium, the analytes will occupy localized regions of the parabolic flow profile based on their diffusion coefficients. Having higher diffusion coefficients, the smaller particles/molecules will move upwards towards the center of the flow profile, while the larger particles/molecules will be pushed towards the accumulation wall. Since the drift velocity varies at different points of the flow profile, the sample will elute at different time points, with the smaller particles eluting first. Knowing the retention time t_r , the analyte's diffusion coefficient D can be determined using the following equation [64]

$$\text{Fehler! Textmarke nicht definiert. } D = \frac{t^0 F_c w^2}{6V^0 t_r}$$

2.1

where t^0 is the void time, F_c is the cross flow rate, w is the channel thickness, and V^0 is the void volume of the channel [64]. Using the Stokes-Einstein equation, the particle size can be related to the retention time as follows:

$$d_H = \frac{2kTV^0 t_r}{\pi \eta t^0 F_c w^2} \quad 2.2$$

where d_H is the hydrodynamic diameter, k is the Boltzmann constant, T is the temperature, and η is the viscosity of the carrier liquid [64].

It is thus evident that FFF can be used for separation as well as size determination. However, this is not usually the case, since the retention time may be

affected by the interaction between the analytes and the ultrafiltration membrane [62]. More reliable methods are thus coupled to FFF for the determination of size and molar mass of the analytes, namely multi-angle light scattering (MALS).

The theory underlying MALS is based on the fact that the intensity of the scattered light depends on many factors, including the scattering angle θ , the weight average molar mass (M_w), and the root mean square radius (RMS radius, r_g^\dagger) as follows [64, 67]

$$R_\theta = KM_w c P(\theta) [1 - 2A_2 M_w P(\theta) c] \quad 2.3$$

where R_θ is the Rayleigh ratio (excess of scattering of the macromolecular solution above that scattered by the solvent itself, all divided by the intensity of incident light), M_w is the weight average molar mass, c is the concentration, K is a constant, $P(\theta)$ is the particle scattering function, and A_2 is the second virial coefficient. K and $P(\theta)$ can be given by the following equations [64]:

$$K = \frac{2\pi^2 n_0^2}{\lambda^4 N} \left(\frac{dn}{dc} \right)^2 \quad 2.4$$

$$P^{-1}(\theta) = 1 + \frac{16\pi^2}{3\lambda^2} \langle r_g^2 \rangle \sin^2 \left(\frac{\theta}{2} \right) \quad 2.5$$

where λ is the wavelength of light in vacuum, n_0 is the refractive index of the solvent, N is the Avogadro's number, dn/dc is the refractive index increment of the scattering species in the solvent used.

In very dilute solutions, which is usually the case upon separation with FFF, the term containing A_2 can be neglected. When θ is equal to zero, $P(\theta)$ is equal to unity, and thus

$$\frac{Kc}{R_\theta} = \frac{1}{M_w} \quad 2.6$$

Accordingly measurements are carried out at different angles and different concentrations, and then extrapolated to zero angle and concentration, in what is

[†] The RMS radius depends on the internal mass distribution of the particle/molecule and is independent of the shape. Hence the subscript “g”, which is related to the center of gravity. The misnomer “radius of gyration” is usually used instead of the RMS radius. However, the radius of gyration refers to rotation about an axis fixed in space. Thus each object has an infinite number of radii of gyrations corresponding to the infinite number of axes fixed in space about which an object can rotate [67]. In this text, both designations will be used.

usually known as “Zimm plot”. The intercept of this plot is equal to $1/M_w$ and the slope is equal to [64]:

$$\frac{\partial(Kc/R_\theta)}{\partial \sin^2(\theta/2)} = \frac{16\pi^2}{3M_w\lambda^2} \langle r_g^2 \rangle \quad 2.7$$

Thus the slope depends on M_w and r_g , and can be used to determine the size of the molecules or the particles. Many useful reviews are available on this topic, and the reader can consult them for a more detailed treatment of the light scattering principles [67-70].

Flow FFF is currently applicable in the range from 0.001-50 μm [63]. This includes synthetic and biological macromolecules, as well as particulate systems. It is also possible to use aqueous as well as organic solvents as carrier systems.

2.3.1.2 Results

FFF has been used for the fractionation and molar mass determination of different natural and semi-synthetic polysaccharides, such as ethylhydroxyethyl cellulose [64], native starches [71], amylopectins and glycogen [72] and chemically-modified starches [73]. Such molecules usually have large molar masses and wide distribution. When compared to high performance size exclusion chromatography (HPSEC), the latter has a lower exclusion limit and cannot resolve molecules of extremely large molar masses. On the other hand, FFF can resolve molecules in the range of $5\text{-}10 \times 10^3$ g/mole (which is equal to few nm for most molecules) to 50 μm [72].

dn/dc was determined for the HES samples as shown in Figure 2.2. After correction for the moisture content (ca. 10 % w/w as determined by thermogravimetric analysis), an average of $0.1475 \text{ cm}^3/\text{g}$ was obtained. This value is close to previously reported refractive index increments of HES [74].

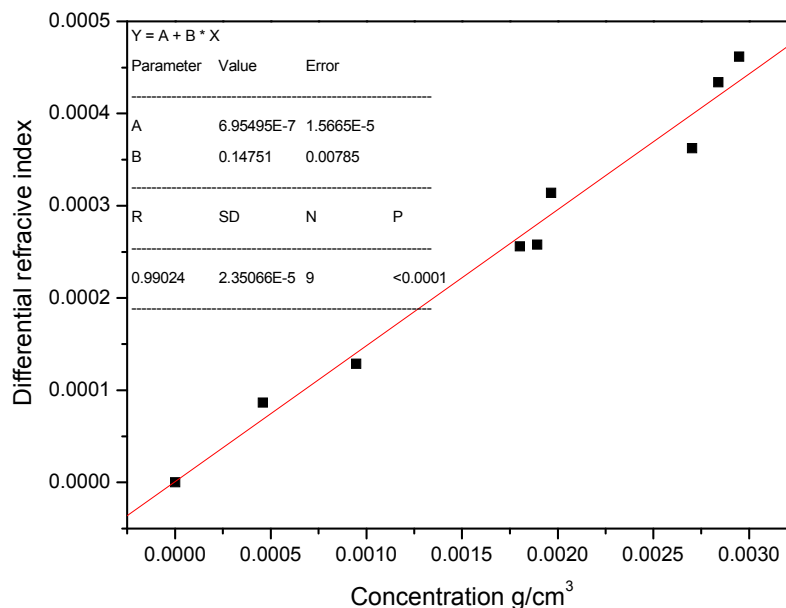


Figure 2.2. Determination of the refractive index increment for HES70

To determine the molar mass of HES, viscosimetric measurements or HPSEC were usually employed [54]. For this study, AF4 was used. Figure 2.3 shows the elugrams for the three HES samples studied, where the light scattering and differential RI signals as well as the molar masses are plotted as a function of elution time. The molar masses and sizes in Table 2.2 are extracted from a Zimm plot. The weight average molar masses (M_w) are quite close to the nominal values reported by the producer. AF4 was used to determine the molar mass of a number of modified starches, including HES450 [73]. Although the used sample had an M_w of 458,012 g/mole determined by HPSEC as reported by the producer, the authors reported a M_w of 564×10^3 g/mole. They attributed this high value to a loss of the lower molar mass fractions, since they used a 10,000 g/mole ultrafiltration membrane. In our case, the use of a 5,000 g/mole membrane seems to prevent the loss of a large portion of the sample, as evidenced by the high recovery (> 85 % w/w) and the agreement of the measured molar masses with the nominal values. Meanwhile, the HES samples show a high polydispersity, ranging from 1.95 for HES70, up to 4.56 for HES450. The polydispersity was proven to be a function of the quality of fractionation [73], where it increased from 2.8 to 3.3 for HES450 samples when the cross flow increased from 1 to 2 ml/min. Our present results are not directly comparable with the mentioned study due to the different supplier, as well as the fact that we used an elution gradient rather than a constant cross-flow. The former is generally known to

have a higher fractionation power, and could have thus led to an increase in polydispersity.

Figure 2.4 shows the molar mass distribution of the HES samples. The samples have a molar mass ranging between $10\text{-}20 \times 10^3$ g/mole and 5×10^5 g/mole (for HES70) and 6×10^6 g/mole (for HES450). The distributions do not show long tails extending to large molar masses, which is important for clinical use [54].

The measurement of molar mass and radius of gyration (r_g) allows the determination of the conformation of macromolecules in solution according to the following equation:

$$r_g = kM^\alpha \quad 2.8$$

where α is the conformational coefficient (also known as the Flory's exponent [75]) and k is the proportionality constant [76]. α is equal to 1 in case of rigid rods, 0.5-0.6 in case of random coils, and 0.33 for hard spheres [75, 76]. Figure 2.5 shows a double logarithmic plot for all 3 HES samples, where a considerable scatter is observed below 10 nm. Accordingly, a linear fit was applied to data larger than 10 nm in order to estimate the values of α . These can be found in Table 2.2. The values for all HES samples are slightly lower than the expected value for a random coil, indicating a slightly compact conformation, which is most probably due to the branching of HES. Wittgren *et. al* [73] determined a value of 0.44 for α , which is in very close agreement to the values determined in this study. It is worth noting that at very high molar masses in case of HES200 and HES450, the slope tends to decrease, indicating that these fractions are even more compact due to higher degrees of branching.

Table 2.2. Molar masses, polydispersity, RMS radius, conformational coefficient α and recovery of the different HES samples as determined by AF4 coupled to MALS.

Sample	M_n $\times 10^3$ (g/mole)	M_w $\times 10^3$ (g/mole)	Polydispersity M_w/M_n	RMS radius (nm)	Conformational coefficient α	Recovery (% w/w)
HES70	35.8 ± 0.8	69.7 ± 2.2	1.95 ± 0.02	5.5 ± 0.5	0.435	86.1 ± 1.1
HES200	59.5 ± 1.0	190.3 ± 6.1	3.20 ± 0.11	11.1 ± 1.0	0.424	96.0 ± 1.4
HES450	102.6 ± 5.9	466.9 ± 7.7	4.56 ± 0.20	19.0 ± 0.2	0.463	93.4 ± 2.4

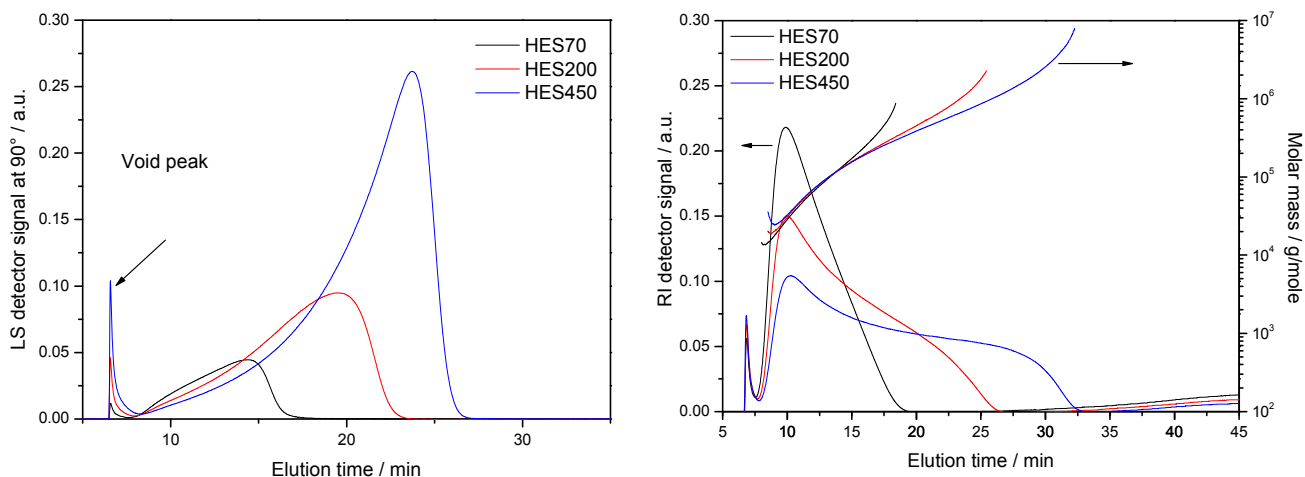


Figure 2.3. Elugrams for the different HES samples showing the LS signal at 90° (left), and the RI signal as well as the molar masses (right).

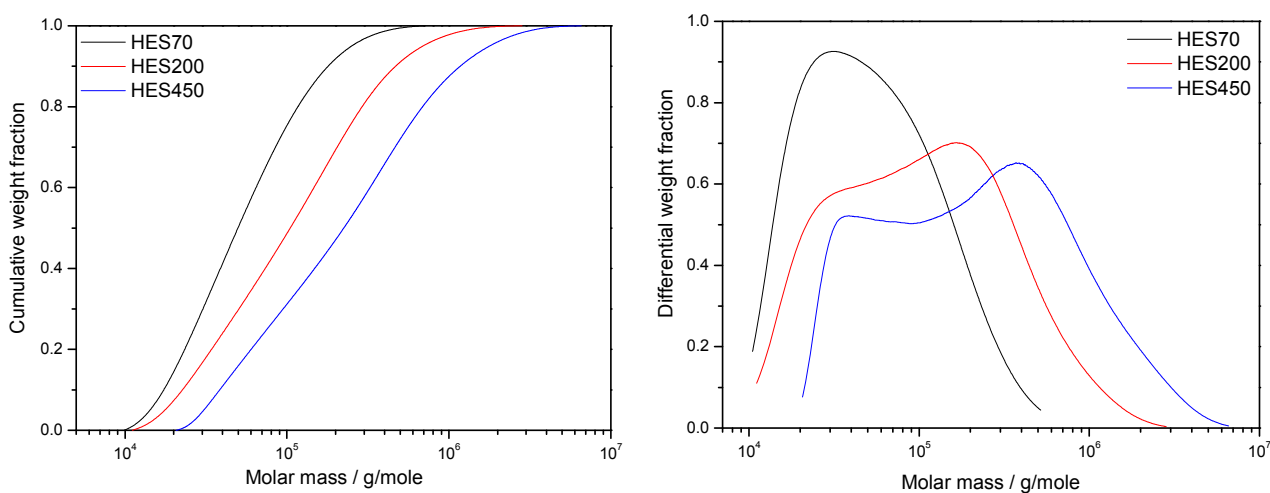


Figure 2.4. Cumulative (left) and differential (right) weight distributions of the molar masses of the different HES samples.

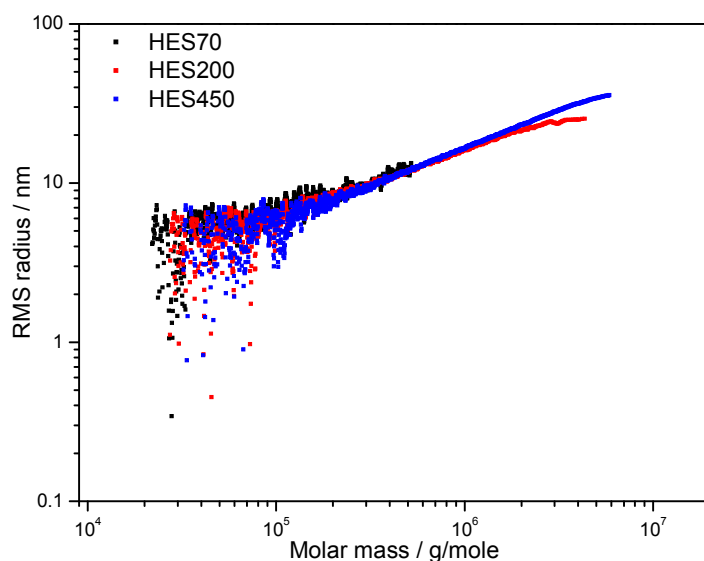


Figure 2.5. A double logarithmic plot of the RMS radius vs. molar mass for the different HES samples.

2.3.2 Dynamic light scattering

The hydrodynamic diameters of the different HES molecules in solution are shown in Table 2.3. As expected, the size increases with the molar mass, ranging between 13.67 nm for HES70 and 32.62 nm for HES450. The polydispersity is rather high for all the HES samples, which is the same observation obtained from AF4 measurements.

The ratio of the radius of gyration to the hydrodynamic radius (r_g/r_h) is known as the ρ -ratio. The latter is a good qualitative indicator for the conformation of macromolecules, where its value is equal to 0.778 for hard spheres, 0.977 for dendrimers, 1.225 for a hyper-branched polymers, and 1.73 for a random coil of polydisperse linear macromolecule in a θ -solvent [77]. Again, the values of the ρ -ratio shown in Table 2.3 indicate that the HES molecules are rather compact due to a relatively high degree of branching.

Table 2.3. Z-average hydrodynamic diameter (d_h), polydispersity index (PDI), hydrodynamic radius (r_h) and ρ -ratio for the different HES samples.

Sample	d_h (nm)	PDI	r_h (nm)	ρ -ratio
HES70	13.67 ± 1.1	0.255	6.84	1.155
HES200	23.34 ± 0.8	0.241	11.67	1.088
HES450	32.62 ± 0.1	0.211	16.31	1.227

2.3.3 ^1H NMR

A typical ^1H NMR spectrum of HES in DMSO-d_6 is shown in Figure 2.6. There is a considerable peak overlapping which precludes the assignment of all peaks in the spectrum. By comparing with spectra of amylose and amylopectin published in the literature [78], it is possible to assign the peaks in the region between 4.5 and 5.6 ppm to the proton attached to C1 of the AGU as well as the 3 hydroxyl groups of each AGU (regardless whether these belong to the AGU directly, or through the hydroxyethyl substitution).

The spectrum of HES in D_2O is more simplified, due to the exchange of the protons of the alcohol groups with deuterium, and thus they disappear from the spectrum. By comparing the spectra with those reported for starch [79] as well as

HES [54], assignment for some of the peaks was possible (see Figure 2.7). The peaks between 5.8 ppm and 5.7 ppm all belong to C1 protons of the AGU. The sharp peak at 5.3 ppm belongs to the C1 protons in case of α 1-4 linkage, at 4.85 ppm belong to those having an α 1-6 linkage, and at 5.6 ppm belong to the C1 protons having hydroxyethyl ethers attached to the neighboring C2. Using these proton NMR spectra, it is possible to determine the degree of branching of the different HES samples. The results shown in Table 2.4 indicate that HES70 has a slightly higher degree of branching (5.15 mol%) compared to HES200 (4.35 mol%) and HES450 (4.05 mol%). In general, these results are close to the degree of branching estimations determined by GC/MS (ranging between 5.5 and 7.17 mol% for 7 different HES samples [49]), and $\{^1\text{H}\}$ - ^{13}C NMR spectroscopy (ranging between 3.1-5.5 mol% for 3 different HES200 samples [54]). ^1H NMR spectroscopy has the advantage of being much simpler than these 2 methods, and can be used for a rapid determination of the degree of branching; however, the above methods can give detailed information about the pattern of hydroxyethylation at C2, C3 and C6 positions, as well as the average molar substitution.

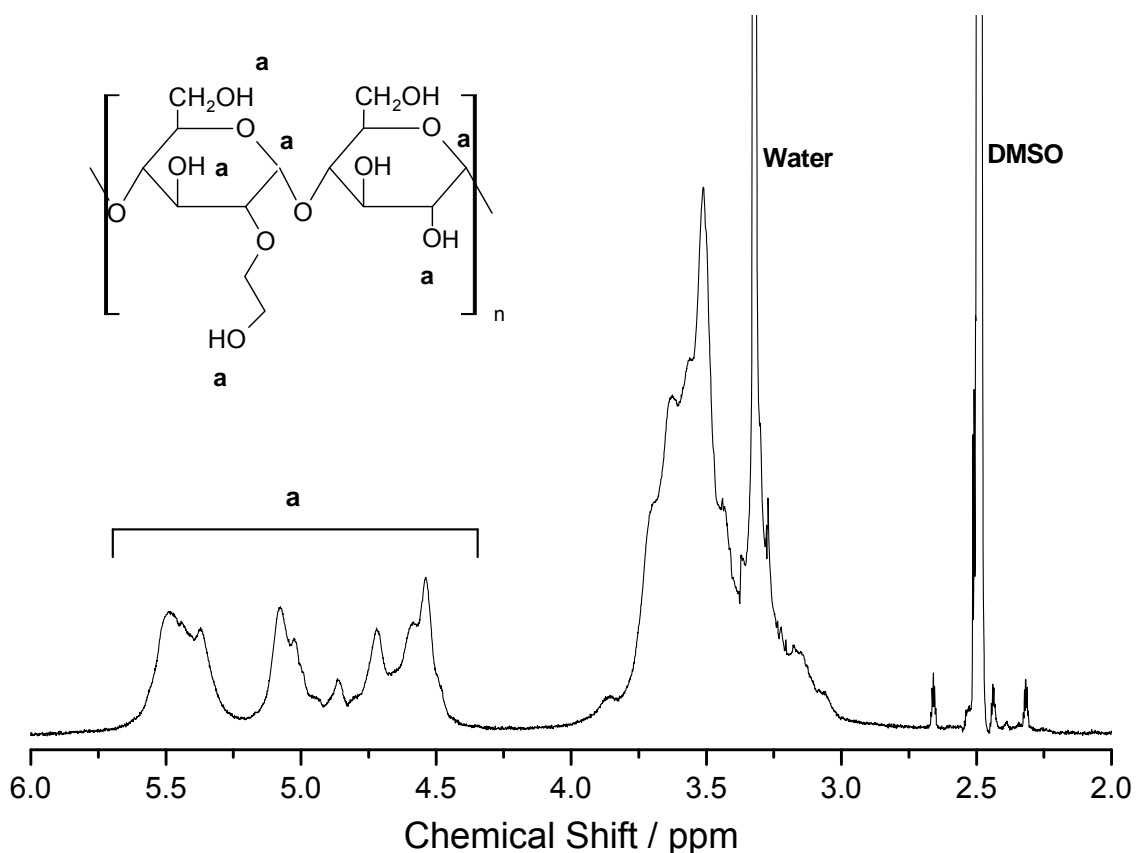


Figure 2.6. ^1H NMR spectrum of HES200 in DMSO-d^6 .

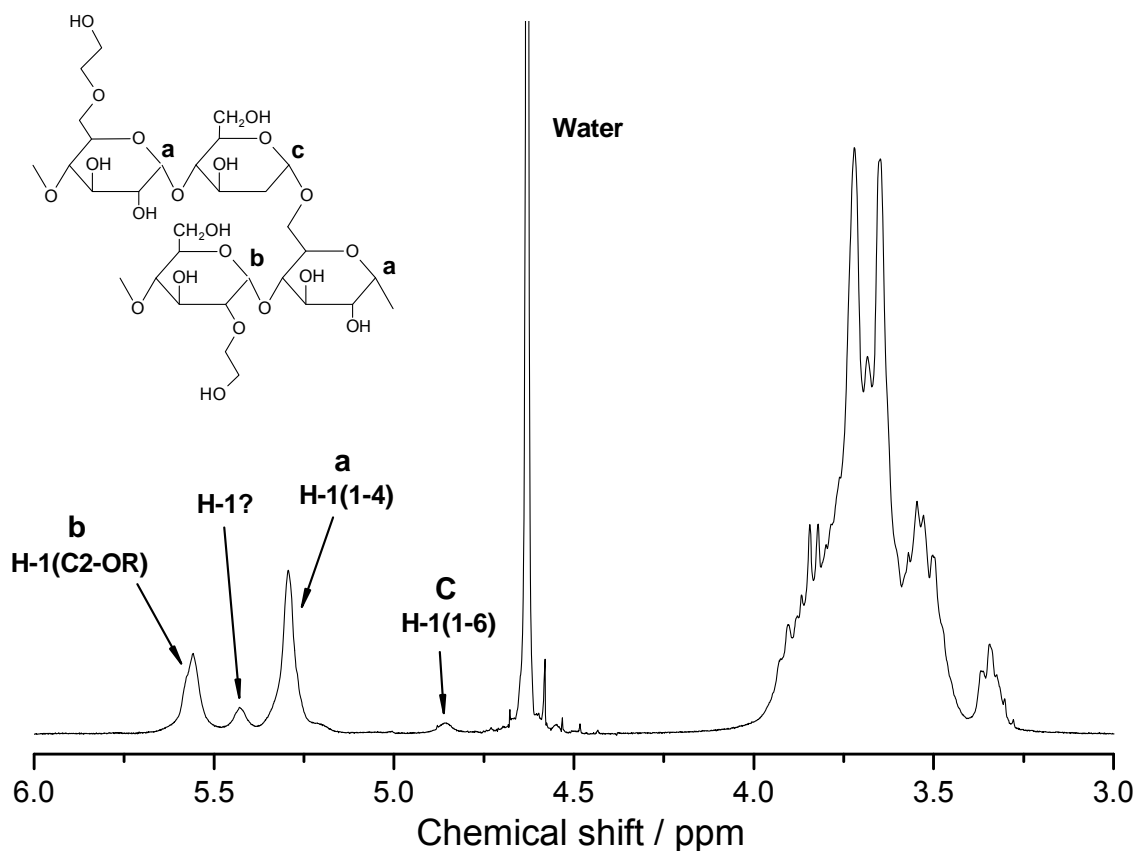


Figure 2.7. ^1H NMR spectrum of HES200 in D_2O .

Table 2.4. Degree of branching of the different HES samples as determined from ^1H NMR spectroscopy of solutions in D_2O .

Sample	Degree of branching (mol%)
HES70	5.15
HES200	4.35
HES450	4.05

2.4 Conclusions and outlook

Using AF4 coupled to MALS, the molar mass of the different HES samples was determined and was found to roughly agree with the nominal values. The polydispersity of the HES samples was high, and despite the fact that this might complicate the characterization of the modified samples (see the next parts), no

measures were taken to fractionate the samples and use a narrowly distributed fraction. The conformation coefficient obtained from a double logarithmic plot of the molar mass and the radius of gyration is lower than that expected for a random coil indicating a somehow compact conformation for the HES samples due to branching.

^1H NMR of the HES samples in DMSO-d^6 could not provide information about the molecular structure due to extensive peak overlapping. Some peaks of the C1 protons could be identified unequivocally for HES solutions in D_2O , thus allowing the determination of the degree of branching. Results were found to agree with previous results determined using GC/MS and $\{^1\text{H}\}$ - ^{13}C NMR spectroscopy. The small degree of branching was responsible for the relatively compact HES coil as determined by AF4 and DLS.

A thorough characterization of the molecular characteristics of the HES samples requires a very cumbersome GC/MS process, involving permethylation, hydrolysis to monosaccharides, reduction, followed by acetylation [49]. This procedure was not carried out, and the above tests were considered sufficient for the analytical characterization of the crude HES.

2.5 References

- [1] O.C. Farokhzad, R. Langer, Nanomedicine: Developing smarter therapeutic and diagnostic modalities. *Advanced Drug Delivery Reviews* 58 (2006) 1456-1459.
 - [2] R. Aston, R. Saffie-Siebert, L. Canham, J. Ogden, Nanotechnology applications for drug delivery. *Pharmaceutical Technology Europe* 17(4) (2005) 21-28.
 - [3] C.N.R. Rao, G.U. Kulkarni, P.J. Thomasa, P.P. Edwards, Metal nanoparticles and their assemblies. *Chemical Society Reviews* 29 (2000) 27-35.
 - [4] Nanomedicine - An ESF – European Medical Research Councils (EMRC) Forward Look report, ESF, 2003.
 - [5] S.M. Moghimi, A.C. Hunter, J.C. Murray, Nanomedicine: current status and future prospects. *FASEB Journal* 19 (2005) 311-330.
 - [6] P. Couvreur, C. Vauthier, Nanotechnology: Intelligent design to treat complex disease. *Pharm Res* 23(7) (2006) 1417-1450.
 - [7] J. Luten, C.F.v. Nostrum, S.C.D. Smedt, W.E. Hennink, Biodegradable polymers as non-viral carriers for plasmid DNA delivery. *Journal of Controlled Release* 126(2) (2008) 97-110.
 - [8] E. Mastrobattista, M.A.E.M.v.d. Aa, W.E. Hennink, D.J.A. Crommelin, Artificial viruses: a nanotechnological approach to gene delivery. *Nature reviews Drug discovery* 5 (2006) 115-121.
 - [9] S.M. Moghimi, C. Hunter, J.C. Murray, Long-Circulating and Target-Specific Nanoparticles: Theory to Practice. *Pharmacological Reviews* (2001) 293-318.
 - [10] C. Toumey, The man who understood the Feynman machine. *Nature Nanotechnology* 2 (2007) 9-10.
 - [11] R. Feynman, There's plenty of room at the bottom. *Engineering and Science* 23 (1960) 22-36.
 - [12] L.Y. Qiu, Y.H. Bae, Polymer architecture and drug delivery. *Pharm Res* 23(1) (2006) 1-30.
 - [13] A. Besheer, J. Kressler, K. Mäder, in: H. S. Nalwa (Ed.), *polymeric nanostructures and their applications*. Vol. 2, American Scientific Publishers, California, 2007, pp. 415-450.
 - [14] K. Letchford, H. Burt, A review of the formation and classification of amphiphilic block copolymer nanoparticulate structures: micelles, nanospheres, nanocapsules
-

-
- and polymersomes. *European Journal of Pharmaceutical and Biopharmaceutics* 65 (2007) 259-269.
- [15] P.A. Vasey, S.B. Kaye, R. Morrison, C. Twelves, P. Wilson, R. Duncan, A.H. Thomson, L.S. Murray, T.E. Hilditch, T. Murray, S. Burtles, D. Fraier, E. Frigerio, J. Cassidy, Phase I clinical and pharmacokinetic study of PK1 [N-(2-hydroxypropyl) methacrylamide copolymer doxorubicin]: First member of a new class of chemotherapeutic agents—drug-polymer conjugates. *Clinical Cancer Research* 5 (1999) 83-94.
- [16] L.W. Seymour, D.R. Ferry, D. Anderson, S. Hesslewood, P.J. Julyan, R. Poyner, J. Doran, A.M. Young, S. Burtles, D.J. Kerr, Hepatic drug targeting: Phase I evaluation of polymer-bound doxorubicin *Journal of Clinical Oncology* 20(6) (2002) 1668-1676.
- [17] J.M. Rademaker-Lakhai, C. Terret, S.B. Howell, C.M. Baud, R.F.d. Boer, D. Pluim, J.H. Beijnen, J.H.M. Schellens, J.-P. Droz, A phase I and pharmacological study of the platinum polymer AP5280 given as an intravenous infusion once every 3 weeks in patients with solid tumors. *Clinical Cancer Research* 10 (2004) 3386-3395.
- [18] R. Duncan, Polymer conjugates as anticancer nanomedicines. *Nature Reviews Cancer* 6 (2006) 688-701.
- [19] H. Maeda, SMANCS and polymer-conjugated macromolecular drugs: advantages in cancer chemotherapy. *Advanced Drug Delivery Reviews* 46(1-3) (2001) 169-185.
- [20] Y. Matsumura, T. Hamaguchi, T. Ura, K. Muro, Y. Yamada, Y. Shimada, K. Shirao, T. Okusaka, H. Ueno, M. Ikeda, N. Watanabe, Phase I clinical trial and pharmacokinetic evaluation of NK911, a micelle-encapsulated doxorubicin. *British Journal of Cancer* 91 (2004) 1775-1781.
- [21] S. Danson, D. Ferry, V. Alakhov, J. Margison, D. Kerr, D. Jowle, M. Brampton, G. Halbert, M. Ranson, Phase I dose escalation and pharmacokinetic study of pluronic polymer-bound doxorubicin (SP1049C) in patients with advanced cancer. *British Journal of Cancer* 90 (2004) 2085-2091.
- [22] W.J. Gradishar, S. Tjulandin, N. Davidson, H. Shaw, N. Desai, P. Bhar, M. Hawkins, J. O'Shaughnessy, Phase III trial of nanoparticle albumin-bound paclitaxel compared with polyethylated castor oil-based paclitaxel in women with breast cancer *Journal of Clinical Oncology* 23(31) (2005) 7794-7803.
- [23] R. Duncan, The dawning era of polymer therapeutics. *Nature Reviews Drug Discovery* 2 (2003) 347-360.
-

-
- [24] M.J. Vicent, R. Duncan, Polymer conjugates: nanosized medicines for treating cancer. *Trends in Biotechnology* 24(1) (2006) 39-47.
- [25] J. Fang, T. Sawa, H. Maeda, in: H. Maeda, A. Kabanov, K. Kataoka and T. Okano (Eds.), *Polymer drugs in the clinical stage - advantages and prospects*, Kluwer Academic Publishers, New York, 2004, pp. 29-50.
- [26] G. Pasut, F.M. Veronese, PEGylation of proteins as tailored chemistry for optimized bioconjugates. *Advances in Polymer Science* 192 (2006) 95-134.
- [27] H. Sato, Enzymatic procedure for site-specific pegylation of proteins. *Advanced Drug Delivery Reviews* 54 (2002) 487-504.
- [28] Y. Kodera, A. Matsushima, M. Hiroto, H. Nishimura, A. Ishii, T. Ueno, Y. Inada, PEGylation of proteins and bioactive substances for medical and technical applications. *Progress in Polymer Science* 23 (1998) 1233-1271.
- [29] F.M. Veronese, Peptide and protein PEGylation: a review of problems and solutions. *Biomaterials* 22 (2001) 405-417.
- [30] J.M. Harris, R.B. Chess, Effect of PEGylation on Pharmaceuticals. *Nature reviews Drug discovery* 2 (2003) 214-221.
- [31] K. Kataoka, A. Harada, Y. Nagasaki, Block copolymer micelles for drug delivery: design, characterization and biological significance. *Advanced Drug Delivery Reviews* 47 (2001) 113-131.
- [32] G.S. Kwon, T. Okano, Polymeric micelles as new drug carriers. *Advanced Drug Delivery Reviews* 21 (1996) 107-116.
- [33] M.-C. Jones, J.-C. Leroux, Polymeric micelles - a new generation of colloidal drug carriers. *European Journal of Pharmaceutical and Biopharmaceutics* 48 (1999) 101-111.
- [34] K. Kataoka, T. Matsumoto, M. Yokoyama, T. Okano, Y. Sakurai, S. Fukushima, K. Okamoto, G.S. Kwon, Doxorubicin-loaded poly(ethylene glycol)-poly(β -benzyl-L-aspartate) copolymer micelles: their pharmaceutical characteristics and biological significance. *Journal of Controlled Release* 64 (2000) 143-153.
- [35] D. Heng, D.J. Cutler, H.-K. Chan, J. Yun, J.A. Raper, What is a Suitable Dissolution Method for Drug Nanoparticles? *Pharm Res* 25(7) (2008) 1696-1701.
- [36] M.G. Garnett, P. Kallinetti, Nanomedicines and nanotoxicology: some physiological principles. *Occupational medicine* 56 (2006) 307-311.
-

-
- [37] K.S. Soppimath, T.M. Aminabhavi, A.R. Kulkarni, W.E. Rudzinski, Biodegradable polymeric nanoparticles as drug delivery devices. *Journal of Controlled Release* 70 (2001) 1-20.
- [38] R.H. Müller, C. Jacobs, O. Kayser, Nanosuspensions as particulate drug formulations in therapy: Rationale for development and what we can expect for the future. *Advanced Drug Delivery Reviews* 47 (2001) 3-19.
- [39] G.C.S. Rao, M.S. Kumar, N. Mathivanan, M.E.B. Rao, Nanosuspensions as the most promising approach in nanoparticulate drug delivery systems. *Pharmazie* 59 (2004) 5-9.
- [40] D.E. Discher, A. Eisenberg, Polymer Vesicles. *Science* 297(5583) (2002) 967-973.
- [41] B.M. Discher, Y.-Y. Won, D.S. Ege, J.C.-M. Lee, F.S. Bates, D.E. Discher, D.A. Hammer, Polymersomes: Tough Vesicles Made from Diblock Copolymers *Science* 284(5417) (1999) 1143-1146.
- [42] M. Antonietti, S. Förster, Vesicles and liposomes: A self-assembly principle beyond lipids. *Advanced Materials* 15(16) (2003) 1323-1333.
- [43] D.E. Discher, V. Ortiz, G. Srinivas, M.L. Klein, Y. Kim, D. Christian, S. Cai, P. Photos, F. Ahmed, Emerging applications of polymersomes in delivery: From molecular dynamics to shrinkage of tumors. *Progress in Polymer Science* 32 (2007) 838-857.
- [44] F. Ahmed, R.I. Pakunlu, A. Brannan, F. Bates, T. Minko, D.E. Discher, Biodegradable polymersomes loaded with both paclitaxel and doxorubicin permeate and shrink tumors, including apoptosis in proportion to accumulated drug. *Journal of Controlled Release* 116(2) (2006) 150-158.
- [45] F. Schortgen, N. Deye, L. Brochard, Preferred plasma volume expanders for critically ill patients: results of an international survey. *Intensive Care Medicine* 30 (2004) 2222–2229.
- [46] J. Treib, J.-F. Baron, M.T. Grauer, R.G. Strauss, An International View of Hydroxyethyl starches. *Intensive Care Medicine* 25 (1999) 258-268.
- [47] M.E. Brecher, H.G. Owen, N. Bandarenko, Alternatives to Albumin: Starch Replacement for Plasma Exchange. *Journal of Clinical Apheresis* 12 (1997) 146–153.
- [48] C. Gosch, T. Haase, W. Kulicke, Molar mass distribution and size of hydroxyethyl starch fractions obtained by continuous polymer fractionation. *Starch* 54 (2002) 375.
-

-
- [49] K. Sommermeyer, U. Hildebrand, F. Cech, E. Pfitzer, K. Henning, B. Weidler, Feinstruktur und Hyperfeinstruktur von klinisch verwendeter Hydroxyethylstärke. *Starch* 44(5) (1992) 173.
- [50] Kolloidaler Volumenersatz aus Bernburg: Infokoll® HES 200/0.5 6 % and 10 %, Product Information Booklet, Serumwerk Bernburg, Germany.
- [51] E. Dellacherie, in: S. Dumitriu (Ed.), *Polysaccharides in medicinal applications*, Marcel Dekker, New York, 1996.
- [52] C. Jungheinrich, T. Neff, Pharmacokinetics of hydroxyethyl starch. *Clinical Pharmacokinetics* 44(7) (2005) 681.
- [53] J. Treib, A. Haass, G. Pindur, U. Seyfert, W. Treib, M. Grauer, F. Jung, E. Wenzel, K. Schimrigk, HES 200/0.5 is not HES 200/0.5 influence of C2/C6 hydroxyethylation ratio of hydroxyethyl starch (HES) on hemorheology, coagulation and elimination kinetics. *Thrombosis and Haemostasis* 74 (1995) 452.
- [54] W. Kulicke, D. Roessner, W. Kull, Characterization of hydroxyethyl starch by polymer analysis for use as a plasma volume expander. *Starch* 45(12) (1993) 445.
- [55] G. Haynes, J. Havidich, K. Payne, Why the Food and Drug administration changed the warning label for hetastarch. *Anesthesiology* 101 (2004) 560.
- [56] D. Metze, S. Reimann, Z. Szepfalusi, B. Bohle, D. Kraft, T. Luger, Persistent pruritis after hydroxyethyl starch infusion therapy: a result of long-term storage in cutaneous nerves. *British Journal of Dermatology* 136 (1997) 553.
- [57] C.T. Knorpp, W.R. Merchant, P.W. Gikas, H.H. Spencer, N.W. Thompson, Hydroxyethyl starch extracellular cryoprotective agent for erythrocytes. *Science* 157(794) (1967) 1312-1313.
- [58] M. Orlando, Modification of proteins and low molecular weight substances with hydroxyethyl starch (HES). Justus Liebig Universität Giessen, Gießen, 2003.
- [59] L. Huang, R. Mehta, P. DeLuca, Evaluation of statistical model for the formation of poly (acryloyl hydroxyethyl starch) microspheres. *Pharm Res* 14 (1997) 475.
- [60] J. Devy, E. Balasse, H. Kaplan, C. Madoulet, M. Andry, Hydroxyethylstarch microcapsules: A preliminary study for tumor immunotherapy application. *International Journal of Pharmaceutics* 307 (2006) 194.
- [61] G. Jiang, W. Qiu, P. DeLuca, Preparation and in vitro/ in vivo evaluation of insulin – loaded poly(acryloyl-hydroxyethyl starch) PLGA composite microspheres. *Pharm Res* 20(3) (2003) 452.
-

-
- [62] W. Fraunhofer, G. Winter, C. Coester, Asymmetrical Flow Field-Flow Fractionation and Multiangle Light Scattering for Analysis of Gelatin Nanoparticle Drug Carrier Systems. *Analytical Chemistry* 76 (2004) 1909-1920.
- [63] J.C. Giddings, in: M. Schimpf, K. Caldwell and J. C. Giddings (Eds.), *Field-Flow Fractionation Handbook*, Wiley-Interscience, New York, USA, 2000, pp. 3-30.
- [64] M. Andersson, B. Wittgren, K.-G. Wahlund, Ultrahigh Molar Mass Component Detected in Ethylhydroxyethyl Cellulose by Asymmetrical Flow Field-Flow Fractionation Coupled to Multiangle Light Scattering. *Analytical Chemistry* 73 (2001) 4852-4861.
- [65] W. Fraunhofer, G. Winter, The use of asymmetrical flow field-flow fractionation in pharmaceuticals and biopharmaceuticals. *European Journal of Pharmaceutics and Biopharmaceutics* 58 (2004) 369–383.
- [66] K.-G. Wahlund, in: M. Schimpf, K. Caldwell and J. C. Giddings (Eds.), *Field-Flow Fractionation Handbook*, Wiley Interscience, New York, USA, 2000, pp. 279-294.
- [67] P.J. Wyatt, Light scattering and the absolute characterization of macromolecules. *Analytica Chimica Acta* 272 (1993) 1-40.
- [68] P.J. Wyatt, The size of macromolecules and some observations on their mass. *Journal of Liquid Chromatography* 14(12) (1991) 2351-2372.
- [69] P.J. Wyatt, Mean square radius of molecules and secondary instrumental broadening. *Journal of Chromatography* 648 (1993) 27-32.
- [70] P.J. Wyatt, Submicrometer Particle Sizing by Multiangle Light Scattering following Fractionation. *Journal of Colloid and Interface Science* 197 (1998) 9-20.
- [71] P. Roger, B. Bauda, P. Colonna, Characterization of starch polysaccharides by flow field-flow fractionation–multi-angle laser light scattering–differential refractometer index *Journal of Chromatography A* 917(1-2) (2001) 179-185.
- [72] A. Rolland-Sabate, P. Colonna, M.G. Mendez-Montealvo, V. Planchot, Branching Features of Amylopectins and Glycogen Determined by Asymmetrical Flow Field Flow Fractionation Coupled with Multiangle Laser Light Scattering. *Biomacromolecules* 8 (2007) 2520-2532.
- [73] B. Wittgren, K.-G. Wahlund, M. Andersson, C. Arfvidsson, Polysaccharide characterization by flow field-flow fractionation-multiangle light scattering: Initial studies of modified starches *International Journal of Polymer Analysis and Characterization* 7(1&2) (2002) 19-40.
-

- [74] W.-M. Kulicke, U. Kaiser, D. Schwengers, R. Lemmes, Measurements of the refractive index increment on hydroxyethyl starch as a basis for absolute molecular weight determinations. *Starch* 43(10) (1991) 392-396.
- [75] C. Augsten, K. Mäder, Characterizing molar mass distributions and molecule structures of different chitosans using asymmetrical flow field-flow fractionation combined with multi-angle light scattering. *International Journal of Pharmaceutics* 351 (2008) 23-30.
- [76] D.J. Nagy, Characterization of nonionic and cationic amine-functional polymers by aqueous SEC-MALLS. *Journal of Applied Polymer Science* 59 (1996) 1479-1488.
- [77] W. Burchard, Solution properties of branched macromolecules. *Advances in Polymer Science* 143(113-194) (1999).
- [78] H. Falk, M. Stanek, Two-Dimensional ^1H and ^{13}C NMR spectroscopy of amylose and amylopectin. *Monatshefte für Chemie* 128 (1997) 777-784.
- [79] G.S. Nilsson, K.-E. Bergquist, U. Nilsson, Lo Gorton, Determination of the degree of branching in normal and amylopectin type potato starch with ^1H -NMR spectroscopy - Improved resolution and two-dimensional spectroscopy. *Starch* 48(10) (1996) 352-357.
-

Part II

Hydrophobically-modified hydroxyethyl starch (HM-HES)

Chapter 3

Synthesis, characterization and self-assembly of hydrophobically-modified hydroxyethyl starch (HM-HES)

3.1 Hydrophobically-modified polysaccharides

Polysaccharides are ubiquitous structural and functional constituents of all living organisms. Their main roles include energy storage (such as starch and glycogen) or structural functions, (such as cellulose in plant cell walls). Furthermore, nature has brilliantly made bioconjugates of proteins and polysaccharides (peptidoglycans, such as mucin to coat mucosal membranes) or lipids and polysaccharides (lipopolysaccharides, such as those in the cell wall of gram negative bacteria that impart an immune resistant character to them). In pursuing new materials that fulfil pressing needs in the biomedical field, man has recently started to realize the wonders of nature and adopt a policy aiming to understand its wisdom and attempting to mimic it.

One of these approaches is the hydrophobic modification of water soluble polysaccharides with fatty acids. Emulsan is an example for such naturally-occurring lipopolysaccharides, produced as an exopolysaccharide in the capsule of the oil-degrading bacterium *Acinetobacter calcoaceticus*. It is a polyanionic heteropolysaccharide containing 3 types of aminosugars, and 5-15 % w/w fatty acid residues (predominantly laurate) attached by ester links [1]. Although it is not

particularly effective in reducing the surface tension, it has a high tendency to bind tightly to interfaces, which makes it an excellent stabilizer for emulsions at relatively small concentrations [1]. Among the possible applications, it was tested successfully for the emulsification and pipeline-transportation of heavy oil, as well as the emulsification and direct combustion of heavy fuel emulsions [1].

Man-made hydrophobically-modified polysaccharides were synthesized and studied for many polymers, including starch [2], dextran [3], pullulan [4, 5], xylan [6], pectin [7] and chitosan [8]. In general, these amphiphilic polymers show a spectrum of different self-assembly behaviours. For example, Francis *et al.* grafted polyethyleneglycolalkyl ether to dextran [9] and hydroxypropyl cellulose [10] and found out that the produced amphiphilic polymers form 20-30 nm micelles in aqueous solutions. Akiyoshi *et al.* reported the formation of monodisperse nanoparticles from pullulan hydrophobized with cholesterol [11], while Liebert *et al.* described the formation of 200-500 nm particles from highly esterified dextran [12]. Polymeric vesicles [13] were reported by Uchegbu *et al.* for the self-assembly of chitosan palmitate. Finally, three-dimensional hydrogel structures were formed from highly concentrated aqueous solutions of hydrophobized pullulan [14].

Such amphiphilic polysaccharide derivatives find a number of applications in the biomedical field. For instance, Durand and Dellacherie studied the properties of hydrophobically-modified dextrans as rheology modifiers [15]. The ability of the polymeric micelles of amphiphilic dextran and hydroxypropyl cellulose to solubilize poorly-soluble drugs was also reported [9, 10]. Rouzes *et al.* used dextran hydrophobized with 3-phenoxy 2-hydroxypropyl residues for the preparation of stable emulsions as well as the stabilization of the surface of poly(styrene) particles prepared by emulsion polymerization [16]. Lauroyldextran with different degrees of modification was investigated as a polymeric coating for tablets to achieve site specific drug delivery to the colon [17]. The hydrophobized polysaccharides can also be used for the surface decoration of liposomes as reviewed by Sihorkar and Vyas [18], while Lemerchand *et al.* reviewed their use for the surface modification of nanoparticles to achieve “stealth” characters and/or site directed delivery [19].

Compared to the widely used cellulose, HES has the advantage of being biodegradable in human body. Furthermore, it has less incidence of hypersensitivity reactions when compared to dextran. Accordingly, hydrophobically modified HES

(HM-HES) is expected to have a better biodegradability and biocompatibility than the aforementioned amphiphilic polymers. In this part of the present thesis, the synthesis of HM-HES prepared by esterification with fatty acids (lauric, palmitic and stearic acids) is reported. The characterization of the modified HES was carried out using ^1H NMR and Raman spectroscopy, and its aqueous self-assembly was studied using FFF and TEM.

3.2 Experimental

3.2.1 Materials

HES with M_w 70 000, 200 000 and 450 000 g/mol and MS 0.5 was a kind gift from Serumwerk Bernburg, Germany. Lauric (C12), palmitic (C16) and stearic (C18) acids as well as dicyclohexyl carbodiimide (DCC) were purchased from Sigma-Aldrich. Dimethyl aminopyridine (DMAP) was from Merck, Darmstadt, Germany. 2-heptadecyl-2,4,5,5-tetramethylimidazole-1-oxyl (HD-TMI) was obtained from Prof. V. Khramtsov, Institute of Chemical Kinetics and Combustion, Novosibirsk, Russia. All other chemicals and solvents were reagent grade and used as received, except dimethylsulfoxide (DMSO) which was stored over a 3 Å molecular sieve for drying.

3.2.2 Synthesis

a) Using lauric acid, DCC and DMAP. 1.5 g HES was dried at 105 °C for 2 h then dissolved in 20 ml dry DMSO. To this solution, a certain amount of the fatty acid (see Table 3.1), DCC and DMAP (in the molar ratio 1:1:0.5, respectively) were added and dissolved while the flask was tightly sealed and left under stirring at room temperature for 24 h (except in the case of stearic acid, where the temperature was raised to 40 °C). During the reaction, DCC converts to dicyclohexyl urea (DCU) which is precipitated and removed by filtration. The filtrate was added to 200 ml precipitating solvent mixture (see Table 3.1). The product was filtered and washed with 100 ml of the same solvent mixture, and then air dried. The dry polymer was dialyzed against distilled water for 3 days then lyophilized.

b) Using vinyl laurate and lyophilized phosphate buffer. 1.5 g HES was dried at 105 °C for 2 h before dissolving in 20 ml dry DMSO. 0.65 ml vinyl laurate were added to the HES solution as well as 50 mg of phosphate buffer pH 7.8 as a lyophilisate. The reaction mixture was shaken for 72 h at 37 °C. Purification took

place by filtration, precipitation with 200 ml isopropanol/ether (1:1), dialysis then lyophilization.

3.2.3 ^1H NMR spectroscopy

For ^1H NMR measurements, 30 mg polymer samples were dissolved in 600 μl d^6 -DMSO and measured at 400 MHz (Gemini 2000, Varian Inc.).

3.2.4 Raman spectroscopy

Raman scattering was recorded at 180° to the incident beam on a Bruker FT-Raman spectrometer RFS 100/S (Bruker Optics, Ettlingen, Germany) using a diode-pumped Nd:YAG laser with wavelength of 1064 nm. The temperature dependence of the Raman spectra of lauric acid was studied in the range from 23 to 55 $^\circ\text{C}$. Temperature variations were performed by flowing tempered air in a glass Dewar cell. After a temperature step, the sample was allowed to equilibrate for 15 min before recording each spectrum. The manipulation and evaluation of the spectra was performed with the Bruker OPUS software.

3.2.5 Asymmetric flow field flow fractionation (AF4)

The water soluble polymers (samples 1-3 in Table 3.1) were studied using AF4 and compared to the original HES. Samples were prepared with a concentration of 5 mg/ml in bidistilled filtered water preserved with 0.02 %w/v sodium azide. HM-HES samples were filtered through 0.2 μm filter before injection. For separation, the same procedure were used as mentioned under section 2.2.2. For the raw HES samples, a dn/dc value equal to 0.146 was obtained from the literature [20]. For the other samples, dn/dc was determined by measuring 3 different concentrations, each repeated three times.

3.2.6 Preparation of nanodispersions

For the study of the self-assembly of the water dispersible HM-HES (samples 4-6 in Table 1), the following procedure for the preparation of a dispersion of the nanoparticles was used. 15 mg polymer was dissolved in 2 ml water/THF 1:1 mixture, and then 2 ml water was added dropwise with stirring. THF was removed by evaporation in a rotary evaporator at 40 $^\circ\text{C}$ and 150 mbar. The polymer concentration in the final nanodispersion was 0.5 % w/v.

3.2.7 Transmission Electron microscopy (TEM)

The water-soluble HES laurate samples were investigated using CryoTEM microscopy (courtesy of Frank Steiniger, Electron Microscopic Center, Friedrich-Schiller-University, Jena, Germany). A few microlitres of polymer solution (5 mg/ml) were placed on a grid (Quantifoil Micro Tools, Jena, Germany) and the excess liquid was removed with filter paper. The samples were cryofixed by rapid immersion into liquid ethane cooled to $-170\text{ }^{\circ}\text{C}$ to $-180\text{ }^{\circ}\text{C}$ in a cryobox (Carl Zeiss NTS GmbH, Oberkochen, Germany). The excess ethane was removed by blotting in the cold. The samples were transferred with a cryotransfer unit (Gatan 626-DH) into the pre-cooled cryoelectron microscope (Philips CM 120, Netherlands) operated at 120 kV and viewed under low dose conditions.

The water-dispersible HES laurates were investigated with negative stain and freeze fracture microscopy. For negative staining, the suspension was mixed with 1% aqueous uranyl acetate (1:1). A copper grid coated with formvar film was placed on a droplet of this mixture for 1 min. Then the liquid was blotted off with filter paper and the grid was air dried. The samples were observed with a transmission electron microscope (EM 900, Carl Zeiss SMT, Oberkochen, Germany) operating at 80 kV.

For freeze fracturing, the samples were cryofixed with a propane jet freezer (JFD 60, BAL-TEC, Liechtenstein) and freeze fractured at $-110\text{ }^{\circ}\text{C}$ using a BAF 060 freeze fracture apparatus (BAL-TEC, Liechtenstein). After freeze etching for 30 s, the surface was shadowed with platinum (2 nm, shadowing angle 45°) and subsequently with carbon (25 nm, shadowing angle 90°). The replica were floated in sodium chloride solution (4 % Cl) for 30 min, rinsed in distilled water (5 min) and washed in 30 % acetone for 30 min. After final washing in distilled water the replica were mounted on grids and observed with a transmission electron microscope (EM 912 OMEGA, Carl Zeiss SMT, Oberkochen, Germany) operating at 80 kV.

3.3 Results and discussion

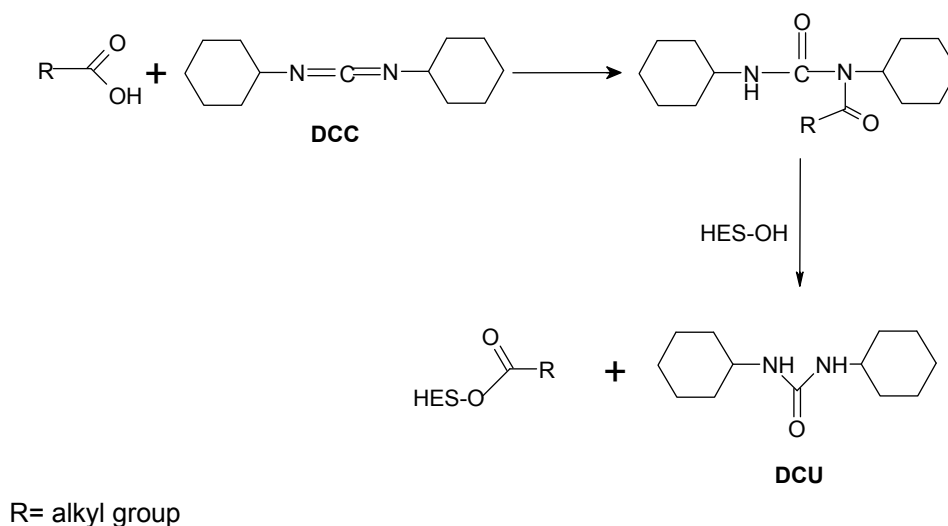
3.3.1 Synthesis and ^1H NMR

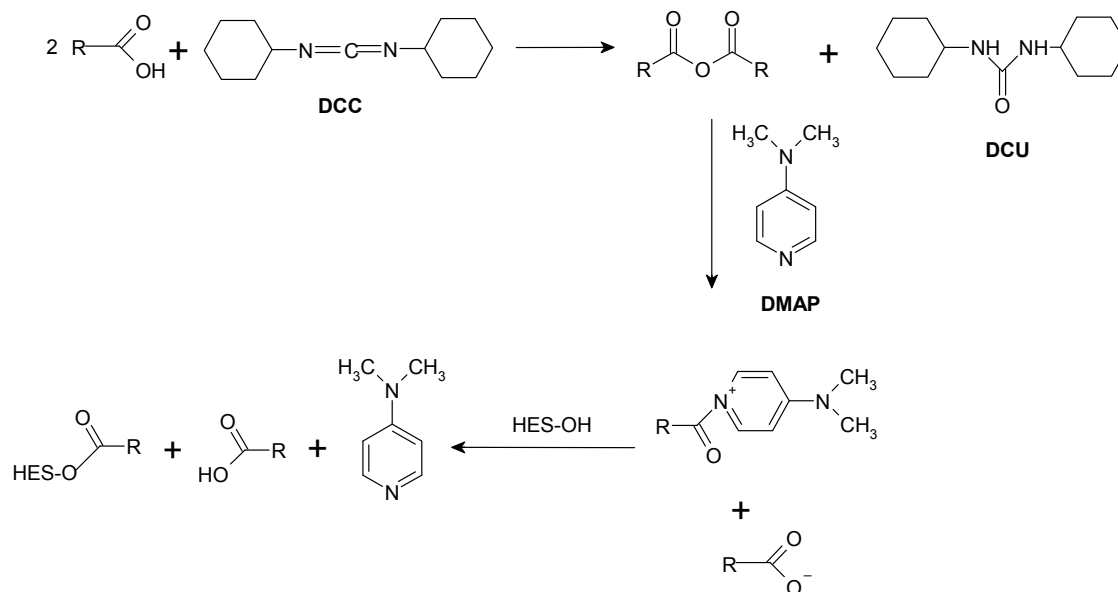
In general, there are various ways to carry out an esterification reaction, however not all of them are suitable to obtain fatty acid esters of HES. For example, the use of acid chlorides is a simple, effective and widely spread method to prepare esters, yet

HCl, the byproduct of the reaction, can lead to acid hydrolysis of starches [21]. Accordingly, we preferred the use of milder reaction conditions. In the first synthetic procedure, DCC and DMAP were used as catalysts, while in the second method, vinyl laurate and a solid salt were used.

The mechanism of the reaction catalyzed by DCC could be explained by two possible pathways; the first involves direct activation of the fatty acid with DCC followed by reaction with HES hydroxyl groups to form the ester (Scheme 3.1) [22]. In the second pathway, the acid is converted to the anhydride through DCC with the formation of DCU as byproduct. The anhydride reacts with DMAP to form an activated acyl pyridinium, that then readily esterifies with the hydroxyl groups (Scheme 3.2) [23]. It was necessary to find a solvent for HES and the reactants to carry out a homogenous reaction, but the choices were limited as HES is soluble only in water, DMSO, DMF and NMP. Water is not suitable for the esterification reaction, and DMSO was chosen as it has a better toxicity profile than DMF and NMP according to the FDA [24].

Scheme 3.1. Direct activation of fatty acid with DCC and subsequent ester formation.



Scheme 3.2. Activation of fatty acid with DCC and DMAP for ester formation.

A typical ^1H NMR spectrum of the modified HES dissolved in $\text{d}^6\text{-DMSO}$ is shown in Figure 3.1. Peak assignment for the fatty acid residues was straightforward (see Figure 3.1 and inset), where the triplet at 0.85 ppm (peak a in Figure 3.1) belongs to the methyl group of the hydrocarbon chain, the peak at 2.29 ppm (peak d) is related to the methylene group beside the carbonyl group, while the one at 1.5 ppm (peak c) is the methylene group directly before it. All the other methylene groups have a peak at 1.23 ppm (peak b). The clear broadening of the peaks for the methylene groups close to the ester bond (at 2.29 and 1.5 ppm) indicates successful esterification. Meanwhile, peak assignment for HES is not easy due to the overlap between the different peaks. By comparing the ^1H NMR spectrum for HES with previously published results [25] and with those of amylose and amylopectin [26, 27] it was possible to assign the peaks between 4.4 and 5.7 ppm to four protons, namely the proton bound to C1 of the AGU, and those found in the three hydroxyl groups of the AGU (regardless whether the OH group is that of glucose or of the attached hydroxyethyl moiety).

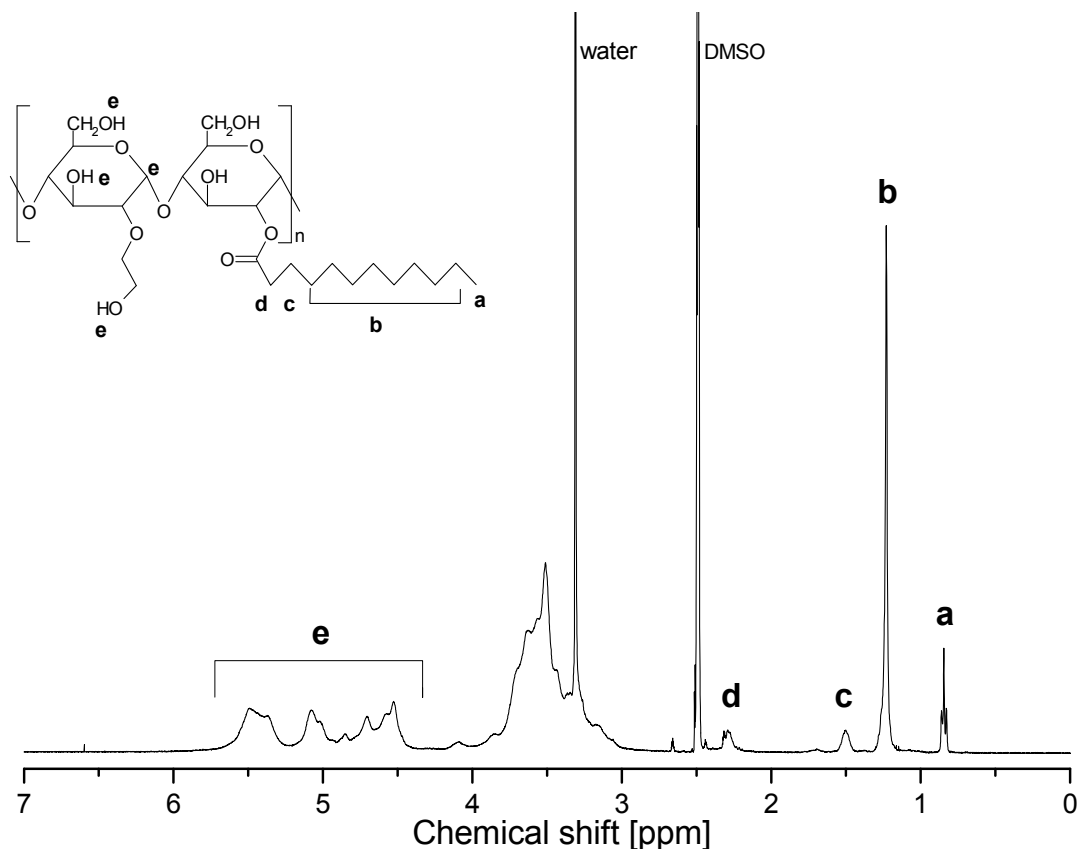


Figure 3.1. ^1H NMR spectrum of HES 200-L0.5. Inset shows the structure of HES laurate and peak assignment.

^1H NMR was used for the calculation of MS of the acyl chains, where it was assumed that each mole of fatty acid removes one mole from the protons of the hydroxyl group after esterification. Thus:

$$MS = \frac{\left(\frac{I_{CH_3}}{3}\right)}{\left(\frac{I_{AGU}}{4 - MS}\right)} \quad 3.1$$

where I_{CH_3} is the integral for the methyl group peak at 0.85 ppm, while I_{AGU} is the integral for the 4 protons of the AGU between 4.4 and 5.7 ppm. Thus $\left(\frac{I_{CH_3}}{3}\right)$ represents one mole of the acyl residue, while $\left(\frac{I_{AGU}}{4 - MS}\right)$ represents one mole of AGU after correction, taking into account that the integral area has decreased due to acylation. By rearranging equation (1), $MS_{\text{fatty acid}}$ can be determined as:

$$MS = \frac{4I_{CH_3}}{3I_{AGU} + I_{CH_3}} \quad 3.2$$

The degree of conversion of the fatty acid (DC) is calculated as:

$$DC = \frac{\text{Actual MS}}{\text{Nominal MS}} \quad 3.3$$

2 different reaction sets were carried out. In the first, lauric, palmitic and stearic acids were reacted with HES using the same molar fatty acid (FA) to AGU ratio. In the second, lauric acid was reacted with HES, where the molar FA:AGU ratio was varied. Results in Table 3.1 show that this simple reaction gave satisfactory DC ranging between 15-55 mol%. With the same fatty acid to AGU ratio, the average $MS_{\text{fatty acid}}$ (average for the 3 different HES molar masses used) increased from lauric acid (9.5 mol %) to palmitic acid (14.7 mol %). On the other hand, HES stearate had a much lower average $MS_{\text{fatty acid}}$ (5.8 mol %). One must note that stearic acid did not dissolve in DMSO at room temperature so that the temperature had to be increased to 40 °C for dissolution. Since relatively low temperatures are required for the reaction of DCC with the acid [28], the elevated temperature used might have led to this reduction in $MS_{\text{fatty acid}}$.

DC increased with increasing the FA:AGU for the lauric acid esterification reaction. This may be due to the fact that the amount of catalysts, particularly DMAP, increased correspondingly. It is worth mentioning that the polymer molar mass seems to have no effect on the $MS_{\text{fatty acid}}$ as it is similar for the reactions using the same fatty acid and polymer: fatty acid ratio.

The second investigated synthetic procedure was a transesterification reaction using vinyl laurate. Transesterification is a process where an ester is converted into another ester by the exchange of the alkoxy moiety [29]. These reactions are usually catalyzed by acids or bases, and lately using different enzymes, such as Lipase [30, 31] and Proteinase [32]. The vinyl groups are good leaving groups that transform into acetaldehyde, and thus shift the reaction forward. Figure 3.2 shows a comparison of the NMR spectra of HES laurate prepared by the DCC method (a) and the vinyl laurate/lyophilized buffer method (b). In case of the DCC catalyzed synthesis, peak 1 at 4.2 ppm for the α -methylene of the esterified primary alcohol is apparent but it is missing in the case of vinyl laurate. This allows the calculation of the proportion of

esterification on primary to secondary alcohol. It turns out that ca. 90 % of the esterification by the DCC occurred at the primary alcohol position, while using the lyophilized salt it occurred exclusively at the secondary alcohols (probably at C2 as it is much more reactive than C3). Another clue is peak **2** at 2.35 ppm which belongs to the α -methylene group of the FA chain. In the case of esterification at the secondary alcohol position, it is much broader due to direct attachment to the polymer backbone, while in case of the primary alcohol esterification, it is less broad, due to the presence of a spacer (C6 of the AGU or the hydroxyethyl group).

Similar results were obtained by Decke during the modification of starch using vinyl esters and different solid salts in DMSO [33]. The regioselectivity of the esterification using vinyl laurate and the lyophilized buffer is attributed to the solvation of starch with DMSO which leads to the activation of the secondary alcohol at C2, while the mechanistic role of the salt in this reaction is not yet known [33]. Meanwhile, the preferential esterification of primary alcohols when using DCC is probably due to the bulkiness of the DCC-activated acyl group.

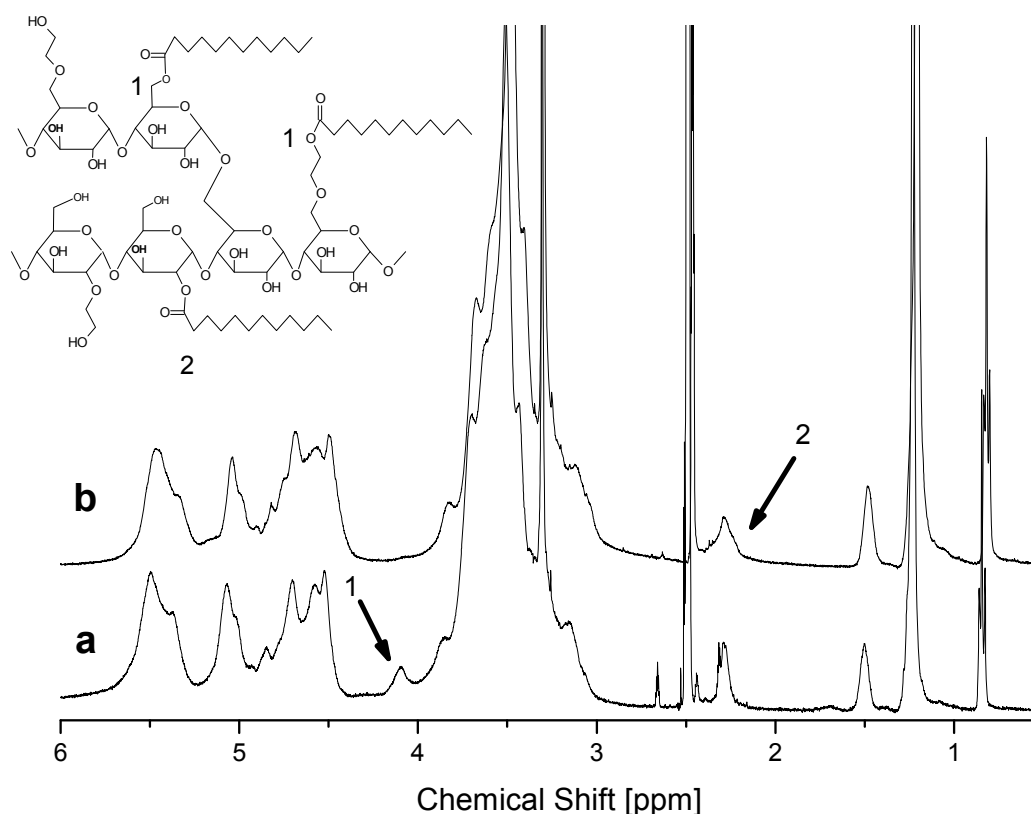


Figure 3.2. ^1H NMR spectrum of HES laurate prepared by the lauric acid/DCC method (a) and the vinyl laurate/lyophilized buffer method (b). Inset shows peak assignment, where **1** is the α -methylene of the esters attached to primary alcohols, and **2** is the α -methylene of the esters bound to secondary alcohols.

Table 3.1. Degree of conversion of the fatty acid, percentage molar substitution as determined by ¹H NMR as well as aqueous solubility.

Serial	Sample	HES M _w ^a x10 ³ g/mol	Reacting FA ^b (wt in g)	FA:AGU ^c	Precipitating solvent	DC _{Fatty acid} ^d mol %	MS _{Fatty acid} ^e mol %	Aqueous solubility
1	HES 70-L2.3 ^f	70	LA (0.25)	1:6.52	Isopropanol/ether 1:1	15	2.3	Water soluble
2	HES 200-L2	200	LA (0.25)	1: 6.52	Isopropanol/ether 1:1	13	2	
3	HES 450-L2	450	LA (0.25)	1: 6.52	Isopropanol/ether 1:1	13	2	
4	HES 70-L10.3	70	LA (0.5)	1:3.26	Isopropanol/ether 1:1	33.7	10.3	Water dispersible
5	HES 200-L8.7	200	LA (0.5)	1:3.26	Isopropanol/ether 1:1	28.4	8.7	
6	HES 450-L9.4	450	LA (0.5)	1:3.26	Isopropanol/ether 1:1	30.6	9.4	
7	HES 70-L19.2	70	LA (1)	1:1.63	Acetonitrile/methanol 1:1	31.3	19.2	Water insoluble
8	HES 200-L27	200	LA (1)	1:1.63	Acetonitrile/ methanol 1:1	44.	27	
9	HES 450-L23.3	450	LA (1)	1:1.63	Acetonitrile/ methanol 2:1	38	23.3	
10	HES 70-P14.5	70	PA(0.64)	1:3.26	Isopropanol/ether 1:1	47.2	14.5	Water insolube
11	HES 200-P16.9	200	PA (0.64)	1:3.26	Isopropanol/ether 1:1	55	16.9	
12	HES 450-P12.6	450	PA (0.64)	1:3.26	Isopropanol/ether 1:1	41.1	12.6	
13	HES 70-S7.5	70	SA (0.7)	1:3.26	Ethanol/ether 1:1	24.4	7.5	Water dispersible
14	HES 200-S5.4	200	SA (0.7)	1:3.26	Ethanol/ether 1:1	17.6	5.4	
15	HES 450-S4.6	450	SA (0.7)	1:3.26	Ethanol/ether 1:1	14.9	4.6	

^a Weight average molar masses are according to the manufacturer. Amount of HES in all reactions was 1.5 g. ^b FA= fatty acid, LA= lauric acid, PA= palmitic acid, SA= stearic acid. ^c molar ratio, AGU= anhydroglucose unit. ^d DC_{Fatty acid}= degree of conversion of the fatty acid. ^e MS_{Fatty acid}= molar substitution of the acyl chains. ^f Sample nomenclature: the numbers 70, 200, 450 refer to the M_w of HES as seen in the 2nd column. The letters L, P or S refer to the type of fatty acid used as seen in the 3rd column. The number after the letter refers to the molar substitution of the acyl chains as seen in the 7th column.

Although the method using the vinyl laurate/lyophilized salt is scientifically intriguing and is worth further investigations of the mechanism of the reaction, this was beyond the scope of the current thesis. Additionally, the method was time consuming, and was thus not pursued for the preparation of the HM-HES. For the rest of the thesis, only the samples prepared using the lauric acid/DCC method were used.

3.3.2 Raman spectroscopy

The esterification was further confirmed with Raman spectroscopy (Figure 3.3 and Figure 3.4). By comparing the spectra of the modified HES to that of lauric acid and native HES, one can notice the appearance of a shoulder (or a peak for higher $MS_{\text{fatty acid}}$) at 1440 cm^{-1} due to the CH_2 scissoring, and at 1300 cm^{-1} due to CH_2 twisting of the alkyl chains, as well as a clear shoulder close to 2852 cm^{-1} due to the symmetric CH_2 stretching of the alkyl chains.

Raman spectroscopy is not only a well known analytical tool for the identification of functional groups in organic compounds, but it can also deliver valuable information about the conformational state, for instance for the hydrocarbon chains [34]. To study this effect, the spectra of crystalline and molten lauric acid at $23\text{ }^\circ\text{C}$ and $55\text{ }^\circ\text{C}$, respectively were compared (N.B., the melting point of lauric acid is $45\text{ }^\circ\text{C}$ as confirmed by DSC measurements). The spectrum of lauric acid at $23\text{ }^\circ\text{C}$ shows the typical features of well ordered hydrocarbon chains [35, 36] (see Table 3.2 for peak assignment). Upon melting, a number of changes could be observed. Most importantly, the antisymmetric C-H stretching at 2880 cm^{-1} , which is very strong and sharp in the crystalline state, collapses into a broad peak upon melting, while the symmetric C-H stretching peak at 2845 cm^{-1} remains sharp and the peak position increases by 7 cm^{-1} . This latter shift of the symmetric C-H stretching versus temperature was found to be sigmoidal, and the midpoint coincides with the melting temperature (see Figure 3.5). Furthermore, the decrease in intensity of the C-C stretching peaks at 1063 and 1127 cm^{-1} , and the CH_3 rocking peak at 893 cm^{-1} as well as the disappearance of the splitting of the CH_2 scissoring band at $1400\text{-}1480\text{ cm}^{-1}$ all indicate a loss of order which means an increase of the gauche/trans ratio of the alkyl chains.

Table 3.2. Raman peaks and their assignment for conformationally sensitive bands in the spectrum of lauric acid at room temperature.

Peak position (cm ⁻¹)	Assignment
893	CH ₃ rocking
1063	C-C antisymmetric stretching for 3 or more trans-trans bonds in sequence
1127	C-C symmetric stretching for 3 or more trans-trans bonds in sequence
1297	CH ₂ twisting
1410	Bending of the CH ₂ group adjacent to COOH
1400-1480	CH ₂ scissoring
2845	CH ₂ symmetric stretching
2880	CH ₂ antisymmetric stretching for 3 or more trans-trans bonds in sequence

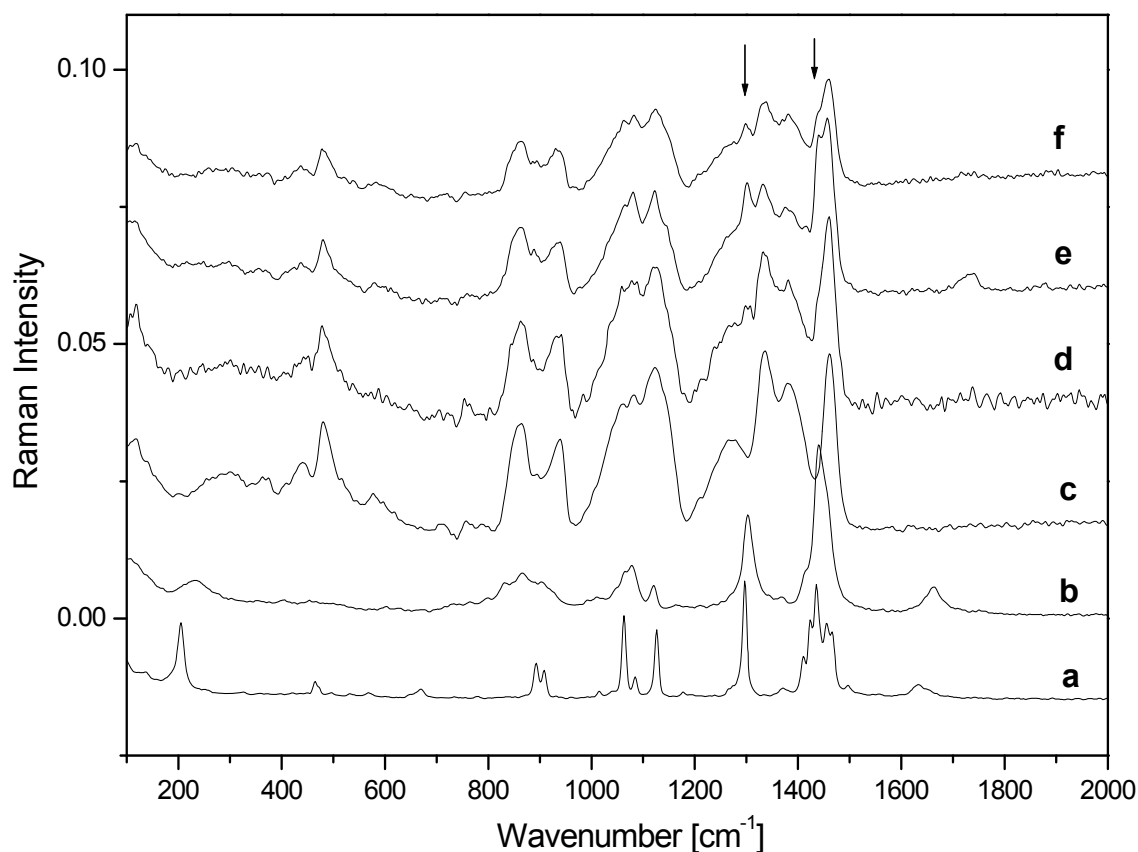


Figure 3.3. Raman spectra in the range from 100-2000 cm⁻¹ for a) lauric acid measured at 23°C, b) lauric acid at 55°C. c) HES 450 (unmodified), d) HES 450-L0.5, e) HES 450-L1, f) HES 450-P0.5. Polymer samples were measured at room temperature.

Figure 3.4. Raman spectra in the range from 2500-3400 cm^{-1} for a) lauric acid measured at 23°C, b) lauric acid at 55°C. c) HES 450, d) HES 450-L0.5, e) HES 450-L1, f) HES 450-P0.5. Polymer samples were measured at room temperature.

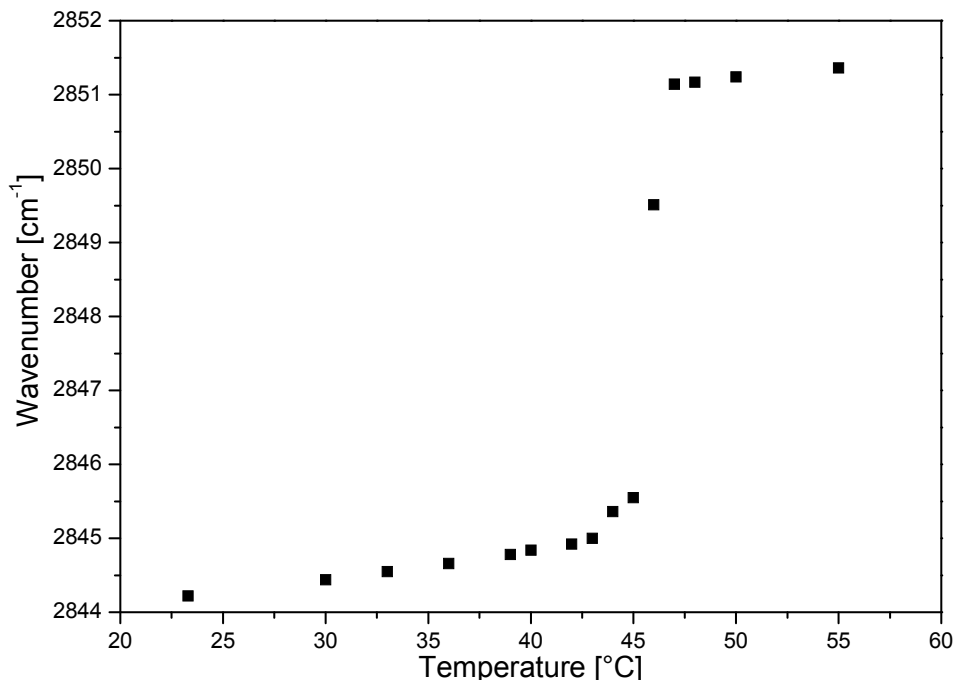
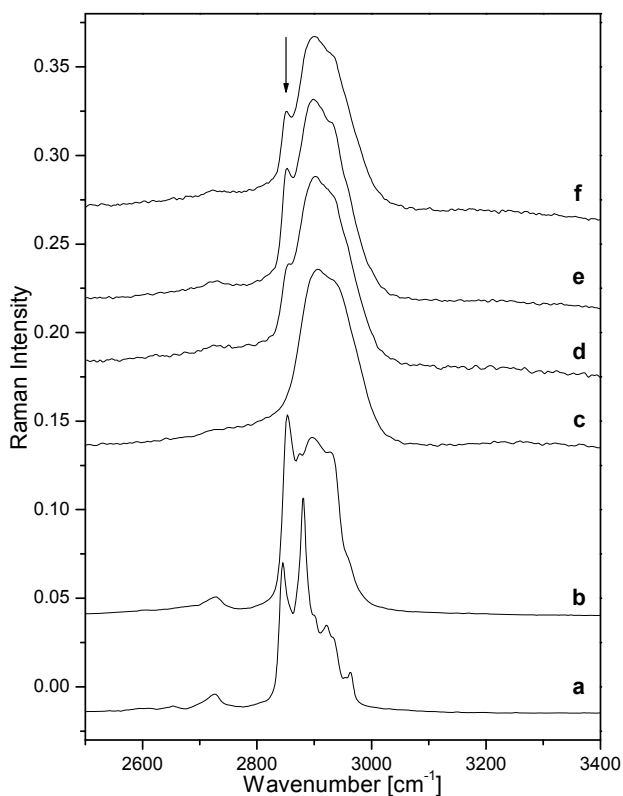
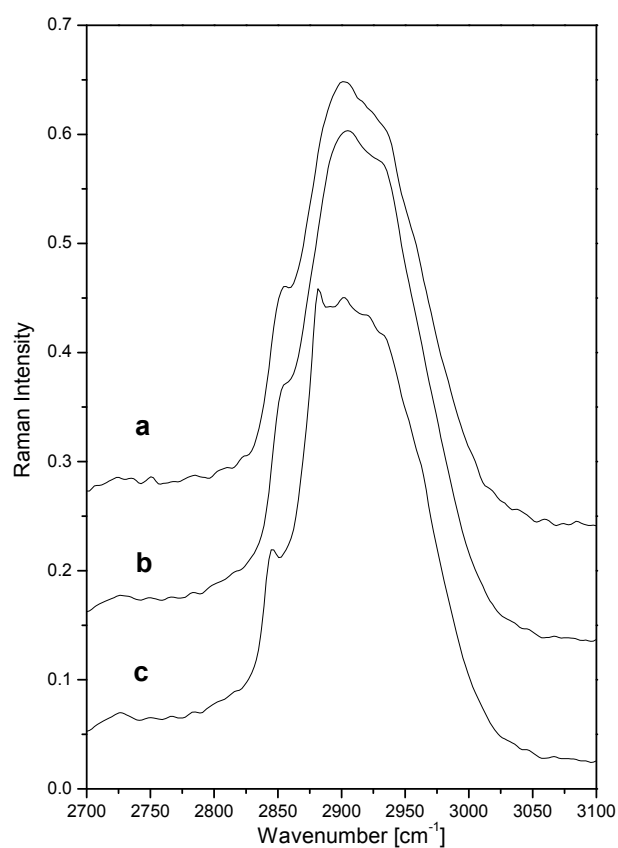


Figure 3.5. Raman shift of the symmetric CH_2 stretching band as a function of temperature.

To find out the conformational state of the lauryl residues attached to HES, a simulated spectrum was calculated by the addition of spectra of crystalline or molten pure lauric acid, respectively, to that of the unmodified HES 450 (90 % of the

spectrum was unmodified HES 450 and 10 % was pure lauric acid to simulate the $MS_{\text{fatty acid}}$ of HES 450-L0.5) and then compared to the experimental spectrum. Figure 3.5 shows the simulated and experimental spectra in the range of CH_2 stretching bands. Obviously, the experimental spectrum does not show the sharp peaks due to the symmetric and anti-symmetric stretching modes of the ordered chains, indicating that the acyl chains are indeed in a non-crystalline state. It is worth noting that similar results were found for all types of fatty acids studied and the different polymeric molar masses used.

Figure 3.6. Raman spectra of a) HES 450-L0.5, b) sum spectrum consisting of 90 % HES 450 and 10 % lauric acid at 55°C, c) sum spectrum consisting of 90 % HES 450 and 10 % lauric acid at 23°C.



3.3.3 Self-assembly of the water soluble HM-HES

3.3.3.1 Asymmetric flow field flow fractionation (AF4)

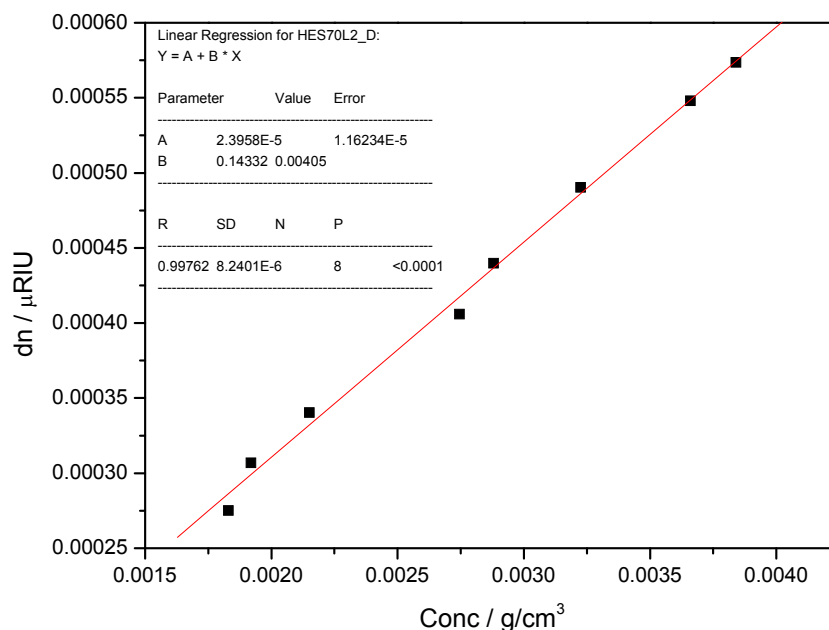


Figure 3.7. dn/dc for HES70-L2 is $0.143 \text{ cm}^3/\text{g}$.

AF4 coupled to MALS was used to study the water soluble HM-HES samples which have a low degree of modification, and compare them to the original HES (see section 2.3.1). The refractive index increment for the water soluble HES laurates was $0.143 \text{ cm}^3/\text{g}$ as seen in Figure 3.7. The elugrams for the unmodified original HES are shown in Figure 3.8, while those for HM-HES are in Figure 3.9, and a summary of the data evaluation is given in Table 3.3.

Upon esterification with lauric acid, the elugrams show considerable changes. The refractive index signals show either a second peak (as in the case of HES70-L2) or a significant broadening of the polymer peak and extension to longer elution times, as in HES200-L2, while HES450-L2 shows a small shift to higher elution times. The LS detector shows an increase in the elution times corresponding to those observed from the RI detector. The molar masses show a considerable increase over the original HES, as well as an increase over the expected/calculated M_w based on ^1H NMR results (see Table 3.3). Moreover, the polydispersity also increases, particularly for HS70-L2 and HES200-L2. The increase in molar mass above the theoretical value based on NMR measurements is probably because the amphiphilic polymers aggregated to form micelles. However, it was not possible to completely separate the

micelles from the soluble molecules due to the high polydispersity of the original HES.

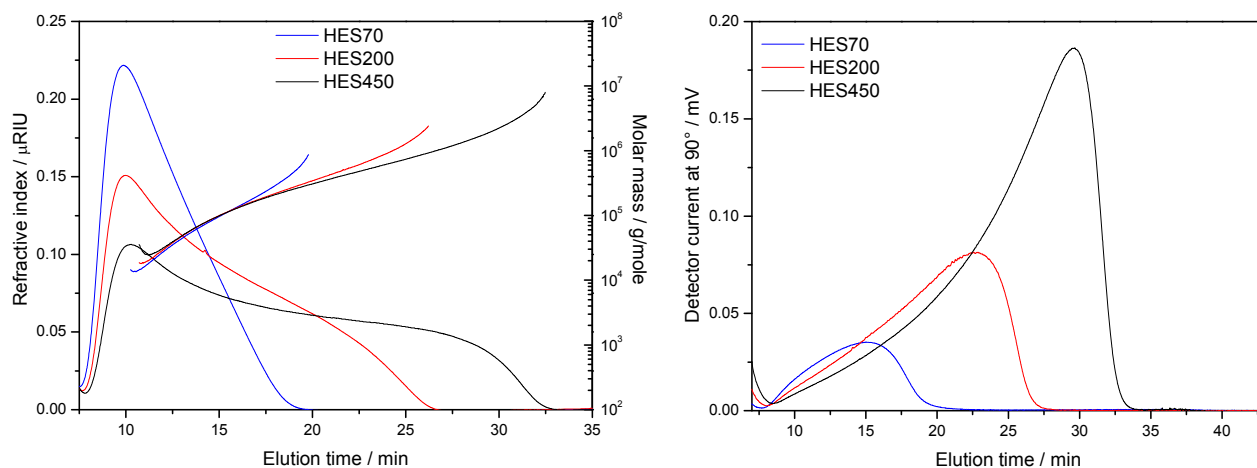


Figure 3.8. Elugrams for the original HES samples showing the refractive index and molar mass (left) as well as the light scattering signal (right) as determined by AF4 coupled to MALS.

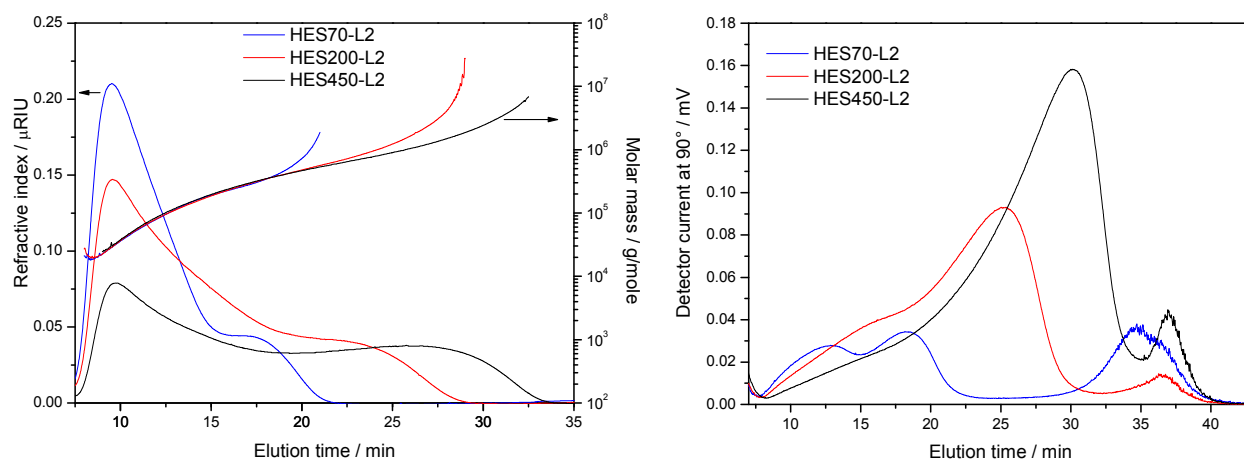


Figure 3.9. Elugrams for the soluble HM-HES samples showing the refractive index and molar mass (left) as well as the light scattering signal (right) as determined by AF4 coupled to MALS.

Table 3.3. Weight average and number average molar masses as well as the polydispersity, recovery and RMS radius of the original and modified HES samples as measured by AF4 coupled to MALS.

	M_n ($\times 10^3$ g/mole)	M_w ($\times 10^3$ g/mole)	Calc. M_w ($\times 10^3$ g/mole)	PDI	Recovery (% w/w)	RMS radius (nm)
HES70	35.8 ± 0.8	69.7 ± 2.2	-	1.95	86 ± 1	5.5 ± 0.5
HES200	59.5 ± 1.0	190.3 ± 6.1	-	3.20	96 ± 1	11.1 ± 1.0
HES450	102.6 ± 5.9	466.9 ± 7.7	-	4.56	93 ± 2	19.0 ± 0.2
HES70-L2	46.1 ± 0.3	105.9 ± 1.7	72	2.30	72 ± 7	6.8 ± 0.7
HES200-L2	70.3 ± 1.9	292.8 ± 11.8	204	4.17	84 ± 5	14.8 ± 0.3
HES450-L2	137.4 ± 1.6	650.0 ± 2.9	470	4.73	63 ± 2	19.8 ± 0.3

An additional peak is observed between 30-40 min for all three samples in the LS elugram. The fact that there is no RI signal in this region of the elugram indicates that the concentration of these large particles is rather small. The peaks appearing between 30-40 min were analysed for their particle size using the “particle mode” option available in the software. This option uses the fact that it is possible to calculate particle size from light scattering measurements without the knowledge of concentration, dn/dc or the molar mass [37]. Results show that those aggregates lie between 120-150 nm in diameter. To elucidate the nature of these larger aggregates, cryoelectron microscopy was carried out (see the next section)

3.3.3.2 TEM

The results of the CryoTEM of the water soluble HESlaurates are shown in Figure 3.10. Vesicular structures were observed, having a membrane thickness of 7 nm. This indicates that the HM-HES could self-assemble into polymeric vesicles, also known as polymersomes.

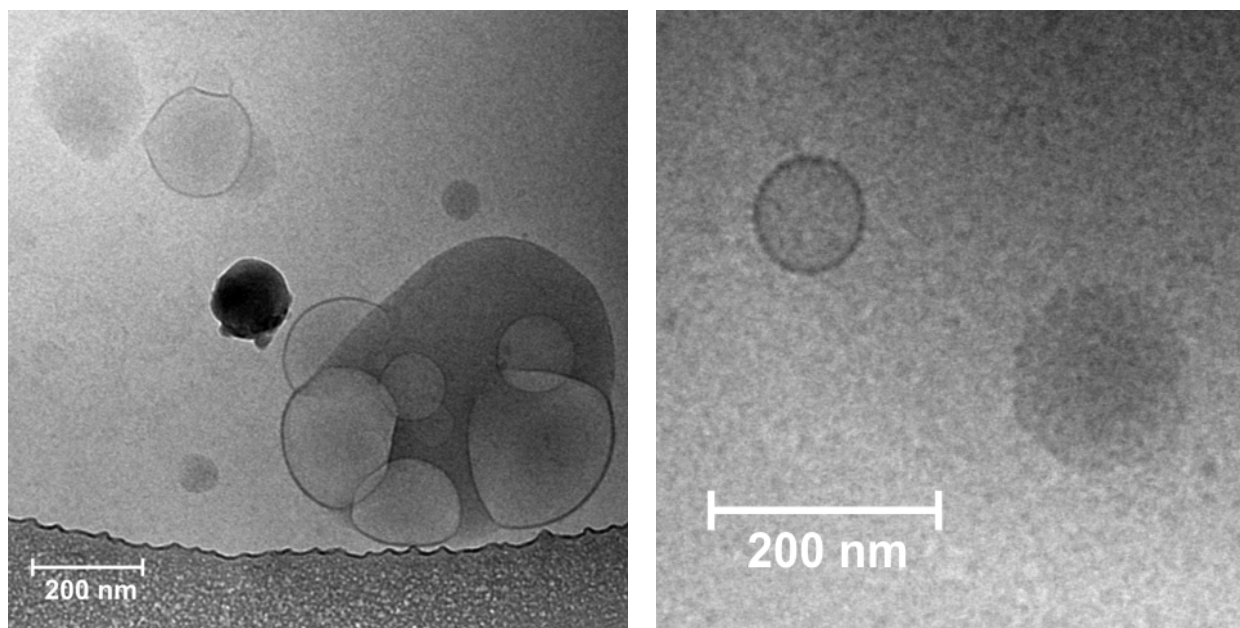


Figure 3.10. CryoTEM micrographs for HES70-L2 samples, concentration 5 mg/ml.

Similarly, HES modified with lauric acid and with medium $MS_{\text{fatty acid}}$ (samples 4-6 in Table 3.1) formed polymersomes as shown in the TEM micrographs of negatively stained samples (Figure 3.11a). This observation was supported with freeze fracture EM (Figure 3.11b). In the latter, the vesicles were not intact after fracture, but the fracture plane passed through the vesicles, forming a cross section in the vesicle that was clear after etching and shadowing (see Figure 3.11c). The size of the vesicular structure from freeze-fracture TEM is in the range of 100-500 nm, and the electron micrographs show a broad size distribution.

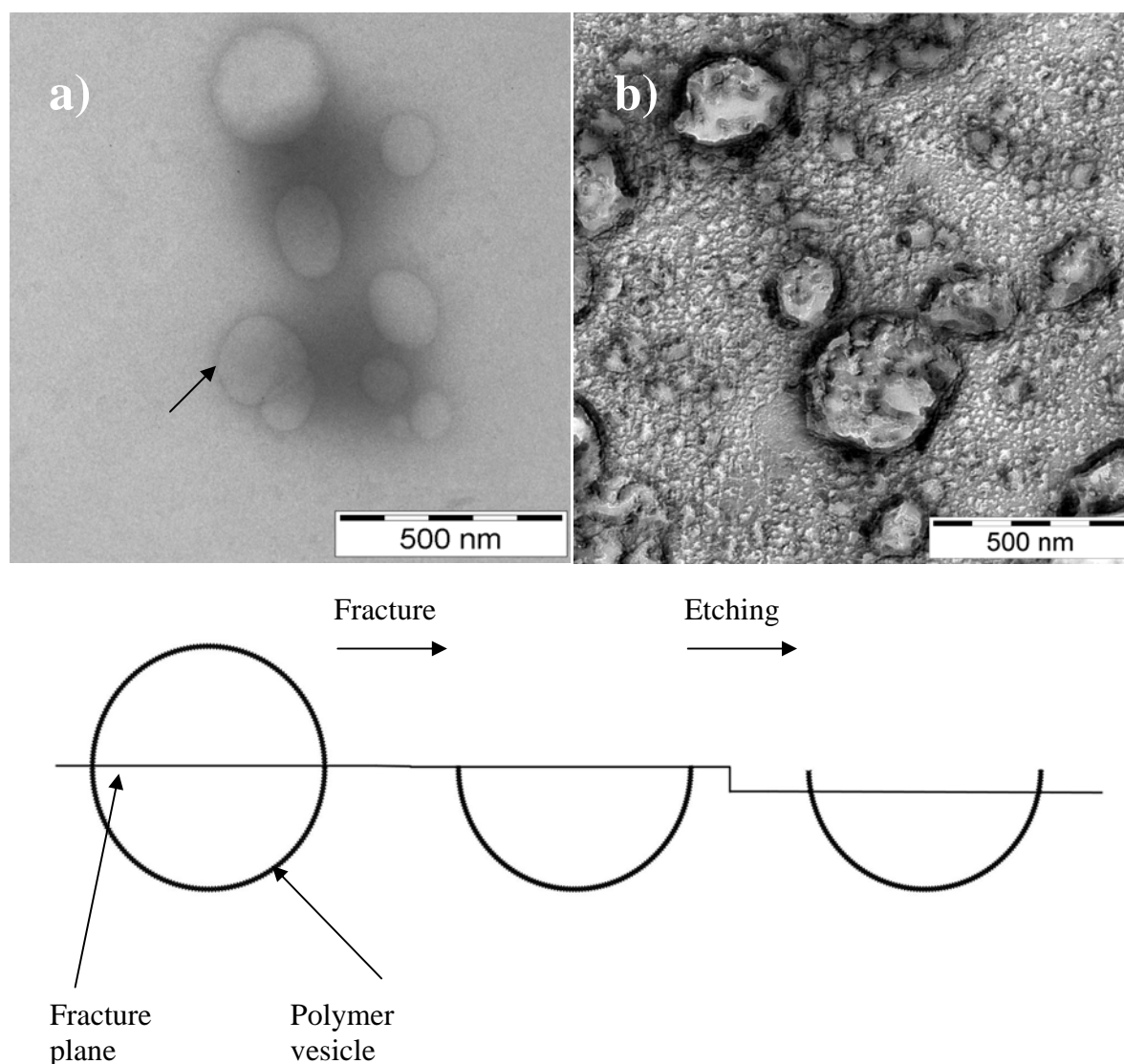


Figure 3.11. a) Negative stain TEM micrograph of HES 200-L0.5 nanodispersion (0.5 % w/v) showing polymeric vesicles. Arrow points to overlapping vesicles. b) Freeze fracture micrograph of the same sample c) schematic for the freeze fracture of the polymer vesicle and the etching.

In general, the interest in polymersomes has increased a lot in the last decade from an academic and practical point of view [38, 39]. This is because they have an aqueous core which can entrap proteins, polypeptides or nucleotides [40, 41], and compared to liposomes, they have higher stability, lower membrane fluidity, lower transmembrane permeability and larger membrane thickness [42]. An examination of the literature reveals that the majority of publications dealing with polymeric vesicles are reports for the self-assembly of di-, tri- or multi-block copolymers [38, 42-45]. In this case, it is easy to extend the physicochemical formalisms developed for the small surfactant molecules that form vesicles, such as phospholipids or nonionic

emulsifiers. This includes the packing factor and interfacial curvature [39]. Only very few papers describe the formation of polymersomes from non-block copolymers. For instance, the hyperbranched polymer (poly(3-ethyl-3-oxetanemethanol)–star PEO) self assembled into giant polymersomes, 100 μm in diameter [46]. Uchegbu *et al.* reported the formation of vesicles from palmitate-modified glycol chitosan [13, 47], where it self-assembled into vesicular structures in the presence of cholesterol as stabilizer. Recently, Dan *et al.* reported the spontaneous formation of polymeric vesicles from alternating copolymer of hydrophobic alkyl maleates and hydrophilic polyhydroxy vinyl ethers [48]. These vesicles were found to have a very thin membrane (1.5 ± 0.3 nm), and showed relatively rapid release characteristics similar to liposomes. (N.B. Release experiments were carried out using a dialysis membrane. In this case, the diffusion through the dialysis membrane is usually the rate limiting step and may interfere with the actual release kinetics. [49, 50])

Little is known about how graft copolymers can form polymeric vesicles. Ringsdorf *et al.* [51] have mentioned that hydrophobized polymers cannot self-assemble into vesicles unless there is a hydrophilic spacer molecule between the lipid and the polymer backbone. This is necessary to decouple the movement of the grafted lipid and the stiff backbone, otherwise, a high degree of polymeric cooperativity is needed which makes vesicle-formation very difficult to achieve. The presence of hydroxyethyl units and oligo(ethylene glycol) chains in HES satisfy this necessary prerequisite for such assembly. A detailed study of the mechanism of formation of the vesicles needs a more defined molecular architecture. This could be achieved by using the fatty acid esters of unbranched polysaccharide, such as dextrin, as well as coupling poly(ethylene oxide) alkyl chains to the same molecule to see the effect of the spacer molecule.

3.4 Conclusions and outlook

HES was hydrophobically modified with lauric, palmitic and stearic acids by mild esterification using DCC and DMAP. The molar substitution of the acyl chains ($MS_{\text{fatty acid}}$) was determined using ^1H NMR. Three groups of HES laurates were produced having had an average $MS_{\text{fatty acid}}$ of 2, 9.5 and 19-27 mol%. These were water

soluble, water dispersible and water insoluble, respectively. Using the same FA:AGU molar ratio, an average $MS_{\text{fatty acid}}$ of 9.5 and 14.7 mol% were obtained for lauric and palmitic acid respectively, while stearic acid showed a lower $MS_{\text{fatty acid}}$ (5.8 mol%) due to the higher temperature necessary to dissolve it in DMSO. Raman spectroscopy confirmed the esterification and showed that the hydrocarbon chains lost their crystalline form after esterification. The water-soluble HES laurates were studied using AF4, and were found to have a larger size and molar mass compared to the unmodified HES. The 100-150 nm aggregates detected in the AF4 measurements were found to be polymeric vesicles (polymersomes) as visualized using TEM. This is one of the few reports describing the formation of polymersomes from non-block copolymers. The architecture of the macromolecule needs to be optimized in order to increase the amount of produced polymersomes. The ability of these polymersomes to encapsulate hydrophilic and/or hydrophobic molecules needs to be estimated as well as the release characteristics.

Chapter 4

Application of HM-HES for the surface modification of PLGA nanospheres

4.1 Introduction

Polymeric nanoparticulate systems are promising drug delivery vehicles that can control the pharmacokinetics and biological fate of encapsulated drugs [52]. In this regard, surface properties proved to be crucial for the behaviour of these nanoparticles, where untreated particles are rapidly removed from the circulation by the mononuclear phagocytic system (MPS) [53]. This takes place because these particles can easily adsorb opsonins from the blood plasma, thus facilitating their identification and elimination from the circulation [54]. To prevent this rapid uptake, engineering the surface properties of nanoparticles is essential [55]. This can produce long-circulating or “stealth” particles and allow both passive and/or active targeting. The general conditions for the stealthiness of colloidal drug carriers were reviewed by Vonarbourg *et al.* [56]. These include having a small size, with a neutral and hydrophilic surface, as well as a thick, well-anchored and flexible coating.

Accordingly, the use of hydrophilic polymer-coatings to nanoparticulates is now a common practice to achieve a long circulation time. The most commonly used polymer for this purpose is poly(ethylene glycol) (PEG) [57] due to its high hydrophilicity and extreme flexibility. It is generally accepted that these PEG coats prevent opsonization by imparting an entropically-driven steric hindrance for protein adsorption, which mainly depends on the degree of surface coverage and their molar

mass [58]. However, this may not be the only mechanism. Another possible explanation is that the PEG coats allow the selective adsorption of some serum proteins that are sometimes known as dysopsonins, i.e. plasma components which are believed to prevent opsonization [59, 60]. This is supported by the observation that liposomes carrying gangliosides (a group of naturally occurring glycolipids) on their surface show an extended circulation time, despite the fact that their very thin hydrophilic coats cannot impart the necessary steric hindrance. This is explained by their ability to adsorb selectively some dysopsonins [61]. Additionally, the group of R. H. Müller has provided evidence that the selective adsorption of blood proteins can alter the fate of nanoparticles, by, for example, allowing their targeting to the brain, in what they called “differential protein adsorption” [62]. To summarize, it may be the selective adsorption, and not the prevention of adsorption, that alters the pharmacokinetics and fate of nanoparticles.

In this study, Pluronics are used to modify the surface of poly(lactic-co-glycolic acid) PLGA nanospheres. Pluronics (also known as poloxamers) are a group of ABA triblock copolymers with hydrophilic PEG outer blocks and a hydrophobic poly(propylene oxide) (PPO) as a middle block. They have been extensively studied as surface coatings that can modify the pharmacokinetics and fate of nanoparticles [63-67]. For example, Pluronic F127 (poloxamer 407) was found to prolong the circulation of PLGA nanospheres, where 44 % and 5.9 % of the nanospheres were found in the blood after 3 and 24 h respectively, compared to 6.4 and 1.6 % for the bare nanospheres [65]. However, Pluronics are not biodegradable, and despite the long history, no commercial product using F127 was approved for parenteral administration until now.

Polysaccharides have also been suggested as biomimetic polymer coatings for nanoparticles [19]. For example, a heparin coating on poly(methyl methacrylate) nanoparticles increased their half-life from a few minutes up to 5 h [68]. Similarly, coating superparamagnetic iron oxide nanoparticles (SPIONs) with dextran increased their half-life up to 4.5 h [69]. However, caution should be exercised upon clinical administration to avoid hypersensitivity reactions due to dextran [19]. Meanwhile, hydroxyethyl starch (HES) is a semisynthetic polysaccharide that is used as a plasma volume expander. HES is currently investigated at the industrial level as a biodegradable substitute for PEG, so that HESylation of proteins would substitute

PEGylation [70], however the ability of HES to stabilize nanoparticulate systems was not studied before. We have reported earlier the synthesis, characterization and self-assembly of hydrophobically modified hydroxyethyl starch (HM-HES) [71]. In this manuscript, the ability of HES laurate to stabilize PLGA nanospheres and the interaction of these stabilized nanospheres with phagocytic cells *in vitro* are reported, in comparison to Pluronics.

4.2 Experimental

4.2.1 Materials

Resomer RG 502 (PLGA, molar mass 12-13 kDa) was purchased from Boehringer Ingelheim, Germany, Lutrol F68 (Pluronic F68, PEO₇₉-PPO₂₈-PEO₇₉^{*}, molar mass 8.594 kDa [72]) and Lutrol F127 (Pluronic F127, PEO₁₀₁-PPO₅₆-PEO₁₀₁^{*}, molar mass 12.154 kDa [73]) were purchased from BASF, Germany. Different HES laurate polymers were synthesized as in section 3.2.2. Only the water soluble and water dispersable esters were used in this study (samples 1-6 in Table 3.1). Triton-X 100, fibrinogen (from bovine plasma) and the fluorescent probes 1,1'-dioctadecyl-3,3',3',3'-tetramethylindocarbocyanine perchlorate (Dil) and 3,3'-dioctadecyloxacarbocyanine perchlorate (DiO) were from Sigma-Aldrich, Germany. Human serum albumin (HSA) was from Pharma Dessau GmbH, Germany. All other chemicals and solvents were reagent grade and were used as received.

4.2.2 Nanosphere preparation

A stock dispersion of the nanospheres was prepared by adding 3.5 ml of distilled acetone containing 25 mg PLGA to 10 ml bidistilled water with stirring at 1000 rpm. Acetone was removed by evaporation in a rotary evaporator, and the sample weight was adjusted to 10 g using bidistilled water. The polymer-stabilized nanospheres were prepared by dissolving the amphiphilic polymer in the nanospheres dispersion to a final concentration of 7.5 mg/ml.

For the cell uptake experiments (see below), a very hydrophobic fluorescent dye was entrapped in the nanospheres during preparation. 1 mg of a fluorescent probe, Dil, was dissolved in 10 ml acetone stock solution and used during the nanospheres preparation. Its final concentration in the nanospheres dispersion was 50 µg/ml. For

* The degree of polymerization is an average number

these experiments, it was not possible to prepare a stock solution of PLGA nanospheres without using a stabilizer, since the nanospheres encapsulating the fluorescent probe precipitated during the evaporation of acetone. Therefore, the stabilizing polymers were dissolved in water before the addition of the organic PLGA solution. This led to the formation of stable nanospheres.

4.2.3 Physicochemical characterization

Particle size was determined using dynamic light scattering (DLS). Samples were diluted 1:20 in bidistilled water, and the hydrodynamic diameter of the nanospheres was determined at 25 °C using the back scattering mode (HPPS, Malvern Instruments, UK).

The thickness of the adsorbed polymer layer (also known as fixed aqueous layer thickness, FALT [74]) was determined using DLS, as well as zeta potential (ζ) measurements as a function of electrolyte concentration [75]. In the case of DLS, the thickness of the adsorbed polymer layer (δ) was determined according to the following equation (1) [66]:

$$\delta = \frac{d_a - d_o}{2} \quad 4.1$$

where d_a is the hydrodynamic size after polymer adsorption and d_o is the hydrodynamic size of the bare nanospheres.

The zeta potential-based measurements of the adsorbed polymer layer are derived from the approximation of the Guy-Chapmann theory, which expresses the decrease of the electrostatic potential as a function of the distance from the surface as follows [76].

$$\psi_x = \psi_o e^{-\kappa x} \quad 4.2$$

where ψ_x is the potential at a distance x from the surface, ψ_o is the surface potential, and κ^{-1} is the Debye length, which is the length characterizing the decrease with distance of the potential in the double layer. The Debye length decreases as the concentration of electrolytes increases. This approximation applies only in case of using neutral polymers, and using monovalent electrolytes [77]. Since ζ is the potential measured at the slip plane (also called plane of shear), then a plot of $\ln \zeta$ vs.

κ will give the thickness of the adsorbed polymer layer, where κ is equal to $3.33\sqrt{c}$ (c is the molality of electrolytes) [78].

For zeta potential measurements, samples were diluted 1:10 with a NaCl solution (in bidistilled water) so that the final electrolyte concentration is 0, 1, 2, 4, 6, 8 and 10 mM. Samples were measured using a Zetamaster (Malvern Instruments, UK).

4.2.4 Protein adsorption

In order to test protein adsorption, the nanospheres were prepared in bidistilled water or in a phosphate buffered saline (PBS) pH 7.4 (according to the EP). However in the latter case, bare nanospheres were not stable, probably because PBS reduces the zeta-potential necessary for their stabilization. Therefore, the amphiphilic polymers were dissolved in PBS during nanospheres preparation to stabilize them. Please note that the HES laurates with high molar substitution were not soluble in PBS, and thus not used for this experiment.

Nanospheres stabilized with the different amphiphilic polymers were incubated with different concentrations of HSA (0, 10, 15 and 20 mg/ml dissolved in bidistilled water or in PBS pH 7.4) or FBG (0, 1, 2 and 3 mg/ml in PBS pH 7.4) for 3 h at room temperature, after which samples were diluted 1:20 and the hydrodynamic radius was measured using DLS (HPPS, Malvern Instruments, UK).

4.2.5 Phagocytosis of the nanospheres

The murine monocyte-macrophage cell line J774.2 was used to study the phagocytic uptake of the different PLGA nanospheres [79, 80]. Cells were maintained in Dulbecco's Modified Eagle Medium (DMEM, Biochrom GmbH, Berlin Germany) supplemented with 10 % v/v fetal bovine serum (FBS, Biochrom) and 1 % w/v antibiotic/antimycotic solution (Sigma, Deisenhofen, Germany) at 37 °C and 5 % v/v CO₂. For phagocytosis experiments, the cells were scraped mechanically at 70 – 90 % confluence from the bottom of tissue culture flask, and counted using a hemacytometer. The cells were suspended in DMEM with 10 % v/v FBS at a concentration of 5×10^5 cells/ml.

100 μ l of the cell suspension were added per well in a 96-well plate (Cellstar, Greiner bio-one GmbH, Germany), and incubated for 2 h. To each well, 100 μ l test suspension were added, consisting of 9 parts DMEM supplemented with FBS and 1

part nanospheres dispersion, and then incubated at 37 °C for 6 h. Thereafter, the wells were washed twice with DMEM and incubated for 1 h with 100 µl of 1 % v/v Triton X-100 as a cell lyses solution. The resulting cell lysate was transferred to a black poly(propylene) 96-well plate to measure the fluorescence intensity using a fluorescent plate reader (Lumistar Optima, BMG, Jena, Germany) with excitation filter of 544 nm, and emission filter of 590 nm. The fraction of nanospheres phagocytosed was determined by dividing the measured fluorescence intensity to that of the original nanospheres preparation diluted 1:10 in 1 % v/v Triton X-100 solution. Since phagocytosis does not take place at 4 °C [81], the same experiment was carried out simultaneously at 4 °C to determine the extent of surface adsorption of the nanospheres to the cells.

4.2.6 Confocal laser scanning microscopy (CLSM)

Preparation of the DiO solution [82]: 3 mg DiO were dissolved in 0.9 ml ethanol plus 0.1 ml DMSO. The solution was filtered through a 0.45 µm nylon filter. 0.7 ml dye solution was diluted to 10 ml with DMEM to a final concentration of ca. 0.2 mg/ml.

Cell staining, fixation and mounting: Glass cover slides 15 x 15 mm were placed into a 12 well plate (Cellstar, Greiner bio-one GmbH, Germany). To each well, 0.5 ml of the diluted DiO solution in the culture medium was added. 0.5 ml of the cell suspension in DMEM with 10 % v/v FBS at a concentration of 5×10^5 cells/ml were added to each well. Cells were incubated in a CO₂-incubator at 37 °C for 2 h to allow cell adhesion and staining. Then, the medium was aspirated, and adherent cells were washed once with DMEM. 1 ml of Dil-encapsulating nanospheres, diluted 1:10 in DMEM medium with FBS, was added per well and incubated at 37 °C. After 6 h, the medium was aspirated, and the cells washed with PBS. RotiHistofix was used for cell fixation, followed by washing with PBS. The cover slides were mounted on objective glass slides using Mowiol 4-88 solution, then left to dry at 4 °C for at least 2 days before CLSM.

Images of cells and nanoparticles were obtained using a Leica DM-IRE2 confocal microscope (Leica Microsystems Heidelberg GmbH, Mannheim, Germany) equipped with a computer-controlled, motorized scan stage. An argon laser for DiO excitation at 488 nm was used, while a 543 nm He-Ne laser was used for the excitation of Dil. 2

band-pass filters were used between 493-538 nm and 548-630 nm, for the DiO and the Dil emission signals, respectively. For each cell, 20 optical planes were scanned, each having a thickness of 0.3 μm .

4.3 Results and discussion

4.3.1 Physicochemical characterization

The process of nanoprecipitation can produce nanoparticles with a size range of 100 – 300 nm and with a narrow unimodal distribution [83]. Results in Table 4. 4.1 show that the produced nanospheres follow the same pattern, with an average size of 110 nm for the bare nanospheres, and a considerable low PDI (< 0.1 , c.f. emulsions with PDI > 0.2) . The thickness of the adsorbed polymer layer obtained from DLS measurements are close to those mentioned in the literature for Pluronic F68 (3-6 nm depending on particle size [84]) and F127 (7 nm [65]). In the case of HES laurate, it is possible to notice that the thickness increases with the increase of the average molar mass from 70 to 450 kDa, particularly in the group with low degree of substitution. It is also worth mentioning that the adsorbed layer is thinner in the case of high fatty acid substitution. This is probably because the macromolecule bends to form loops and trains that are anchored to the surface with the hydrophobic fatty acid. Due to the higher fatty acid content, the number of loops is higher and the thickness is thus lower (Figure 3.12).

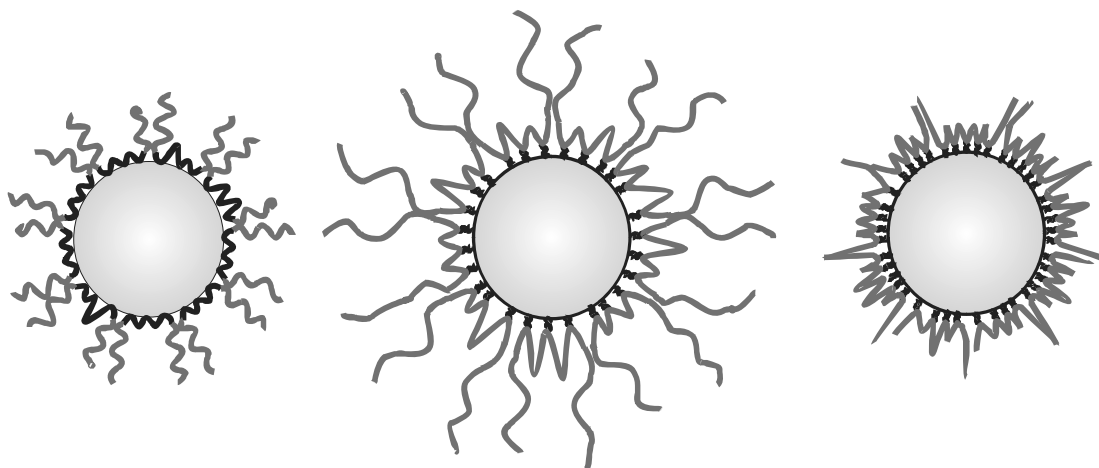


Figure 3.12. A simplified schematic representation showing the adsorption of Pluronics on the surface of PLGA nanospheres (left), where the PPO blocks (black) adsorb to the surface, while the PEG chains (grey) extend to the surrounding aqueous phase. In the middle, the HM-HES with low substitution is anchored to the surface through the alkyl chains (black) and the HES backbone (grey) forms loops and tails. To the right, the HM-HES with high substitution shows a more tight anchorage due to the higher number of fatty acid chains and the thickness of the adsorbed layer is smaller.

As seen in Table 4.1, the increase of the molar mass (and thus the adsorbed layer thickness) is accompanied with a decrease in the zeta potential. This is due to the outward shift of the slip plane due to the increase in the thickness of the adsorbed polymer layer. The adsorbed layer thickness determined from zeta potential measurements is slightly higher for the Pluronics than that determined by DLS, but is nearly identical in the case of HES laurates. It is worth mentioning that the thickness of the adsorbed polymer layer is method-dependent. For example, Stolnik *et. al* [66] found a difference in the results of the thickness of the polymer layer when determined by field flow fractionation (FFF) and DLS. Similarly, Rube *et al.* [85] found the thickness of Pluronic F68 adsorbed on PLA nanocapsules to be 17 nm using small angle neutron scattering. In this regard, the differences between the 2 methods used in this study can be regarded as minor.

Table 4.1. Z-Average diameter, polydispersity index (PDI), zeta potential and the thickness of the adsorbed polymer layer determined using DLS and zeta potential measurements for PLGA nanospheres (NS) stabilized with different amphiphilic polymers.

	Z-Av ± S.D.	PDI	Thickness of the adsorbed polymer layer from DLS (nm)	Zeta Potential (mV)	Thickness of the adsorbed polymer layer from zeta potential (nm)
Bare NS	110.5 ± 1.1	0.06	0	- 34.5	0
F68	116.9 ± 0.8	0.07	3.17	- 23.1	5.4 +/- 0.16
F127	122.8 ± 0.8	0.06	6.12	- 23.5	8.9 +/- 1.10
HES 70-L2	126.3 ± 0.9	0.07	7.87	-19.2	7.4 +/- 1.40
HES 200-L2	132.9 ± 0.5	0.10	11.20	- 16.4	11.9 +/- 1.00
HES 450-L2	140.7 ± 1.2	0.07	15.07	-15.6	14.2 +/- 2.40
HES 70-L10.3	116 ± 0.4	0.12	2.75	n.d.	n.d.
HES 200-L8.4	118.8 ± 0.4	0.11	4.15	n.d.	n.d.
HES 450-L9.4	119 ± 0.9	0.12	4.25	n.d.	n.d.

(n.d. = not determined)

Both Pluronic F68 and F127 have 2 PEG chains, each having an average[†] of 76 and 100 monomeric units, respectively. Note that the radius of gyration of a polymer in a theta solvent is equal to:

$$R_g = aN^{1/2} \quad 4.3$$

And in a good solvent

$$R_g = aN^{3/5} \quad 4.4$$

where a is the segment length (which is 0.36 nm in case of PEG [76], and 0.515 nm in case of the anhydroglucose unit (AGU) [87]), and N is the degree of polymerization. A comparison between the expected diameters from Table 4.2 and the thickness of the adsorbed polymer layers shows that the values for Pluronic are close to the theoretical values for a random coil, while they are much lower than

[†] The average molar mass copolymer distribution which conforms to the USP requirement for Pluronic F68 is 7680-9510 Da, and for Pluronic F127 is 9840-14600 Da. Batch-to batch variations and differences between different producers were observed by different researchers [86]

theoretical for the HES-Laurates. This discrepancy could be for a number of reasons, including the fact that HES is a branched polymer with a rather large polydispersity, and more importantly, that HM-HES is expected to bend on the surface forming loops and trains in order to accommodate the hydrophobic fatty acid groups on the surface of the nanospheres.

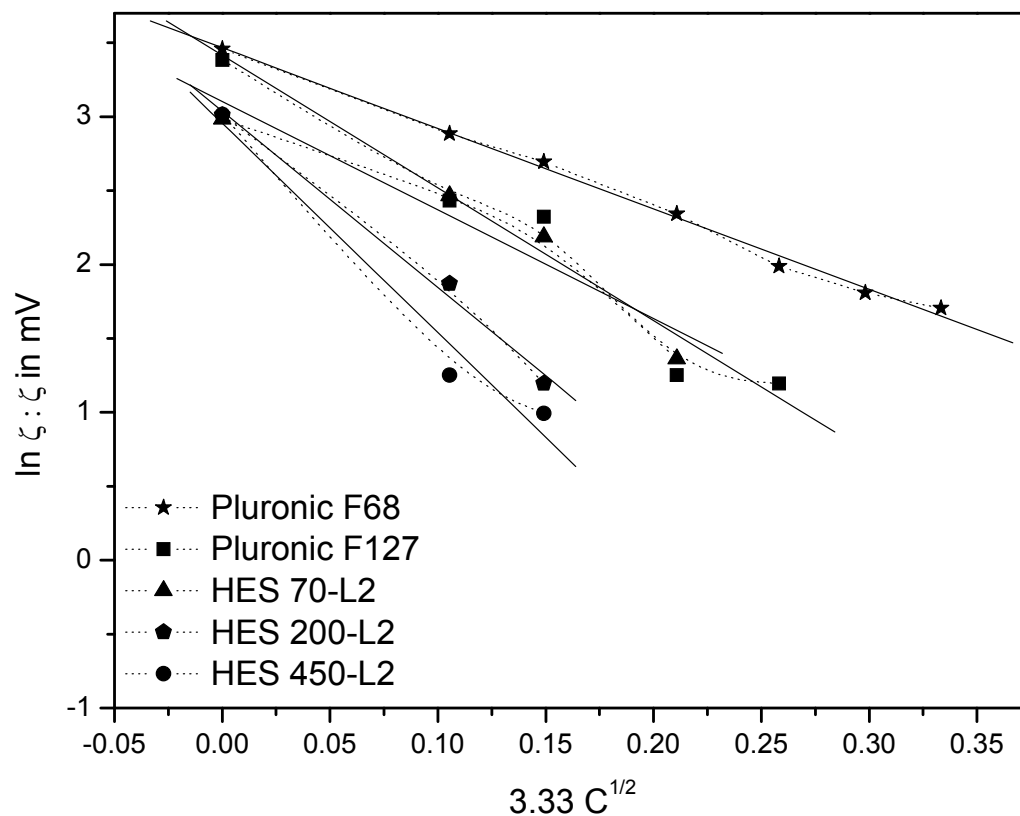


Figure 3.13. Plot of $\ln \zeta$ vs. $3.33 \sqrt{c}$ ($= \kappa$). The slope gives the thickness of the adsorbed polymer layer.

Table 4.2. Number of monomeric units for the different amphiphilic polymers, together with the radius of gyration in theta- and good solvents.

	Number of monomers	R _g in theta solvent (nm)	Diameter in theta solvent (nm)	R _g in good solvent (nm)	Diameter in good solvent (nm)
One PEG chain of Pluronic F68	76	3.14	6.28	4.84	9.68
One PEG chain of Pluronic F127	100	3.6	7.2	5.7	11.4
HES 70-L2	379	10	20	18.15	
HES 200-L2	1084	16.96	33.92	34.1	68.2
HES 450-L2	2439	24.69	49.38	55.48	110.96

4.3.2 Protein adsorption

Figure 3.14 shows the results of incubation of the bare and the polymer-stabilized PLGA nanospheres with different concentrations of HSA in bidistilled water. The bare PLGA nanospheres show an increase in the hydrodynamic radius of 33 nm with the 10 mg/ml HSA concentration, which then decreases to approximately 10 nm for the higher concentrations. Lee *et al.* [88] have reported similar results for HSA adsorption on polystyrene nanospheres. They attributed the initial high apparent increase in the hydrodynamic radius at a protein/polymer ratio ≤ 5 due to bridging of nanospheres with the albumin molecules. Higher concentrations give a constant increase in thickness of approximately 8 nm due to a monolayer of adsorbed albumin [88].

Tan *et al.* [64] reported that Pluronic F68 and F108 (the latter having 2 PEG chains each with approximately 129 monomeric units) were effective in preventing the adsorption of HSA on polystyrene nanospheres. Similarly, our results show that Pluronics prevent the adsorption of HSA on PLGA nanospheres as indicated by the constant hydrodynamic radius of the nanospheres. On the other hand, not all the HES laurates behaved in the same manner. Those having a low degree of

substitution were effective in preventing the protein adsorption, while the ones with a higher degree of substitution showed a slight increase in size with 15 mg/ml HSA probably due to protein adsorption, and a large increase in size with eventual precipitation with higher protein concentration due to bridging and destabilization of the nanospheres. Albumin is known to have 4 binding sites for fatty acids [89]. It is possible that some alkyl chains are extending to the aqueous environment in the case of the high degree of substitution, and thus act as adsorption sites and bridging points for HSA. Upon using PBS pH 7.4 instead of bidistilled water, no adsorption was observed in the case of Pluronics or low substitution HES laurates (Figure 3.15). It is worth mentioning that the increase in ionic strength due to using PBS reduces the effect of electrostatic repulsion. This indicates that indeed the prevention of adsorption was due to steric hindrance from the polymer coat. HES laurates with high degree of substitution were not used in this experiment because they were not soluble in PBS.

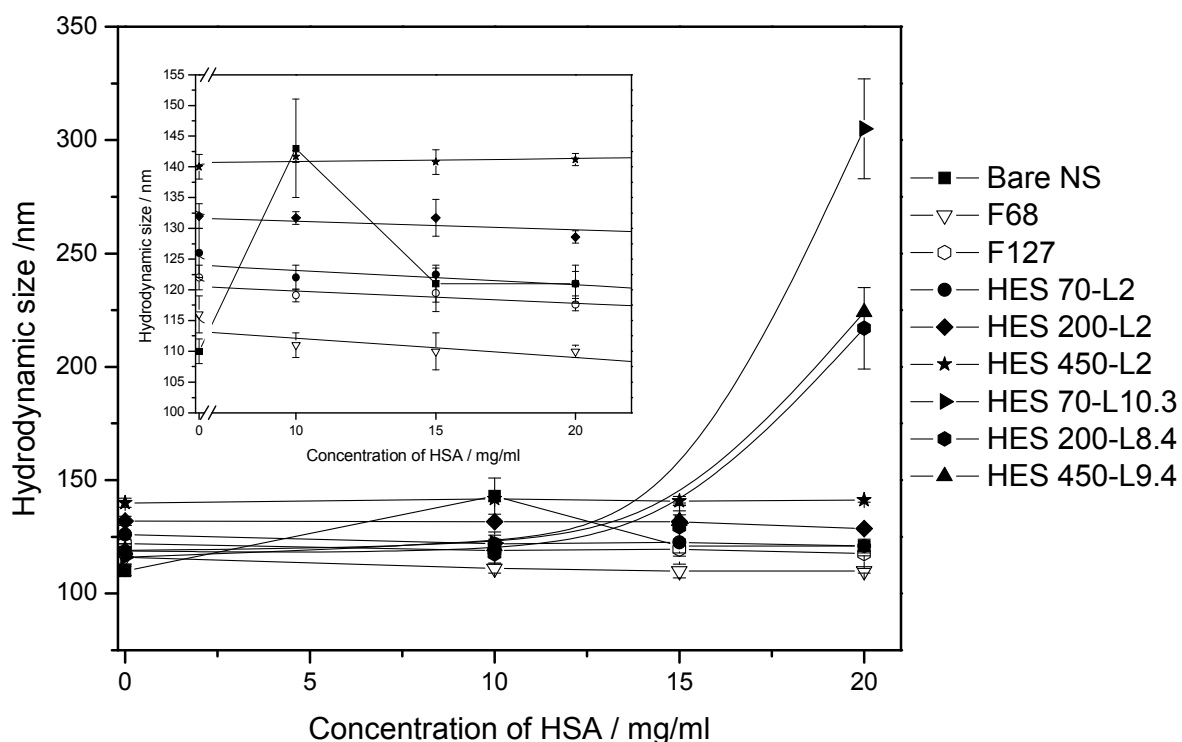


Figure 3.14. Hydrodynamic radius of PLGA nanospheres stabilized using different amphiphilic polymers before and after incubation with 10, 15 and 20 mg/ml HSA in bidistilled water at room temperature for 3 h. For better visibility, the inset shows the same data excluding the results of HES laurates with high degree of modification.

Fibrinogen is known to have a higher penetrating/anchoring ability due to its semi-flexible α -chains, and thus a higher affinity to hydrophobic surfaces [88]. As seen in

Figure 3.16, Pluronic F68 failed to prevent the adsorption of fibrinogen, while F127 as well as the low substitution HES laurates showed no adsorption.

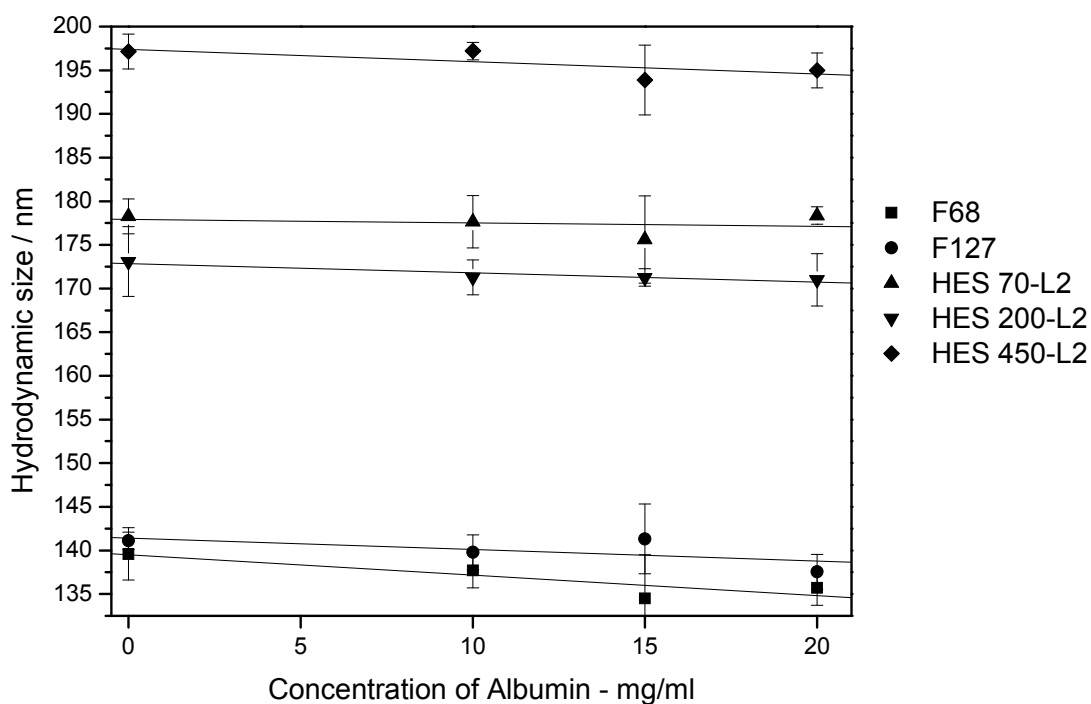


Figure 3.15. Hydrodynamic radius of PLGA nanospheres stabilized using different amphiphilic polymers before and after incubation with 10, 15 and 20 mg/ml HSA in PBS pH 7.4 at room temperature for 3 h.

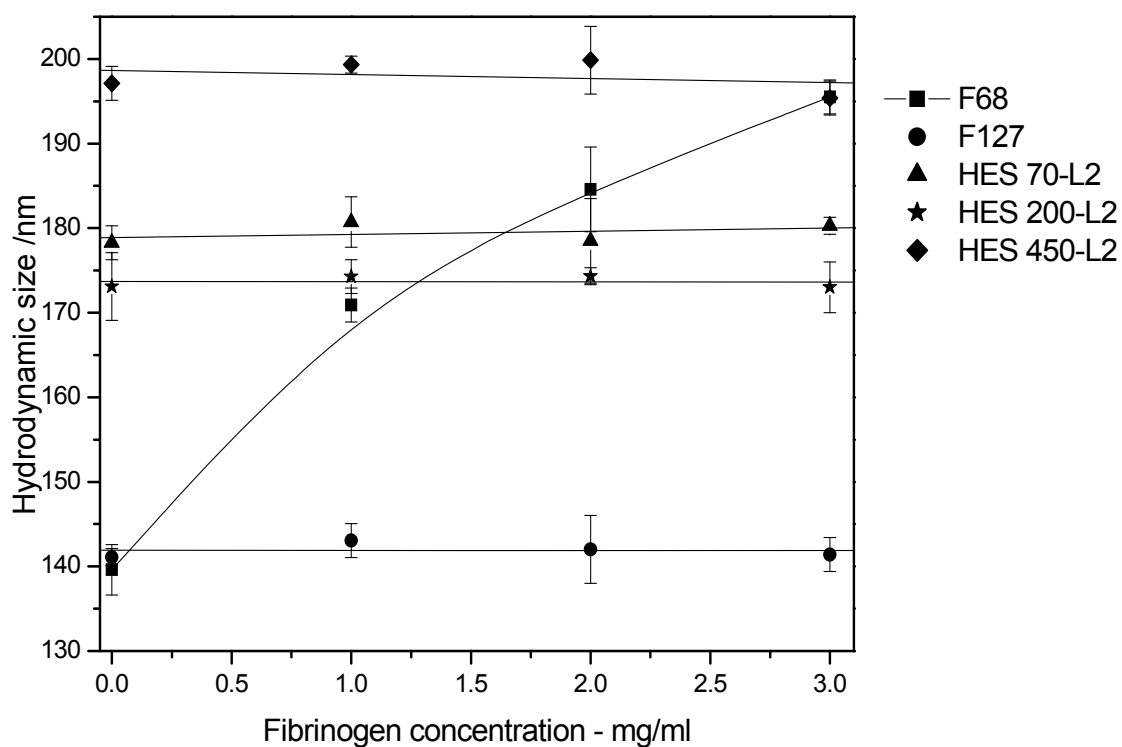


Figure 3.16. Hydrodynamic radius of PLGA nanospheres stabilized with different amphiphilic polymers incubated with 0, 1, 2 and 3 mg/ml fibrinogen in PBS pH 7.4 at room temperature for 3 h.

4.3.3 Phagocytosis of nanospheres

It is well known that pluronic F68 and F127 can reduce the uptake of nanospheres by phagocytic cells in vitro [65, 67]. However, the reduction of phagocytosis in the case of Pluronic F68 is concentration dependent, and decreases by dilution [90], implying a reversible adsorption. Figure 3.17 shows the quantities of nanospheres associated with cells after 6 h of incubation with the particles at 4 °C and 37 °C. The fluorescence intensity (FI) was lower at 4 °C with no statistically significant differences between the various polymeric coats ($P \leq 0.001$). Since phagocytosis is inhibited at 4 °C [81], one can assume that nanospheres are only adhering to the cell surface at this temperature. By contrast at 37 °C, significantly elevated FI can be observed for all nanospheres modifications indicating phagocytosis of nanospheres. Pluronic F68 expressed the highest FI indicating highest particle uptake, while Pluronic F127 and HES 450-L2 showed a statistically significant reduction (40-50 % reduction in uptake) compared to Pluronic F68. Figure 3.18 shows the effect of the amphiphilic polymer concentration on the uptake of nanospheres at 37 °C. As expected for Pluronic F68, the reduction in uptake was concentration dependent, and increased with increasing concentration. By contrast, it was rather constant in the case of HES 450-L2 in the studied concentration range. This points to the relatively firm attachment of HES 450-L2 to the surface, which is probably due to the presence of multiple anchoring points, and the need for a statistically less likely cooperative motion of the polymer backbone for the desorption of the macromolecule.

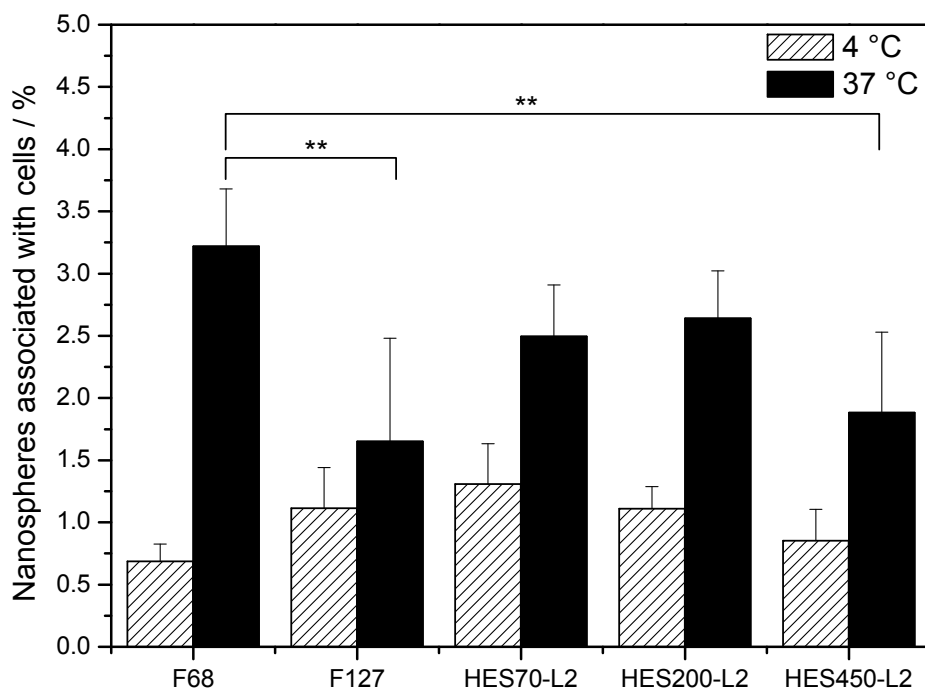
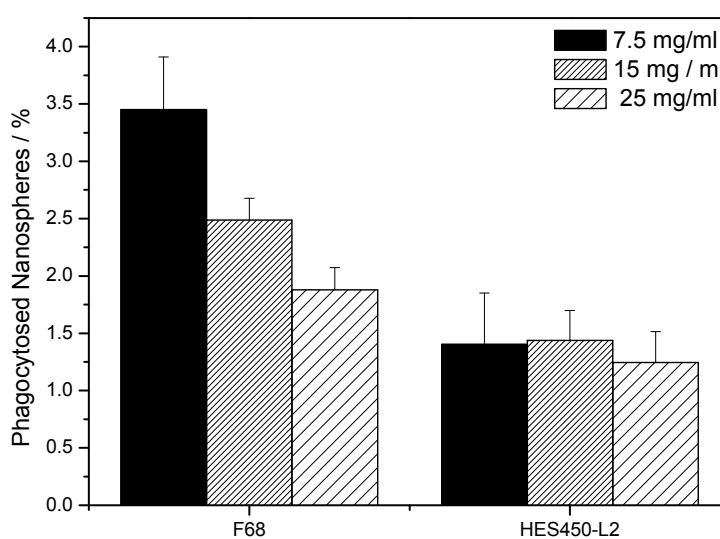


Figure 3.17. Adsorption and uptake of PLGA nanospheres stabilized with different amphiphilic polymers upon incubation with J774.2 phagocytic cell line for 6 h at 4 °C (dashed bars), and 37 °C (black bars). Statistical significance was calculated using 2-tailed unpaired t-test, $P \leq 0.001$. (Average of 2 experiments, $n=10$).

Figure 3.18. Effect of the amphiphilic polymer concentration on the phagocytic uptake of PLGA nanospheres stabilized with Pluronic F68 vs. HES 450-L2 and incubated with J774.2 cell line at 37°C for 6 h.



The confocal micrographs in Figure 3.19 represent optical sections in the middle of the cells (slice 11 out of 20). Cells were incubated with nanospheres, stabilized with different polymers, for 6 h at 37 °C. The micrograph in Figure 3.8a shows the appearance of cells labelled with DiO only, which stains mainly lipids. The cells have a strong green background, while the nuclear region appears black. A specific staining of internal vesicles, which may represent endosomes and other organelles, is visible. Cells incubated with Pluronic F68-stabilized nanospheres shown in Figure 3.8b, express a large number of red dots (see arrows), which represent nanospheres stained with DiI. These dots are mainly visible inside the cells. The orange colour of most of them indicates a mixing with the green staining of intracellular vesicles. This is probably attributed to the trafficking of the nanospheres to cell organelles, such as the endosomes or lysosomes. By contrast, only a few nanospheres stabilized with F127 and HES 450-L2 (Figure 3.8c and d) can be seen associated with cells. Moreover, the nanospheres stabilized with F68 showed a higher tendency for surface adsorption than those stabilized with F127 or HES 450-L2 (see arrows in Figure 3.8b). Overall, confocal microscopy confirms qualitatively the findings of quantitative phagocytosis assay, that nanospheres stabilized with F68 undergo a considerable uptake while those covered with F127 or HES 450-L2 possess a stealth character since their uptake was considerably lower.

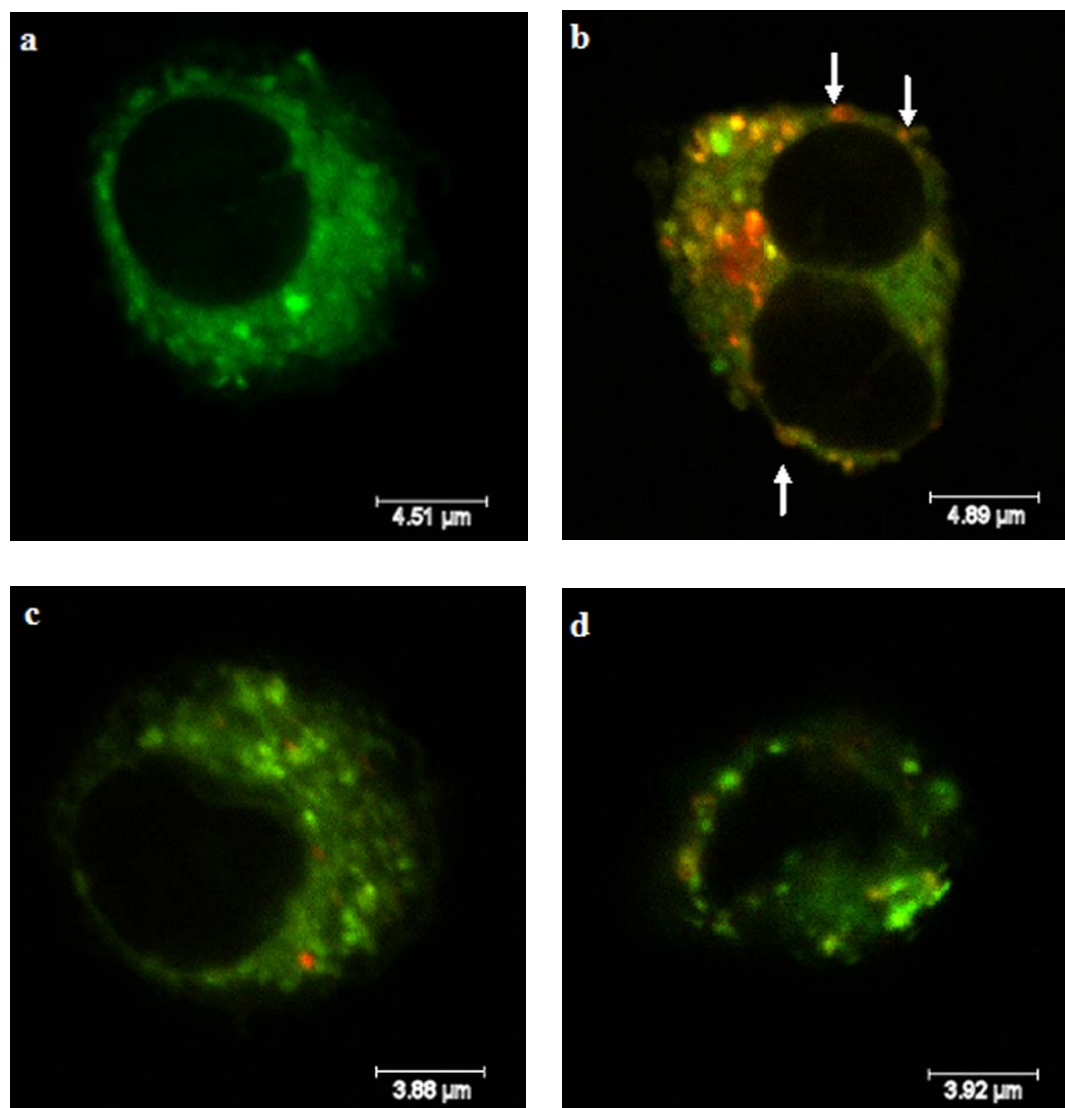


Figure 3.19. CLSM micrographs of a control cell (not incubated with nanospheres) stained with DiO (green) (a), cells incubated with PLGA nanospheres stabilized with Pluronic F68 (b), Pluronic F127 (c), and HES 450-L2 (d) at 37 °C for 6 h. nanospheres are stained with Dil (red)

4.4 Conclusions and outlook

In this study, the ability of HES laurates - having different molar masses and different degrees of modifications - to stabilize PLGA nanospheres was evaluated, in comparison to Pluronic F68 and F127. Nanospheres with an average particle size of 110-140 nm were produced. The thickness of the adsorbed polymer layer increases with the increase in molar mass, and is generally higher for HES laurates than the

studied Pluronics. The adsorption of HSA on the nanospheres was prevented by Pluronic F68, F127 as well as the HES laurates with low molar substitution, while the ones stabilized with medium substitution HES laurate aggregated in the presence of HSA. This is probably due to the presence of fatty acid binding sites on HSA, so that it acts as bridges between the nanospheres. Meanwhile, HES laurates with low molar substitution and F127, but not F68, prevented the adsorption of the more hydrophobic protein fibrinogen. The phagocytosis experiments showed that the HES laurates, particularly HES450-L2, could reduce the uptake of the nanospheres better than F68 and comparable to F127. This points to the significant role of an efficient steric repulsion to prevent protein adsorption and phagocytosis. In general, HES laurates with low degree of substitution may be a biodegradable alternative to Pluronic F127 for stabilization and in vivo administration of PLGA nanospheres. However, the question remains open; how they would perform in vivo, which should be the focus of future investigations.

4.5 References

- [1] D.L. Gutnick, The emulsan polymer: Perspectives on a microbial capsule as an industrial product. *Biopolymers* 26(S0) (1987) S223-S240.
 - [2] J. Wootthikanokkhan, S. Santikunakorn, Effects of propionyl content on the morphology, mechanical properties, and biodegradability of esterified cassava starch/polycaprolactone blends *Journal of Applied Polymer Science* 96(6) (2005) 2154-2162.
 - [3] M. Suzuki, T. Mikami, T. Matsumoto, S. Suzuki, Preparation and antitumor activity of O-palmitoyldextran phosphates, O-palmitoyldextrans, and dextran phosphate. *Carbohydrate Research* 53(2) (1977) 223-229.
 - [4] C. Duval-Terrié, J. Huguet, G. Muller, Self-assembly and hydrophobic clusters of amphiphilic polysaccharides. *Colloids and Surfaces A: Physicochemical and Engineering Aspects* 220(1-3) (2003) 105-115.
 - [5] W. Henni, M. Deyme, M. Stchakovsky, D. LeCerf, L. Picton, V. Rosilio, Aggregation of hydrophobically modified polysaccharides in solution and at the air–water interface *Journal of Colloid and Interface Science* 281(2) (2005) 316-324.
 - [6] K. Mazeau, C. Moine, P. Krausz, V. Gloaguen, Conformational analysis of xylan chains. *Carbohydrate Research* 340(18) (2005) 2752-2760.
 - [7] M.C. Miralles-Houzelle, P. Hubert, E. Dellacherie, Hydrophobic Alkyl Chains-Pectin Conjugates. Comparative Study of Some Physicochemical Properties in Relation to Covalent Coupling vs Ionic Association *Langmuir* 17(5) (2001) 1384-1391.
 - [8] X.-G. Chen, C.M. Lee, H.-J. Park, O/W Emulsification for the Self-Aggregation and Nanoparticle Formation of Linoleic Acid-Modified Chitosan in the Aqueous System. *Journal of Agricultural and Food Chemistry* 51(10) (2003) 3135-3139.
 - [9] M.F. Francis, L. Lavoie, F.M. Winnik, J.-C. Leroux, Solubilization of cyclosporin A in dextran-g-polyethyleneglycolalkyl ether polymeric micelles. *European Journal of Pharmaceutical and Biopharmaceutics* 56 (2003) 337-346.
 - [10] M.F. Francis, M. Piredda, F.M. Winnik, Solubilization of poorly water soluble drugs in micelles of hydrophobically modified hydroxypropylcellulose copolymers *Journal of Controlled Release* 93(1) (2003) 59-68.
-

-
- [11] K. Akiyoshi, S. Deguchi, N. Moriguchi, S. Yamaguchi, J. Sunamoto, Self-aggregates of hydrophobized polysaccharides in water. Formation and characteristics of nanoparticles. *Macromolecules* 26 (1993) 3062-3068.
- [12] T. Liebert, S. Honig, S. Hesse, T. Heinze, Nanoparticles on the basis of highly functionalized dextrans. *Journal of the American Chemical Society* 127 (2005) 10484-10485.
- [13] I.F. Uchegbu, A.G. Schatzlein, L. Tetley, A.I. Gray, J. Sludden, S. Siddique, E. Moshia, Polymeric chitosan-based vesicles for drug delivery. *Journal of Pharmacy and Pharmacology* 50(5) (1998) 453-458.
- [14] K. Kuroda, K. Fujimoto, J. Sunamoto, K. Akiyoshi, Hierarchical self-assembly of hydrophobically modified pullulan in water: Gelation by networks of nanoparticles *Langmuir* 18(10) (2002) 3780-3786.
- [15] A. Durand, E. Dellacherie, Aqueous solutions of native and hydrophobically modified polysaccharides: Temperature effect. *Biomacromolecules* 7 (2006) 958-964.
- [16] C. Rouzes, A. Durand, M. Leonard, E. Dellacherie, Surface Activity and Emulsification Properties of Hydrophobically Modified Dextrans *Journal of Colloid and Interface Science* 253(1) (2002) 217-223.
- [17] S. Hirsch, V. Binder, V. Schehlmann, K. Kolter, K.H. Bauer, Lauroyldextran and crosslinked galactomannan as coating materials for site-specific drug delivery to the colon. *European Journal of Pharmaceutical and Biopharmaceutics* 47 (1999) 61-71.
- [18] V. Sihorkar, S.P. Vyas, Potential of polysaccharide anchored liposomes in drug delivery, targeting and immunization. *Journal of Pharmacy and Pharmaceutical Sciences* 4(2) (2001) 138-158.
- [19] C. Lemarchand, R. Gref, P. Couvreur, Polysaccharide-decorated nanoparticles *European Journal of Pharmaceutics and Biopharmaceutics* 58(2) (2004) 327-341.
- [20] W.-M. Kulicke, U. Kaiser, D. Schwengers, R. Lemmes, Measurements of the refractive index increment on hydroxyethyl starch as a basis for absolute molecular weight determinations. *Starch* 43(10) (1991) 392-396.
- [21] J. Aburto, I. Alric, E. Borredon, Preparation of long-chain esters of starch using fatty acid chlorides in the absence of an organic solvent. *Starch* 51(4) (1999) 132-135.
- [22] H.G. Khorana, The chemistry of carbodiimides. *Chemical Reviews* 53 (1953) 145-164.
-

-
- [23] Z.B. Zhang, C.L. McCormick, Structopendant unsaturated cellulose esters via acylation in homogeneous lithium chloride/N,N-dimethylacetamide solutions. *Journal of Applied Polymer Science* 66(2) (1997) 293-305.
- [24] FDA, International conference on harmonization; guidance on impurities: residual solvents, . Federal Register 62 (1997) 67378 (www.fda.gov/cder/guidance/61907fnl.pdf).
- [25] M. Lepistö, P. Artursson, P. Edman, T. Laakso, I. Sjöholm, Determination of the degree of derivatization of acryloylated polysaccharides by Fourier transform proton NMR spectroscopy *Analytical Biochemistry* 133(1) (1983) 132-135.
- [26] H. Falk , M. Stanek, Two-Dimensional ^1H and ^{13}C NMR spectroscopy of amylose and amylopectin. *Monatshefte für Chemie* 128 (1997) 777-784.
- [27] K.B. Wesslén, B. Wesslén, Synthesis of amphiphilic amylose and starch derivatives *Carbohydrate Polymers* 47(4) (2002) 303-311.
- [28] K. Arai, Y. Shitara, T. Ohyama, Preparation of photochromic spiropyrans linked to methyl cellulose and photoregulation of their properties. *Journal of Material Chemistry* 6 (1996) 11-14.
- [29] J. Otera, Transesterification. *Chemical Reviews* 93 (1993) 1449-1470.
- [30] I. Ikeda, A.M. Klivanov, Lipase-catalyzed acylation of sugars solubilized in hydrophobic solvents by complexation. *Biotechnology and Bioengineering* 42 (1993) 788-791.
- [31] S. Chakraborty, B. Sahoo, I. Teraoka, L.M. Miller, R.A. Gross, Enzyme-catalyzed regioselective modification of starch nanoparticles. *Macromolecules* 38 (2005) 61-68.
- [32] P. Potier, A. Bouchu, G. Descotes, Y. Queneau, Proteinase N-catalysed transesterifications in DMSO–water and DMF–water: preparation of sucrose monomethacrylate. *Tetrahedron Letters* 41 (2000) 3597-3600.
- [33] R. Dicke, A straight way to regioselectively functionalized polysaccharide esters. *Cellulose* 11(255-263) (2004).
- [34] S. Wartewig, R.H.H. Neubert, Pharmaceutical applications of Mid-IR and Raman spectroscopy. *Advanced Drug Delivery Reviews* 57 (2005) 1144-1170.
- [35] G. Zerbi, G. Conti, G. Minoni, S. Pison, A. Bigotto, Premelting phenomena in fatty acids: An infrared and Raman study. *Journal of Physical Chemistry* 91 (1987) 2386-2393.
-

-
- [36] S. Abbate, G. Zerbi, S.L. Wunder, Fermi resonances and vibrational spectra of crystalline and amorphous polymethylene chains. *Journal of Physical Chemistry* 86 (1982) 3140-3149.
- [37] P.J. Wyatt, Light scattering and the absolute characterization of macromolecules. *Analytica Chimica Acta* 272 (1993) 1-40.
- [38] D.E. Discher, A. Eisenberg, Polymer Vesicles. *Science* 297(5583) (2002) 967-973.
- [39] M. Antonietti, S. Förster, Vesicles and liposomes: A self-assembly principle beyond lipids. *Advanced Materials* 15(16) (2003) 1323-1333.
- [40] D.R. Arifin, A.F. Palmer, Polymersome encapsulated hemoglobin: A novel type of oxygen carrier. *Biomacromolecules* 6 (2005) 2172-2181.
- [41] J.C.-M. Lee, H. Bermudez, B.M. Discher, M.A. Sheehan, Y.-Y. Won, F.S. Bates, D.E. Discher, Preparation, stability, and in vitro performance of vesicles made with diblock copolymers. *Biotechnology and Bioengineering* 73 (2001) 135-145.
- [42] A. Taubert, A. Napoli, W. Meier, Self-assembly of reactive amphiphilic block copolymers as mimetics for biological membranes. *Current Opinion in Chemical Biology* 8 (2004) 598-603.
- [43] K. Kita-Tokarczyk, J. Grumelard, T. Haefele, W. Meier, Block copolymer vesicles - using concepts from polymer chemistry to mimic biomembranes. *Polymer* 46(11) (2005) 3540-3563.
- [44] B.M. Discher, Y.-Y. Won, D.S. Ege, J.C.-M. Lee, F.S. Bates, D.E. Discher, D.A. Hammer, Polymersomes: Tough Vesicles Made from Diblock Copolymers *Science* 284(5417) (1999) 1143-1146.
- [45] D.E. Discher, V. Ortiz, G. Srinivas, M.L. Klein, Y. Kim, D. Christian, S. Cai, P. Photos, F. Ahmed, Emerging applications of polymersomes in delivery: From molecular dynamics to shrinkage of tumors. *Progress in Polymer Science* 32 (2007) 838-857.
- [46] Y. Zhou, D. Yan, Supramolecular self-assembly of giant polymer vesicles with controlled sizes. *Angewandte Chemie International Edition* 43 (2004) 4896-4899.
- [47] W. Wang, A.M. McConaghy, L. Tetley, I.F. Uchegbu, Controls on polymer molecular weight may be used to control the size of palmitoyl glycol chitosan polymeric vesicles. *Langmuir* 17(3) (2001) 631-636.
- [48] D. Wu, L. Abezgauz, D. Danino, C.-C. Ho, C.C. Co, Alternating polymer vesicles. *Soft Matter* 4 (2008) 1066-1071.
-

-
- [49] Washington, Drug release from microdisperse systems: a critical review. *International Journal of Pharmaceutics* 58 1-12.
- [50] D. Heng, D.J. Cutler, H.-K. Chan, J. Yun, J.A. Raper, What is a suitable dissolution method for drug nanoparticles? *Pharm Res* 25(7) (2008) 1696-1701.
- [51] H. Ringsdorf, B. Schlarb, J. Venzmer, Molecular architecture and function of polymeric oriented systems: Models for the study of organization, surface recognition, and dynamics of biomembranes. *Angewandte Chemie International Edition* 27 (1988) 113-158.
- [52] A. Besheer, J. Kressler, K. Mäder, in: H. S. Nalwa (Ed.), *polymeric nanostructures and their applications*. Vol. 2, American Scientific Publishers, California, 2007, pp. 415-450.
- [53] V.P. Torchilin, V.S. Trubetskoy, Which polymers can make nanoparticulate drug carriers long-circulating? *Advanced Drug Delivery Reviews* 16 (1995) 141-155.
- [54] D.E. Owens, N.A. Peppas, Opsonization, biodistribution, and pharmacokinetics of polymeric nanoparticles. *International Journal of Pharmaceutics* 307 (2006) 93–102.
- [55] K.S. Soppimath, T.M. Aminabhavi, A.R. Kulkarni, W.E. Rudzinski, Biodegradable polymeric nanoparticles as drug delivery devices. *Journal of Controlled Release* 70 (2001) 1-20.
- [56] A. Vonarbourg, C. Passirani, P. Saulnier, J.-P. Benoit, Parameters influencing the stealthiness of colloidal drug delivery systems. *Biomaterials* 27 (2006) 4356–4373.
- [57] R. Gref, A. Domb, P. Quellec, T. Blunk, R.H. Müller, J.M. Verbavatz, R. Langer, The controlled intravenous delivery of drugs using PEG-coated sterically stabilized nanospheres. *Advanced Drug Delivery Reviews* 16 (1995) 215-233.
- [58] S.J. Sofia, V. Premnath, E.W. Merrill, Poly(ethylene oxide) Grafted to Silicon Surfaces: Grafting Density and Protein Adsorption. *Macromolecules* 31 (1998) 5059-5070.
- [59] S.M. Moghimi, I.S. Muir, L. Illum, S.S. Davis, V. Kolbachofen, Coating Particles with a Block-Copolymer (Poloxamine-908) Suppresses Opsonization but Permits the Activity of Dysopsonins in the Serum. *Biochimica Et Biophysica Acta* 1179(2) (1993) 157-165.
- [60] S.M. Moghimi, H.M. Patel, Serum-mediated recognition of liposomes by phagocytic cells of the reticuloendothelial system – The concept of tissue specificity. *Advanced Drug Delivery Reviews* 32 (1998) 45-60.
-

-
- [61] Y.S. Park, L. Huang, Effect of Chemically Modified G(M1) and Neoglycolipid Analogs of G(M1) on Liposome Circulation Time - Evidence Supporting the Dysopsonin Hypothesis. *Biochimica Et Biophysica Acta* 1166(1) (1993) 105-114.
- [62] R.H. Müller, C. Jacobs, O. Kayser, Nanosuspensions as particulate drug formulations in therapy: Rationale for development and what we can expect for the future. *Advanced Drug Delivery Reviews* 47 (2001) 3-19.
- [63] L. Illum, L.O. Jacobsen, R.H. Müller, E. Mak, S.S. Davis, Surface characteristics and the interaction of colloidal particles with mouse peritoneal macrophages. *Biomaterials* 8 (1987) 113-117.
- [64] J.S. Tan, D.E. Butterfield, C.L. Voycheck, K.D. Caldwell, J.T. Li, Surface modification of nanoparticles by PEO/PPO block copolymers to minimize interactions with blood components and prolong blood circulation in rats. *Biomaterials* 14(11) (1993) 823-833.
- [65] S.E. Dunn, A.G.A. Coombes, M.C. Garnett, S.S. Davis, M.C. Davies, L. Illum, In vitro cell interaction and in vivo biodistribution of poly(lactide-co-glycolide) nanospheres surface modified by poloxamer and poloxamine copolymers. *Journal of Controlled Release* 44 (1997) 65-76.
- [66] S. Stolnik, B. Daudali, A. Arien, J. Whetstone, C.R. Heald, M.C. Garnett, S.S. Davis, L. Illum, The effect of surface coverage and conformation of poly(ethylene oxide) (PEO) chains of poloxamer 407 on the biological fate of model colloidal drug carriers. *Biochimica et Biophysica Acta* 1514 (2001) 261-279.
- [67] L. Illum, I.M. Hunneyball, S.S. Davis, The effect of hydrophilic coatings on the uptake of colloidal particles by the liver and by peritoneal macrophages. *International Journal of Pharmaceutics* 29 (1986) 53-65.
- [68] C. Passirani, G. Barratt, J.P. Devissaguet, D. Labarre, Long-circulating nanoparticles bearing heparin or dextran covalently bound to poly(methylmethacrylate). *Pharm Res* 15 (1998) 1046-1050.
- [69] R. Weissleder, A. Bogdanov, E.A. Neuwelt, M. Papisov, Long circulating iron oxides for MR imaging. *Advanced Drug Delivery Reviews* 16 (1995) 321-334.
- [70] M. Orlando, Modification of proteins and low molecular weight substances with hydroxyethyl starch (HES). Justus Liebig Universität Giessen, Gießen, 2003.
- [71] A. Besheer, G. Hause, J. Kressler, K. Mäder, Hydrophobically Modified Hydroxyethyl Starch: Synthesis, Characterization, and Aqueous Self-Assembly into Nano-Sized Polymeric Micelles and Vesicles. *Biomacromolecules* 8 (2007) 359-367.
-

-
- [72] Lutrol® F 68, Technical information, March 2007, BASF AG, Ludwigshafen, Germany.
- [73] Lutrol® F 127, Technical information, August 2005, BASF AG, Ludwigshafen, Germany.
- [74] Y. Sadzuka, A. Nakade, R. Hirama, A. Miyagishima, Y. Nozawa, S. Hirota, T. Sonobe, Effects of mixed polyethyleneglycol modification on fixed aqueous layer thickness and antitumor activity of doxorubicin containing liposome. *International Journal of Pharmaceutics* 238(1-2) (2002) 171-180.
- [75] Y. Sadzuka, I. Sugiyama, T. Tsuruda, T. Sonobe, Characterization and cytotoxicity of mixed polyethyleneglycol modified liposomes containing doxorubicin. *International Journal of Pharmaceutics* 312 (2006) 83-89.
- [76] L.C. McCormick, G.W. Slater, A.E. Karger, W.N. Vreeland, A.E. Barron, C. Desruisseaux, G. Drouin, Capillary electrophoretic separation of uncharged polymers using polyelectrolyte engines. Theoretical model. *Journal of Chromatography A* 924(1-2) (2001) 43-52.
- [77] A.T. Poortinga, Electrical double layer interactions in bacterial adhesion and detachment. Groningen University, Groningen, 2001.
- [78] B. Shi, C. Fang, Y.Y. Pei, Stealth PEG-PHDCA niosomes: Effects of chain length of PEG and particle size on niosomes surface properties, in vitro drug release, phagocytic uptake, in vivo pharmacokinetics and antitumor activity. *Journal of Pharmaceutical Sciences* 95(9) (2006) 1873-1887.
- [79] E. Chnari, J.S. Nikitzuk, K.E. Uhrich, P.V. Moghe, Nanoscale anionic macromolecules can inhibit cellular uptake of differentially oxidized LDL. *Biomacromolecules* 7(2) (2006) 597-603.
- [80] C. Lemarchand, R. Gref, C. Passirani, E. Garcion, B. Petri, R. Muller, D. Costantini, P. Couvreur, Influence of polysaccharide coating on the interactions of nanoparticles with biological systems. *Biomaterials* 27(1) (2006) 108-118.
- [81] M. Roser, D. Fischer, T. Kissel, Surface-modified biodegradable albumin nano- and microspheres. II: effect of surface charges on in vitro phagocytosis and biodistribution in rats. *European Journal of Pharmaceutics and Biopharmaceutics* 46 (1998) 255-263.
- [82] M.G. Honig, R.I. Hume, Fluorescent Carbocyanine Dyes Allow Living Neurons of Identified Origin to Be Studied in Long-Term Cultures. *The Journal of Cell Biology* 103 (1986) 171-187.
-

-
- [83] U. Bilati, E. Allemann, E. Doelker, Development of a nanoprecipitation method intended for the entrapment of hydrophilic drugs into nanoparticles. *European Journal of Pharmaceutical Sciences* 24 (2005) 67-75.
- [84] J.-T. Li, K.D. Caldwell, N. Rapoport, Surface Properties of Pluronic-Coated Polymeric Colloids. *Langmuir* 10 (1994) 4475-4482.
- [85] A. Rübe, G. Hause, K. Mäder, J. Kohlbrecher, Core-shell structure of Miglyol/poly(d,l-lactide)/Poloxamer nanocapsules studied by small-angle neutron scattering. *Journal of Controlled Release* 107 (2005) 244-252.
- [86] S.M. Moghimi, A.C. Hunter, Poloxamers and poloxamines in nanoparticle engineering and experimental medicine. *Trends in Biotechnology* 18 (2000) 412-420.
- [87] A. Pramanik, P.K. Chowdhury, Polyelectrolyte Configuration of Low Molecular Weight Sodium Amylose Xanthate in Aqueous and Salt Solutions *Journal of Macromolecular Science – Chemistry A* 5(7) (1971) 1149-1167.
- [88] J. Lee, A. Martic, J.S. Tan, Protein Adsorption on Pluronic Copolymer-Coated Polystyrene Particles. *Journal of Colloid and Interface Science* 131(1) (1989) 252-266.
- [89] A.A. Spector, Fatty acid binding to plasma albumin. *Journal of Lipid Research* 16 (1975) 165-179.
- [90] V.C.F. Mosqueira, P. Legrand, J.-L. Morgat, M. Vert, E. Mysiakine, R. Gref, J.-P. Devissaguet, G. Barratt, Biodistribution of Long-Circulating PEG-Grafted Nanocapsules in Mice: Effects of PEG Chain Length and Density. *Pharm Res* 18(10) (2001) 1411-1419.
-

Part III

Gd-HES: A macromolecular MRI contrast agent

Chapter 5

Synthesis, Characterization and in-vivo evaluation of Gd-HES

5.1 Introduction

Since its first implementation by Lauterbur [1], magnetic resonance imaging (MRI) has become a powerful non-invasive diagnostic tool in the clinical setting. It depends on the phenomenon of nuclear magnetic resonance (NMR), whereby atomic nuclei exposed to a strong magnetic field absorb electromagnetic waves at a characteristic frequency, which falls in the radio frequency (RF) range [2]. Using special 3D-encoding techniques, MRI gives a spatial distribution of the density (and relaxation) of protons [3]. When compared to other clinical imaging techniques like computerized tomography (CT) or positron emission tomography (PET), MRI has the advantage of (i) using non-ionizing radiations, and (ii) high versatility, since the procedure used to acquire the images can be easily tailored to enhance the visibility of specific organs or tissues.

Despite its high ability to differentiate between internal organs, MRI contrast agents may be used for tissue specific enhancement of the MRI images. Depending on their pharmacokinetics and biodistribution, which in turn depend on their physicochemical properties, size and molar mass, these contrast agents can differentially enhance certain pathological conditions, thus sparing the patient from carrying out a biopsy or other expensive and invasive procedure [4]. For the sake of clarifying the background for the experiments described in this section, this

introduction will include a brief overview of the basics of MRI and the contrast agents used for image enhancement.

5.1.1 Magnetic resonance imaging

5.1.1.1 Theory

Medical magnetic resonance uses the signal from the nuclei of hydrogen atoms (protons) for image construction. As a rotating mass carrying a positive charge, the proton possesses a magnetic moment, i.e. it behaves like a small magnet. In an external magnetic field, the nucleus precesses along the direction of the field (see Figure 5.1). The speed of precession is proportional to the applied magnetic field [5], and is called the “Larmor frequency” ω_o ,

$$\omega_o = \gamma_o \times B_o \quad \text{Eq. 1}$$

where γ_o is the gyromagnetic ratio* and B_o is the external magnetic field. For protons exposed to an MRI magnetic field, the Larmor frequency lies in the radiofrequency range.

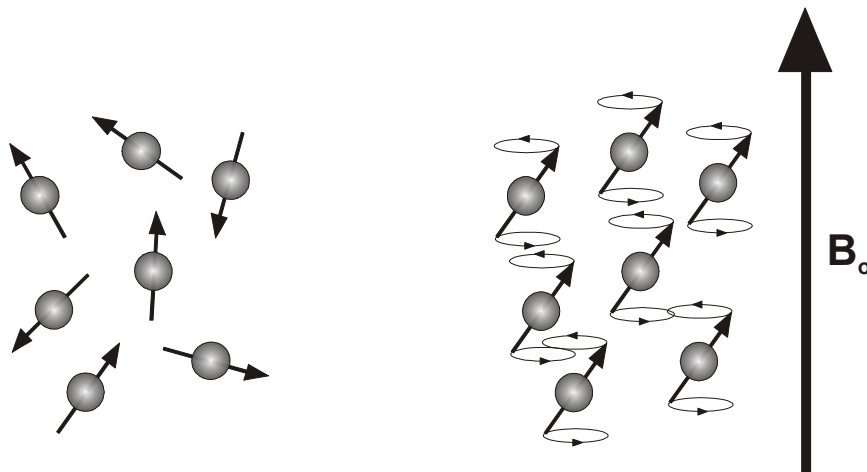


Figure 5.1. A schematic diagram illustrating the alignment of nuclei in an external magnetic field. Left, random orientation of the nuclei. Right, precession of the nuclei along the direction of the external magnetic field B_o .

* The gyromagnetic ratio for a nucleus is the ratio of the nuclear magnetic dipole moment to its angular momentum.

The net magnetic field of all nuclei is the vector sum of the magnetic moments of all the protons, and is called the nuclear magnetization \mathbf{M} [2]. Under equilibrium conditions, there is a small net magnetization in the longitudinal direction (parallel to static field \mathbf{B}_0), while the transverse component (perpendicular to \mathbf{B}_0) is equal to zero. By applying a short pulse of oscillating magnetic field at exactly the Larmor frequency (RF signal), the nuclear magnetization can be tipped away from the longitudinal axis, producing a finite component in the transverse plane. Since the nuclei precess in phase, they produce an oscillating magnetic field that can be detected with an RF receiver coil. The signal is thus proportional to the transverse component of \mathbf{M} . When the RF signal is turned off, the transverse magnetization will gradually decay to zero and the signal disappears [6].

The RF excitation is quantified by the flip angle (FA) through which the net magnetization is tipped away from the longitudinal axis, and FA is equal to

$$FA = \gamma\beta_1\tau \quad \text{Eq. 2}$$

where β_1 is the magnetic field component of the RF signal, and τ is the pulse duration.

The maximum achievable signal is obtained with an FA of 90° , which transfers all the longitudinal magnetization into the transverse plane. The amplitude of the signal is then limited only by the magnitude of the equilibrium magnetization \mathbf{M}_0 . This, in turn, is determined by the strength of the static magnetic field \mathbf{B}_0 . Accordingly, MRI instruments with stronger fields have a higher sensitivity.

5.1.1.2 Spin relaxation

Excitation of nuclei by means of an RF pulse makes a number of spins precess in synchrony, producing a rotating magnetic field that can be detected with an RF coil. However, the signal will not persist indefinitely, because the nuclei will lose the phase coherence among the spins with a corresponding attenuation of the transverse magnetization. This loss of phase coherence is called „transverse relaxation“, and the time scale over which it occurs is known as T2. Since the MR signal represents the transverse component of the magnetization, T2 determines how quickly an MR signal fades after excitation. Simultaneously, the nuclei lose energy to their surroundings, leading to the recovery of the longitudinal magnetization to the original equilibrium

state. This loss in energy is called „longitudinal relaxation“, and its time scale is T_1 . Thus T_1 determines the time required for the spins to recover and be available for the next excitation. In many cases, the decrease in the MR signal due to T_2 relaxation takes around 100-300 ms, while the recovery of the longitudinal magnetization takes 0.5-5 s [5].

5.1.1.2.1 Longitudinal relaxation time T_1

Longitudinal relaxation (also known as spin-lattice relaxation) arises from loss of the excitation energy to the surroundings due to fluctuations in the local magnetic field. The latter is the sum of the external field and the smaller fields generated by the neighboring nuclei, electrons and molecules. As the molecule tumbles, the protons experience a fluctuating magnetic field. The excited protons can lose their energy to the surrounding environment when these fluctuations (or the molecular tumbling rate) approach the Larmor frequency. Thus T_1 depends on the molecular mobility, which varies with molecular size and the surrounding environment [6].

5.1.1.2.2 Transverse relaxation time T_2

Transverse relaxation (also known as spin-spin relaxation) occurs more rapidly than longitudinal relaxation, because it involves a number of mechanisms, both microscopic and mesoscopic. The component caused by microscopic processes is a spin-spin interaction accompanied by energy transfer between spins. This process takes place on a time scale denoted T_2 , and occur most efficiently if the molecular tumbling rate is low.

Dephasing over a mesoscopic scale further shortens the relaxation time of the transverse magnetization to a value denoted T_2^* . It is a result of magnetic field inhomogeneities, which is due to differences in magnetic susceptibility. The latter alters the strength of the field both within the tissue itself and in its immediate neighborhood. Most biological materials are diamagnetic, meaning that they have a small negative susceptibility. A few biological substances, mostly blood proteins, such as deoxyhemoglobin, are paramagnetic and have a small positive susceptibility. Whenever a sample contains tissues of different susceptibility, the strength of the magnetic field changes across their boundaries, causing spin dephasing and shortening the T_2^* value. This occurs around air-filled cavities, such as the sinuses, and in tissues containing deoxygenated blood or byproducts of hemorrhage.

5.1.1.3 Measurement of T_1 and T_2

Several pulse sequences can be used to measure the relaxation times. The simplest pulse sequence is the application of a single 90° RF pulse. The subsequent attenuation of the transverse magnetization is known as the free induction decay (FID). Since it is affected by both spin-spin relaxation and field inhomogeneities, it occurs on a T_2^* timescale.

The dephasing caused by mesoscopic field inhomogeneities can be reversed using a refocusing procedure. The method uses a 180° RF pulse (the refocusing pulse) to give the slower spins a head start, while the faster spins need longer time to refocus. As the spins precess back under the influence of the same field inhomogeneities (this eliminating their effect), they gradually come back into phase, producing a brief signal recovery known as a “spin echo”. The time taken for the spins to rephase exactly equals the time during which they were allowed to dephase, and the total is known as the “echo time, TE ”. Since the effect of the mesoscopic field inhomogeneities are neutralized, the decay of the spin echo train is governed by T_2 relaxation and not T_2^* .

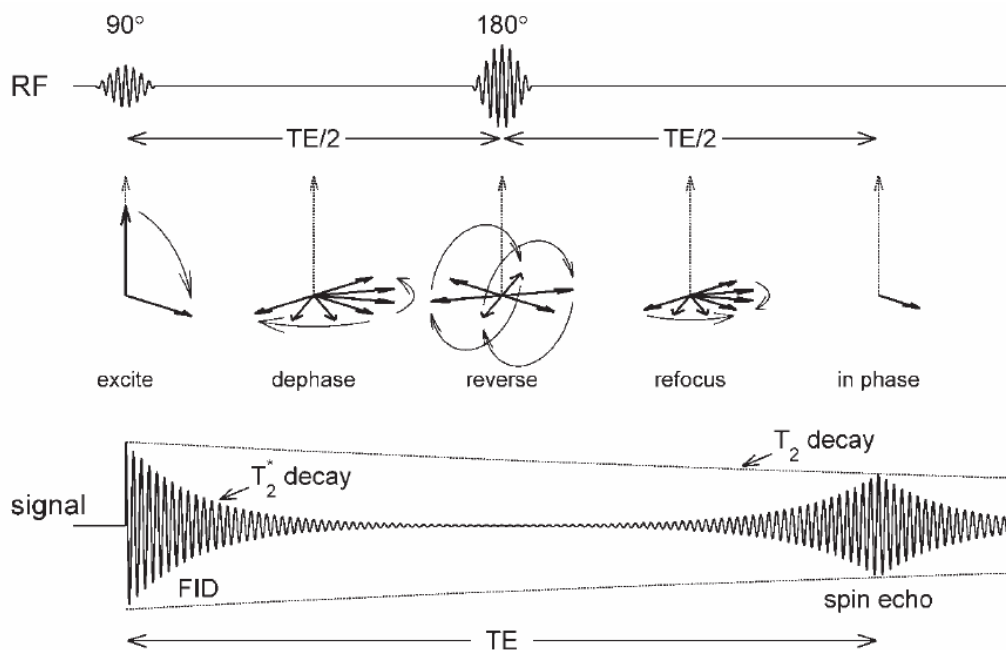


Figure 5.2. The use of a 180° refocusing pulse results in the elimination of the effect of field inhomogeneities and the formation of a spin echo. The amplitude of the spin echo is determined by the T_2 relaxation that has occurred during the echo time TE (from reference [6]).

The above sequence (90° pulse followed by 180° , known as the Hahn spin echo) can be replaced by a more refined one for T_2 measurement, namely the CPMG (Carr-Purcell-Meiboom-Gill) sequence. If there is an error in the 180° RF pulse (175° instead of 180°), the magnetization will not be in the x-y plane, and thus the signal will be smaller than expected. To avoid this, a second 180° pulse is applied to recover the echo exactly in plane.

T_1 is usually measured by the inversion recovery sequence. A 180° pulse is applied flipping the magnetization in the negative z-direction. After a certain time period, τ , a 90° pulse is applied to tip the magnetization in the x-y plane in order to measure its magnitude. Before the 90° pulse, the longitudinal magnetization will tend to recover its original (positive) magnitude due to the spin-lattice relaxation. After applying the 90° pulse, and for small values of τ , the magnetization will still have a negative value, which then increases for larger values of τ , passing through zero (see) [7].

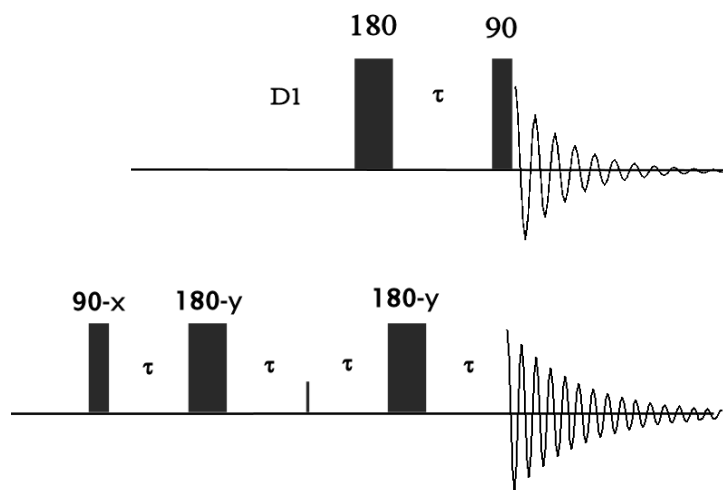


Figure 5.3. Pulse sequence for inversion recovery (top) and CPMG (bottom).

5.1.1.4 T_1 - and T_2 -weighted images

To produce a good signal-to-noise ratio during imaging, the process of excitation and signal acquisition needs to be repeated several times in succession. The repetition time between successive excitations, TR, is important in determining the signal amplitude from a given tissue type. If the TR is short with respect to T_1 of the tissue, the longitudinal magnetization will not have fully recovered to its equilibrium value before the next excitation. Because the magnetization remains partially

saturated, no further excitation is possible, and the signal from the tissue is reduced accordingly. By comparison, a tissue with a faster relaxation rate will be less saturated and will exhibit a relatively higher signal. If a long TR is selected, all tissues will have enough time to return to the equilibrium state and thus will give similar signals. Therefore, if TR is chosen to be sufficiently short that the signal from each tissue depends heavily on its T1 value, the resulting image is described as being 'T1-weighted.'

In imaging, spin-echo acquisitions provide T2 weighting, whereas FID acquisitions provide T2* weighting. The degree of T2-weighting is determined by the value of TE, which for a spin-echo sequence may range from a few milliseconds to hundreds of milliseconds. If a relatively long TE is chosen, tissues with a short T2 look dark since they have lost most of their signal, while tissues with a long T2 still produce a signal and appear bright. Because spin-echo sequences employ large FA, they require long TR to allow adequate recovery of the longitudinal magnetization. Typical TR values range from hundreds of milliseconds to several seconds, the shorter values producing greater degrees of T1-weighting.

Table 5.1. Summary for T1- and T2-weighting (adapted from reference [5])

-
- Short TR (approximately < 600 ms) gives a strong T1 weighting
 - Long TE (approximately > 60 ms) gives a strong T2 weighting

 - Tissues with a short T1 appear bright on T1-weighted images.
 - Tissues with a long T1 appear dark on T1-weighted images.
 - Tissues with a short T2 appear dark on T2-weighted images.
 - Tissues with a long T2 appear bright on T2-weighted images.
-

5.1.1.5 Spatial encoding for image acquisition

To construct an MRI image, the nuclei in a certain body slice are excited. Nuclei can absorb energy from the RF field only if their Larmor frequency exactly matches the frequency of the RF field. Slice-selective excitation is achieved by applying the RF field in the presence of a magnetic field gradient. The gradient produces a linear variation in the strength of the static field, B_0 , which gives rise to a spatial variation in the value of the Larmor frequency. Only those spins whose Larmor frequency exactly matches the frequency of the applied RF field will be excited.

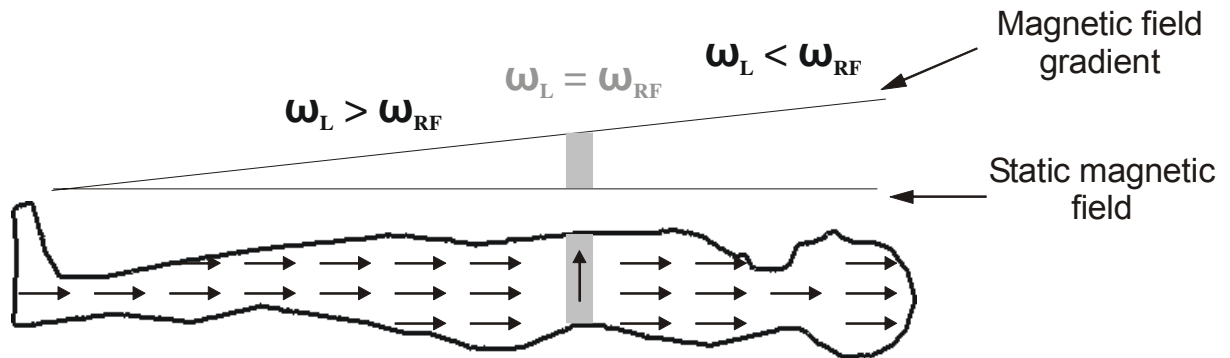


Figure 5.4. Slice selection. To acquire an image of a particular slice of tissue, the scanner must excite the nuclear magnetization only within that slice. Slice-selective excitation is achieved by applying an RF pulse in the presence of a magnetic field gradient. The gradient produces a linear variation in the strength of the static field, which gives rise to a spatial variation in the value of the Larmor frequency. Only those spins whose Larmor frequency, ω_L , exactly matches the frequency of the applied RF field, ω_{RF} , will be excited.

To obtain information from the 2 dimensions in the slice, frequency encoding is applied in one direction, while phase encoding is applied in the other. (for further details of these techniques, excellent books can be consulted [5, 6].

5.1.2 MRI contrast agents

MRI contrast agents can alter the magnetic relaxation times, thus increasing the contrast between tissues that would otherwise be difficult to obtain, particularly soft tissues such as the liver, GIT, cardiovascular system, lymphatic system and the lung. MRI contrast agents can alter T1 and T2 to varying degrees. Those that alter T1 and T2 by roughly the same amounts generate a positive contrast in T1-weighted images. These positive contrast agents are usually paramagnetic complexes of Gd^{3+} or Mn^{2+} ions [4, 8]. By contrast, super paramagnetic iron oxide nanoparticles (SPIONs) lead to a pronounced decrease in T2 compared to T1, and usually give dark spots (negative contrast) in T2-weighted images [4, 8].

The commercially available positive MRI contrast agents, such as Gd-DTPA, Gd-DOTA or Gd-BOPTA have low molar masses. This causes several drawbacks, such as 1) extravasation after administration resulting in low image quality; and 2) rapid elimination through the kidneys (Gd-DTPA has a half-life of only 20 minutes in rats [9]). One approach to overcome these drawbacks is to conjugate these chelates to a

polymeric carrier. Such polymeric contrast agents have additional advantages. These include 1) the ability to reduce toxicity of metal ions 2) persistence in the blood, thus the time window for imaging is not so critical 3) significantly higher contrast 4) the possibility to attach and deliver other ligands including therapeutic modalities 5) they can be conjugated to a homing device to be targeted to specific tissues [10, 11].

The macromolecular contrast agents have a number of applications. Since they are retained in the blood, they can act as a blood pool contrast agent. This can be used to assess tissue perfusion, blood volume, capillary permeability and vascular anatomy [12]. They can also be used to detect pathological conditions with enhanced vascular permeability, such as in case of inflammation, myocardial infarction, atherosclerosis, breakdown of the blood-brain barrier and tumors [11].

Historically speaking, the conjugate of albumin to Gd-DTPA, first synthesized by Ogan *et al.* in 1987 [13], was among the first macromolecular MRI contrast agents. It showed potential utility in angiography, mammography and in characterizing the microvessels of tumors [4]. However, the elimination of the conjugate is incomplete. Accumulation particularly in the liver and bone was observed [4]. Furthermore, albumin is potentially immunogenic. All this have prevented the evaluation of the albumin conjugate in humans and limited it only to animal tests. To avoid these disadvantages, dextran was used instead of albumin and evaluated by several authors [14, 15]. The dextran conjugate has a better toxicity profile and was tested in humans. However, it is worth noting that there is a high incidence of anaphylactic reactions to dextran with a high molar mass. A series of dendrimers with different sizes based on polyamidoamine (PAMAM) and polypropylenimine diaminobutane (DAB) were conjugated to Gd-DTPA or Gd-DOTA and evaluated in animals [16]. Dendrimers 3-6 nm in size were rapidly excreted through the kidneys, while those with 7-12 nm size were retained in the circulation and were better suited as blood pool contrast agents. Despite the fact that these dendrimers have a very narrow polydispersity and their size is readily tailored, concerns about toxicity may arise due to their non-biodegradability. Other polymers include poly(ethylene glycol) [17] and poly(L-glutamic acid) [18].

It is thus clear that a non-immunogenic biodegradable polymer backbone would be the ideal carrier. To this end, hydroxyethyl starch (HES) was chosen in this study. HES, with different molar masses, was coupled to DTPA, and then Gd was chelated

to it. The HES conjugate was characterized using different methods, and finally evaluated in animal models in comparison to low molar mass Gd chelates.

5.2 Experimental

5.2.1 Materials

HES70 and HES200 (Mw 70 x 10³ and 200 x 10³ g/mole, Serumwerke Bernburg, Germany), diethylenetriaminepentaacetic acid (DTPA) (product no. 32320, Fluka), N,N'-Dicyclohexylcarbodiimide (DCC) (product no. 36650, Sigma-Aldrich), N-hydroxysuccinimide (NHS) (product no. 130672, Sigma-Aldrich), N,N-dimethylaminopyridine (DMAP) (Merck). GdCl₃.6H₂O (product no. G7532, Sigma-Aldrich).

5.2.2 Synthesis of the Gd-HES chelates

A predetermined amount of DTPA (see Table 5.2) was dissolved in 10 ml dry DMF by heating and sonication. After addition of DMAP and heating, DTPA dissolved completely. DCC and NHS were dissolved in 5 ml DMF then added to the DTPA solution. The molar ratio of DTPA : DMAP : DCC : NHS was 4:1:2:2. 1.5 g HES70 or HES200 (8.1 mmol of AGU) were dried at 105 °C for 2 h, then dissolved in 10 ml DMF. HES solution was added to the DTPA solution and left to react overnight at room temperature under stirring. The reaction mixture was filtered using a Buchner flask, dialyzed for 4 days (MWCO 6- 8 kDa), then lyophilized.

For chelation of Gd, 500 mg of the HES-DTPA conjugate were dissolved in 5 ml distilled water (DW). 400 mg GdCl₃.6H₂O were dissolved in 5 ml DW and added to the modified HES solution. The mixture was stirred for 1 h, then dialyzed against DW for 3 days and lyophilized.

Table 5.2. Amount of DTPA reacted with 1.5 g of HES to produce the different HES-DTPA conjugates.

Sample	DTPA g (mmol)
HES70-DTPA18 ^a	1.6 (4)
HES70-DTPA25 ^a	2.4 (6)
HES200-DTPA20 ^a	1.6 (4)

^a The 1st number in the sample name stands for the molar mass of the original HES, while the 2nd one represents the molar substitution (MS) of DTPA (see section 5.3.1 for more information)

5.2.3 ¹H NMR spectroscopy

For ¹H NMR measurements, 50 mg polymer samples were dissolved in 600 μl D₂O alone, or with 10 mg NaOH, and measured at 400 MHz (Gemini 2000, Varian Inc., USA).

5.2.4 Conductometric analysis

A solution of GdCl₃·6H₂O was prepared (120 mg/100 ml DW). Solutions of HES-DTPA in 30 ml DW were prepared. Gd solution was added in steps of 0.5 ml and the conductivity was measured. The measurement was carried out 3 times for each of the modified HES.

5.2.5 Asymmetric flow field flow fractionation (AF4)

Samples were prepared with a concentration of 5 mg/ml in a 50 mM NaCl solution preserved with 0.02 % w/v NaN₃. For FFF measurements, the Eclipse FFF system (Wyatt Technology Corp., California, USA) was used. It was coupled to a DAWN EOS MALS detector (Wyatt Technology Corp., California, USA) and an RI detector Shodex 101 (Shoko America, Colorado, USA). Samples were filtered through a 0.2 μm filter and 100 μl of the solution were injected into a channel having a 350 μm spacer and a 5 kDa regenerated cellulose membrane. A channel flow of 2 ml/min was maintained, while a linearly decreasing cross flow from 2 ml/min to 0 ml/min over 30 min was used for separation (see Table 5.3). Data were evaluated using ASTRA software v.4.90.08 (Wyatt Technology Corp., California, USA).

For HES70, a dn/dc value equal to 0.146 was obtained from the literature [19]. For the other samples, dn/dc was determined by measuring 3 different concentrations, each repeated three times.

Table 5.3. Program for sample separation used for AF4 measurements.

	Duration (min)	Cross flow (ml/min)		Focus flow (ml/min)
		Start	End	
Elution	2	2	2	–
Focus	1	–	–	2
Focus+inj	2	–	–	2
Focus	1	–	–	2
Elution	30	2	0	–
Elution	10	0	0	–
Elution+inj	10	0	0	–

5.2.6 Determination of relaxivity

Samples were dissolved in PBS pH 7.4 (EP) and measured at 37 °C in a 20 MHz benchtop MRI spectrometer (Oxford Instruments, UK). For T1 measurement, the inversion recovery pulse sequence was used, while for T2 measurements, the CPMG sequence (Carr-Purcell-Meiboom-Gill sequence) was used (see Figure 5.3). Measurement parameters are included in Table 5.4.

Table 5.4. Parameters for MRI measurements.

	For T1 measurement	For T2 Measurement
RG	5	20
SI	256	1
RD (relaxation delay)	1200000.05	1000000
Tau	135	135
NS (No. of accumulations)	1	64
NECH (No. of echoes)	128	256
DW	10	10

5.2.7 *In vitro* imaging

Contrast enhancement of Gd-HES was judged against that of Gd-DTPA *in vitro*, by comparing the images taken for a tissue culture scaffold. The scaffold preparation is described elsewhere (Nitzsche *et al.*). Briefly, it was made of a composite material of hydroxyapatite, equine collagen type 1 (Lohmann & Rauscher, Neuwied, Germany) and chitosan (Chitoclear FG 95, Primex, Iceland). To impart mechanical stability to the freeze dried scaffolds, dehydrothermal treatment was applied as described in (Nitzsche *et al.*, personal communication).

The scaffolds were incubated in 10 ml phosphate buffer pH 7.4 containing 0.1 % w/v NaN₃ for 3 days. The incubation buffer was exchanged for a solution of the contrast medium (0.548 g/l Gd-DTPA (Sigma-Aldrich), or 1.572 g/l HES70-DTPA18-Gd). For imaging, slices of 3 mm thickness were selected perpendicular to the main magnetic field, with TR of 300 ms, and TE of 2.4 ms. Averages of 16 scans were used resulting in a total measuring time of 10 min.

5.2.8 *In vivo* imaging

Animals: *Nude mice bearing colon carcinoma tumors:* 3 male nude mice (NMRI-Foxn1^{nu}, Harlan Winkelmann, Germany) were used. Their age was approximately 80 d when they were injected subcutaneously with 2 different human colon carcinoma cell lines, namely; HT29 on the right side of the abdomen, and DLD-1 to the left side. In each case, 5 million cells suspended in 100 µl PBS were injected. The imaging experiment was conducted 4 weeks after tumor cell injection.

Normal mice: 3 Balb/c mice (2 males and 1 female) weighing between 15-25 g were used.

Sample preparation: HES70-DTPA18-Gd was dissolved in sterile saline solution to a concentration of 8 % w/v (concentration of Gd is 5 mmol/l). Samples were sterilized by filtration through 0.2 µm filters under aseptic conditions. Gd-BOPTA (Multihance[®]) was diluted 1:100 with sterile saline solution to give a concentration of 5 mmol/l before use.

Administration: Through the tail vein, each animal was injected 150 µl of Gd-BOPTA or 150 µl of HES70-DTPA18-Gd. The injected dose was approximately 0.03 mmol Gd/Kg. **Anaesthesia:** For tumor imaging, animals were anaesthetized with a

continuous stream of isofluran (Forene[®], Abbott) in O₂ (2 Vol%, 2 l/min) using an Isofluran Vet. Med. Vaporizer (Drägerwerk AG, Lübeck, Germany). For angiography, the Balb/c mice were anaesthetized using i.p. injection of a mixture of 6 mg/Kg body weight Rompun[®] (Xylazin) and 90 mg/Kg body weight Ketavet[®] (Ketamin) diluted in 0.9 % w/v NaCl solution. Since the anesthesia was sufficient for 40-60 min, the mice were imaged sequentially over 3 hours.

MR imaging was carried out using a prototype benchtop MRI spectrometer for *in vivo* animal studies (Oxford Instruments, UK), where transaxial images of each anaesthetized mouse were collected using the following parameters: image sequence: T2 spin echo sequence (T2SS), TR 172 ms, TE 9.8 ms, slice width 3 mm, slice separation 3.5 mm, number of slices 5, averages 16, total time 360 s, field of view 40 mm, and images are 512 X 512 pixels. A 50 µl capillary containing a standard solution of Gd-BOPTA was used as a reference (conc. 10 mmol/l).



Figure 5.5. The left photograph shows the Benchtop MRI spectrometer for *in vivo* imaging from Oxford Instruments, UK, while the right one shows an anaesthetized nude mouse with anaesthesia mask (black arrow) and subcutaneously-injected tumors (white arrows).

Image analysis Greyscale images were analyzed using the image analysis software JMicroVision v1.2.5. For the renal sinus and cortex, the average of 36 pixels (6 x 6) was used. The same was applied to the tumor center, while for the tumor rim; the average of 4 positions (36 pixels for each) was used (see Figure 5.6). To be able to compare the measurements, the signal intensity (SI) at the different regions of interest (ROI) was divided by the SI for the reference capillary, and then normalized by dividing it over the signal intensity at time = 0 min.

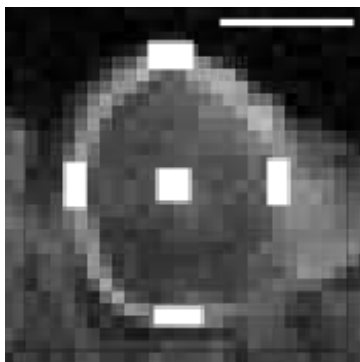


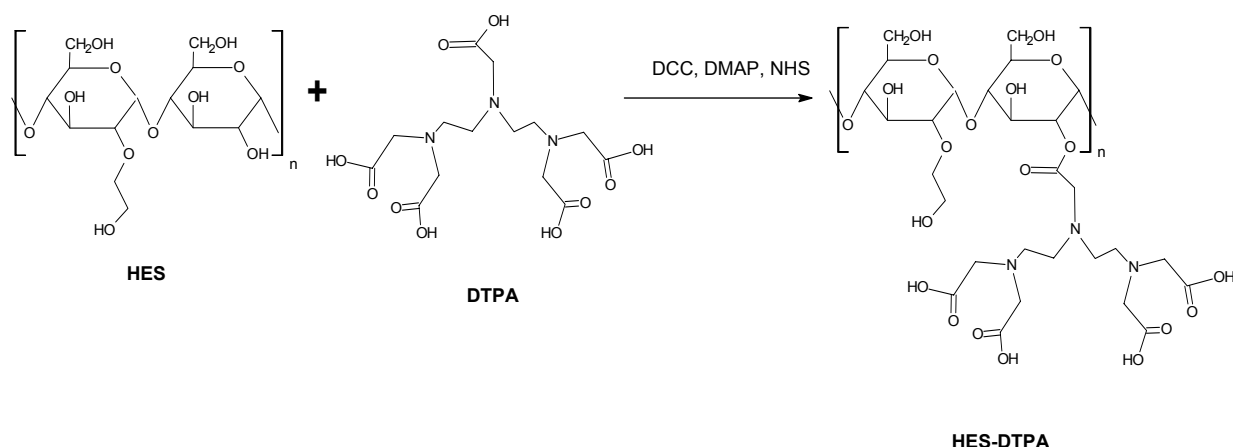
Figure 5.6. A greyscale image of the tumor area, showing the 4 positions of the tumor rim (white bars) and the tumor center (scale bar on top right equals 0.5 cm).

5.3 Results and discussions

5.3.1 ^1H NMR and conductometric titration

For the coupling of DTPA to HES, the esterification using DCC/NHS/DMAP was used as mentioned under HM-HES (see section 3.3.1) It is worth noting that DTPA was not completely soluble in DMF. Upon addition of DMAP, DTPA dissolved with sonication and heating (approximately 70°C for 30-60 min). Due to the fact that DTPA is multifunctional, there is a chance for crosslinking. The use of an excess amount of DTPA in relation to DCC/NHS may reduce the degree of crosslinking. Scheme 5.1 shows the esterification reaction.

Scheme 5.1. Synthesis of HES-DTPA



^1H -NMR was used to determine the degree of esterification of HES with DTPA, as seen in Figure 5.7. When samples were dissolved in D_2O , it was not possible to

assign the peaks for the coupled DTPA due to strong overlapping with the peaks of the polymer backbone. Only the peaks from the protons bound to C1 of the AGU could be unequivocally assigned (peak a), together with an additional peak e. The latter is due to the methylene group of primary alcohols of the polymer backbone which have been esterified. Upon addition of NaOH, peaks for the unbound DTPA can be easily identified, and the peak of the esterified primary alcohols disappears, indicating the hydrolysis of the ester bonds. These spectra were used to determine the molar substitution as seen in Table 5.5.

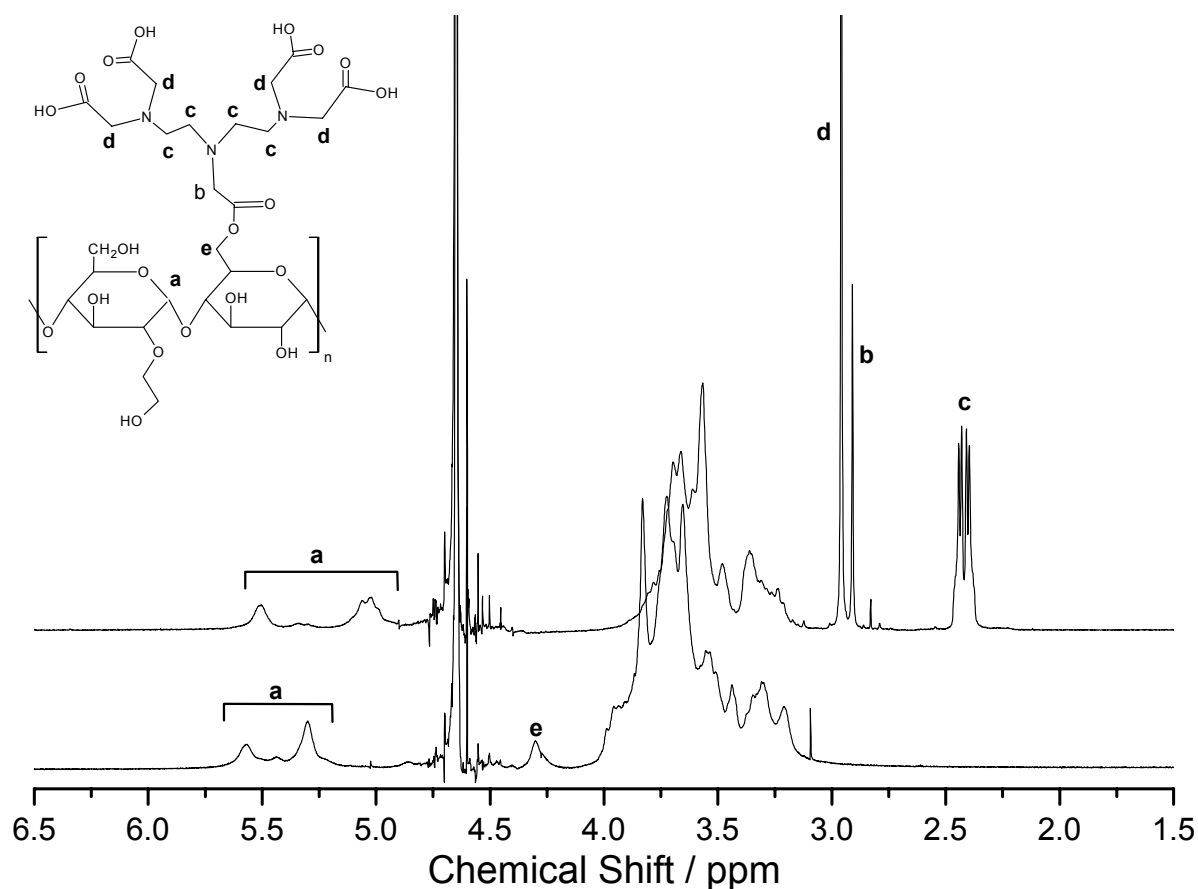


Figure 5.7. ^1H NMR spectrum of HES70-DTPA18 dissolved in D_2O (bottom) and in D_2O plus NaOH (top), together with peak assignment.

Another method was used for the determination of the amount of coupled DTPA, namely conductometric titration. The sharp initial increase in the curve for conductometric titration seen in Figure 5.8 is due to the release of H^+ ions from the DTPA molecule after complexation of Gd^{3+} (see Scheme 5.2). When all the DTPA molecules are saturated by complexing Gd^{3+} , the addition of GdCl_3 leads to an increase in conductivity, however with a clearly lower slope. This can be explained by the large difference in molar conductivity (λ) between the proton ions and the Gd

ions, where it amounts to 349.65, and $201.9 \times 10^{-4} \text{ m}^2\text{Smol}^{-1}$, respectively [20]. Accordingly, the 4 released protons after complexation contribute to the observed large increase in conductivity. It was possible to calculate the amount of Gd complexed per gram of the macromolecule using ^1H NMR and the conductometric titration as seen in Table 5.5, where the results show a good agreement between the 2 methods.

Table 5.5. Molar substitution of the different HES-DTPA conjugates and the amount of Gd complexed per 1 g as determined from ^1H NMR and conductometric titration.

	Molar mass (of original HES) (g/mol)	Molar substitution of DTPA (mol%)	Amount of Gd complexed per 1 g HES-DTPA calculated from ^1H NMR (mMoles)	Amount of Gd complexed per 1 g HES- DTPA from conductometric titration (mMoles) (\pm S.D. in %)
HES70-DTPA18	70,000	18	0.716	0.736 (\pm 0.123 %)
HES70-DTPA25	70,000	25	0.884	0.876 (\pm 0.53 %)
HES200-DTPA20	200,000	20.7	0.7786	0.824 (\pm 9.16 %)

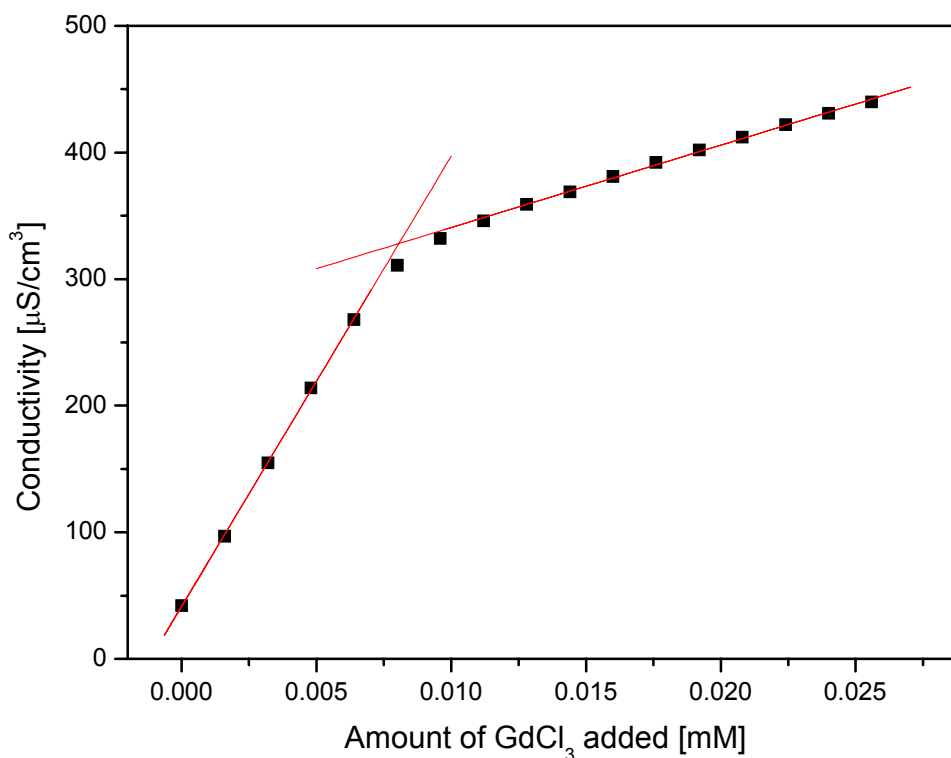
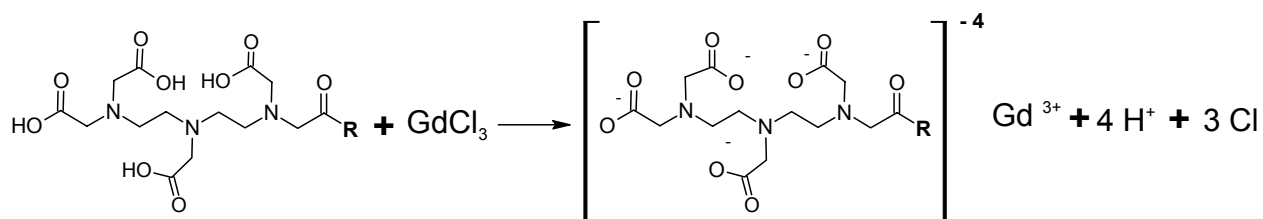


Figure 5.8. Titration of 11.2 mg HES70-DTPA18 with GdCl₃ solution.

Scheme 5.2. Complexation of Gd by HES-DTPA.**5.3.2 Asymmetric flow field flow fractionation (AF4)**

After correction for the moisture content measured by TGA (approximately 8 % w/w), dn/dc was found to be 0.136 for HES70-DTPA18 and HES70-DTPA18-Gd.

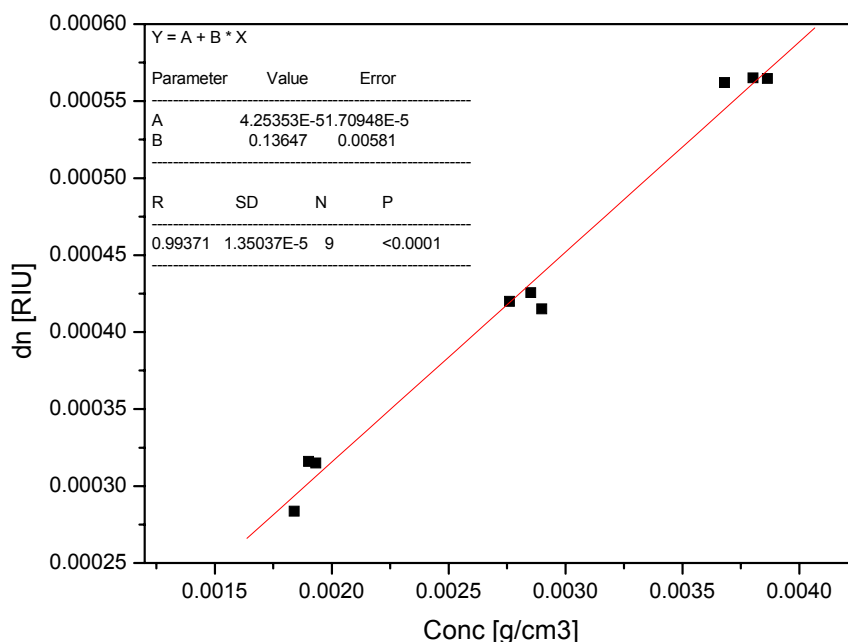


Figure 5.9. Determination of dn/dc for HES70-DTPA18-Gd.

Results for the number average (M_n) and weight average (M_w) molar masses as well as the polydispersity (PDI) and recovery of HES-DTPA and the respective Gd chelates are given in Table 5.6, and are compared to the results of HES70 and HES200 as described in section 2.3.1.3. Upon esterification with DTPA, the molar mass increases considerably, where it reaches approximately 205×10^3 g/mole in case of HES70-DTPA18 and HES70-DTPA24, compared to 69.7×10^3 g/mole for the original HES70. It is worth noting that the recovery is rather low (approximately one half of the sample) indicating that a considerable part of the sample was very large and was thus retained by the $0.2 \mu\text{m}$ filter. Similarly, the measurement of HES200-DTPA20 was not possible, because it could not be filtered through $0.2 \mu\text{m}$ filter.

Rebizak *et al.* reported a considerable increase in the molar mass after the reaction of aminated carboxymethyl dextran with DTPA [21]. They used different methods for the activation of DTPA, including the synthesis of DTPA bisanhydride, the succinimidyl ester of DTPA, and the mixed anhydride. They observed that whatever the activation method used, an increase in the molar mass beyond the theoretically expected level occurred. They attributed this to 2 reasons, namely; a) the intramolecular electrostatic repulsion of the charged macromolecule, and b) polyfunctionalization of DTPA and subsequent crosslinking. A third possible reason is the possibility of formation of self-aggregates, since DTPA is not water soluble. In conclusion, for the DTPA esters of HES, the evaluation of approximately half the sample revealed a considerable increase in molar mass. The rest of the sample was retained by the particle filter due to possible crosslinking/aggregation.

M_w of Gd-HES is clearly higher than that of the original HES, with 205.8×10^3 g/mole for HES70-DTPA18-Gd, 309.7×10^3 g/mole for HES70-DTPA24-Gd, and even more than 3×10^6 g/mole for HES200-DTPA20-Gd. These large molar masses are a clear indication for the occurrence of crosslinking/aggregation. Upon complexation with Gd, there is a marked increase in the recovery up to 80 % w/w, compared to HES-DTPA (see Table 5.6). This increase in recovery is probably due to a decrease in the degree of crosslinking/aggregation, with a subsequent decrease in molecular size and mass, however a direct comparison to the molar mass of HES-DTPA is not possible. Rebizak *et al.* observed a decrease in the molar mass of the aminodextran-DTPA after complexation with Gd, which they attributed to a repulsive electrostatic interaction of the DTPA conjugate, which is masked upon complexation with Gd [21]. Another possible mechanism is the slow metal-catalyzed hydrolysis of the ester bond between DTPA and dextran as reported by Armitage *et al* [22]. The increase in water solubility of the conjugate upon Gd complexation can also decrease the degree of aggregation. All these mechanism could have contributed to a decrease in molar mass, and thus the higher recovery observed for the Gd-containing macromolecular complexes.

Another indicator for the conformational state of the macromolecules can be extracted from Figure 5.13, which shows a plot of the molecular size vs. molar mass for the HES70 derived samples. The slope of this plot is known as the conformational coefficient α derived from Flory's relation between polymer's molar mass and

molecular size (see section 2.3.1.3 for further information) Table 5.6. In the first region of the curve, there is a linear increase in size with molar mass until approximately 10^6 g/mole, after which the slope decreases considerably indicating highly compact structures. The slopes of the curves below 10^6 g/mole are listed in Table 5.6. While the values for the Gd chelating conjugate are quite close to the initial values of the unmodified HES, they are lower for the HES-DTPA conjugate. This points to a more compact structure for the latter, which is probably due to crosslinking or self-aggregation.

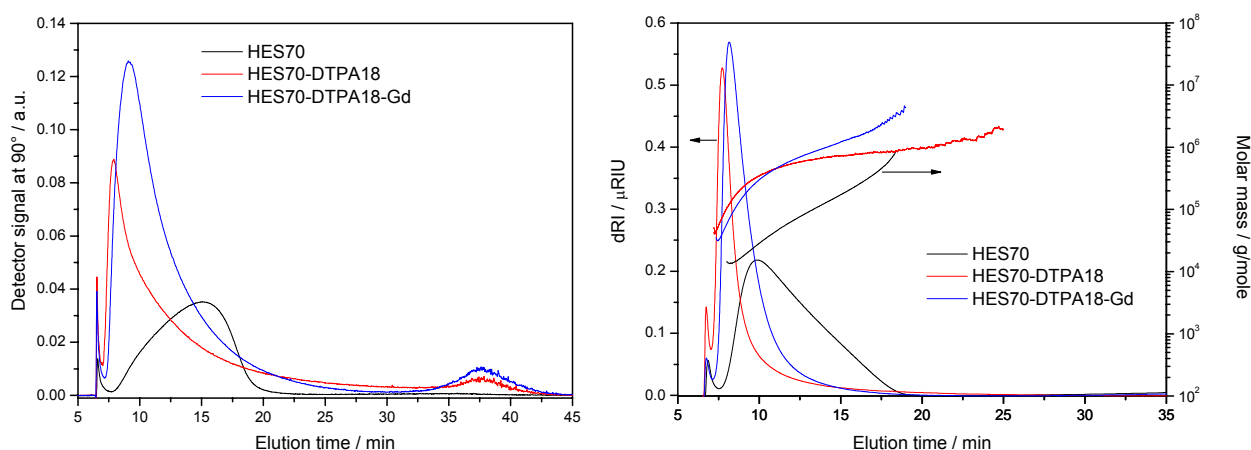


Figure 5.10. AF4 chromatogram for HES70, HES70-DTPA18 and HES70-DTPA18-Gd showing the LS signal (left), and RI signal as well as molar masses (right).

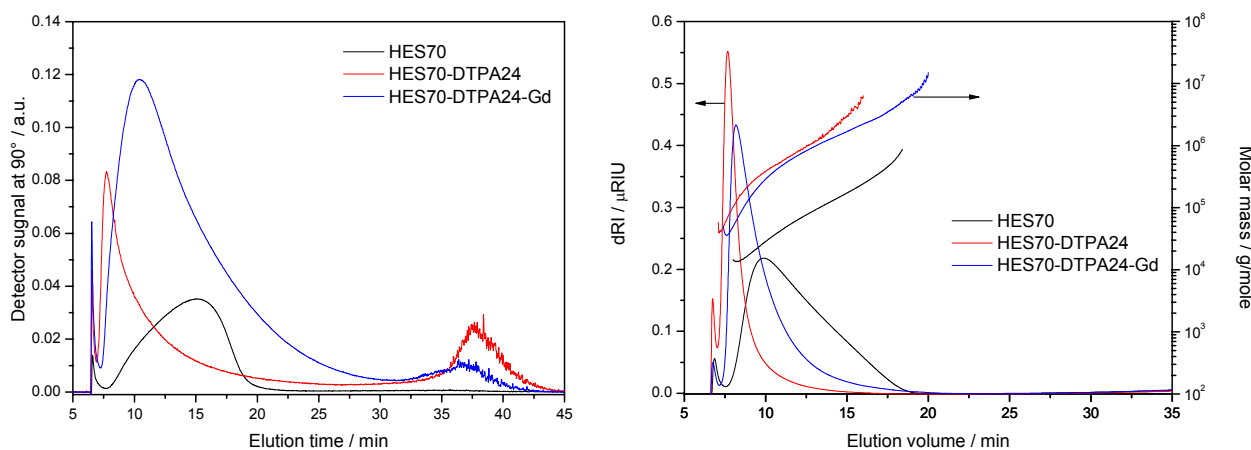


Figure 5.11. AF4 chromatogram for HES70, HES70-DTPA24 and HES70-DTPA24-Gd showing the LS signal (left), and RI signal as well as molar masses (right).

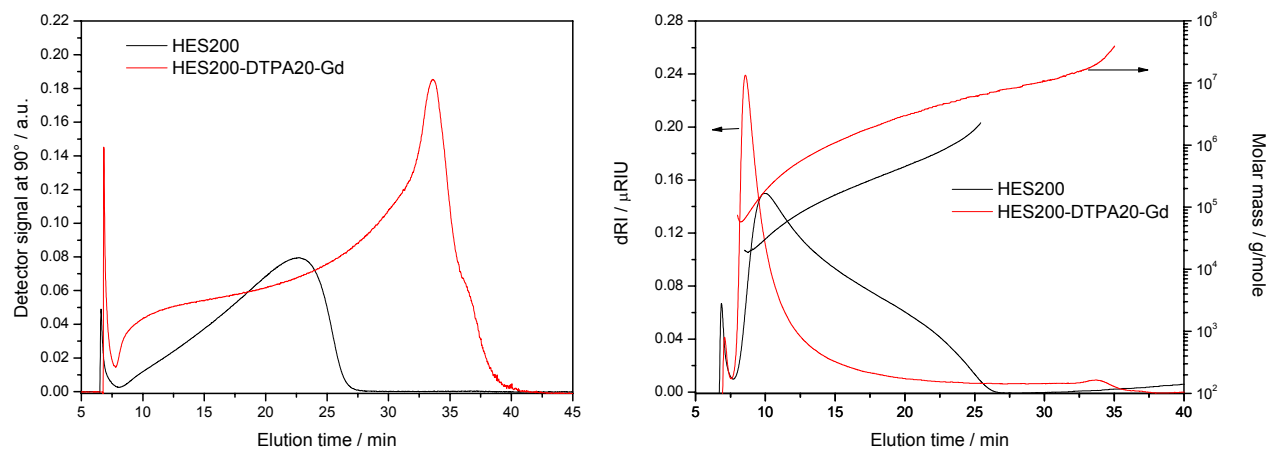


Figure 5.12. AF4 chromatogram for HES200 and HES200-DTPA20-Gd showing the LS signal (left), and RI signal as well as molar masses (right).

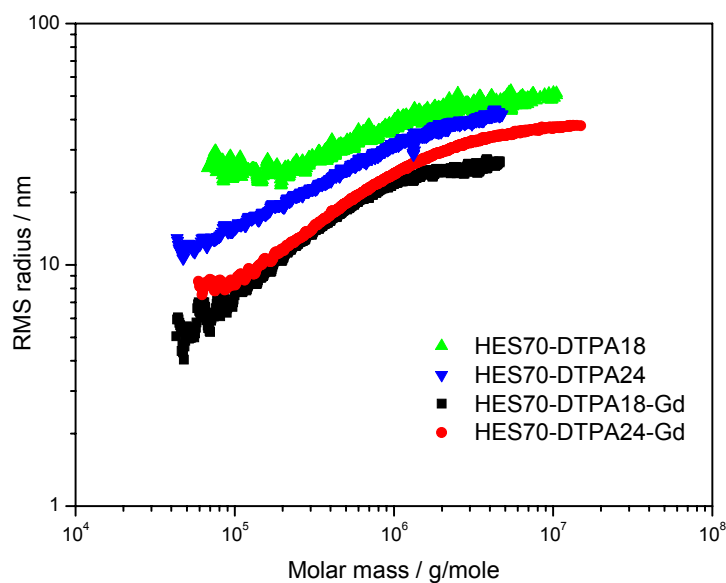


Figure 5.13. A double logarithmic plot of the molar mass vs. RMS radius for the HES70-DTPA conjugates before and after Gd chelation.

Table 5.6. Molar masses, polydispersity and recovery as determined by AF4 coupled to MALS for the HES samples before and after coupling to DTPA and subsequent complexation to Gd.

	M_n (g/mol x 10 ³)	M_w (g/mol x 10 ³)	Polydispersity	Recovery (% w/w)	Conformational coefficient α
HES70	35.8 ± 0.8	69.7 ± 2.2	1.95 ± 0.02	86.1 ± 1.1	0.435
HES200	59.5 ± 1.0	190.3 ± 6.1	3.20 ± 0.11	96.0 ± 1.4	0.424
HES70-DTPA18	94.6 ± 11.7	205.5 ± 29.2	2.17 ± 0.13	54.3 ± 0.08	0.37 ± 0.07
HES70-DTPA24	90.3 ± 9.6	204.9 ± 23.6	2.3 ± 0.2	47.8 ± 0.04	0.36 ± 0.04
HES70-DTPA18-Gd	87.6 ± 4.7	205.8 ± 6.1	2.38 ± 0.03	79.9 ± 0.08	0.44 ± 0.03
HES70-DTPA24-Gd	98.7 ± 1.9	309.7 ± 32.7	3.11 ± 0.29	79.1 ± 0.04	0.47 ± 0.02
HES200-DTPA20-Gd	267.8 ± 140	3,394.3 ± 1,720	12.69 ± 2.5	61.2 ± 20.1	0.41 ± 0.07

5.3.3 Relaxivity

Signal intensity in MRI depends on the local longitudinal relaxation rate $1/T_1$ and transverse relaxation rate $1/T_2$. The signal tends to increase with the increase in $1/T_1$ and to decrease with the increase in $1/T_2$ (see section 5.1.1.4). The longitudinal and transverse relaxivities, r_1 and r_2 , are defined as the increase in $1/T_1$ and $1/T_2$, respectively as a function of the concentration of the paramagnetic agent [8]. Relaxivity can thus be used for an approximate comparison for the efficiency of different contrast agents regarding signal enhancement in MRI.

Results for relaxivity measurements are shown in Figure 5.14 and Table 5.7. The values of r_1 and r_2 for Gd-DTPA (3.53 and 3.99 mM⁻¹s⁻¹, respectively) are close to those reported earlier [8]. When compared to the Gd-HES conjugates, an increase in relaxivity of 2 to 2.5 times can be observed. This increase could be due to one or a combination of reasons [22], namely; a) a decrease of the rotational correlation time due to conjugation to a macromolecule, b) an increase in the number of inner sphere coordinated water and/or their rate of exchange with bulk water, and c) an increase in the number of the outer sphere coordinated water and/or their rate of exchange with bulk water due entrapment by the polysaccharide. One can also observe that the increase in the molar mass of the polymer backbone from 70,000 to 200,000 g/mole

has no significant effect on the relaxivity. Similar results were observed for complexes of Gd with aminodextran-DTPA having different molar masses [23]. This was attributed to the fact that the proton spin relaxation time and the exchange time are short enough to preclude any further decrease in the relaxivity by an increase in molar mass [23]. Another possible explanation is the presence of internal rotations that are similar in the different complexes regardless of the molar mass.

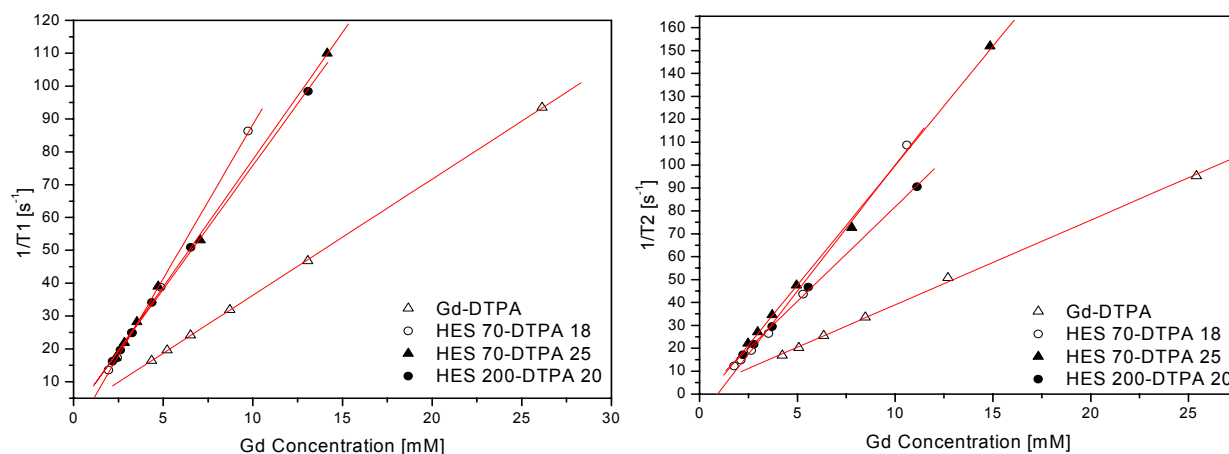


Figure 5.14. Effect of the concentration of Gd on the longitudinal relaxation rate $1/T_1$ (left) and the transverse relaxation rate $1/T_2$ (right).

Table 5.7. Longitudinal relaxivity (r_1) and transverse relaxivity (r_2) for Gd-DTPA and the different Gd-HES samples, measured in phosphate buffer pH 7.4 at 37 °C and 20 MHz.

	Longitudinal relaxivity r_1 ($\text{mM}^{-1} \text{s}^{-1}$)	Transverse relaxivity r_2 ($\text{mM}^{-1} \text{s}^{-1}$)
Gd-DTPA	3.53	3.99
HES 70-DTPA 18	9.4	11
HES 70- DTPA 25	7.74	10.43
HES 200- DTPA 20	7.53	8.261

5.3.4 *In vitro* imaging

Clinical MRI instruments usually operate in the range of 1.5 - 3 T. In addition to being very strong, the magnetic field must also be very stable. To achieve this, electromagnets are used, where the coils are made from superconducting materials that need extremely low temperatures. The use of liquid helium (4 K) thus increases the running costs of the instrument. For research purposes however, a low cost MRI instrument would be highly favourable. Oxford Instruments has recently introduced a low cost, Bench-top 0.5 T MRI instrument. The new instrument uses a permanent magnet, which also decreases the running costs to a large extent. Although the instrument has a relatively low resolution compared with stronger field instruments, it appeared to be quite satisfactory for the purpose of investigating the efficiency of Gd-HES, both *in vitro* and *in vivo*.

Results of the *in vitro* imaging show that in addition to the higher relaxivity and thus higher MRI signal enhancement, the macromolecular contrast agent gives better images than the small molecule of Gd-DTPA. For instance, Gd-HES gives a sharper image of the scaffold after 10 min compared to the Gd-DTPA (see Figure 5.15). Over time, Gd-DTPA diffuses rapidly through the scaffolds, leading to blurred images, while with Gd-HES, a slow diffusion over time is observed, allowing the visualization of details of the internal structure. It is possible to detect channels that extend from the edges to the centre (after 46-56 min). These are important for tissue culture scaffolds, as they can facilitate the mass transfer of nutrients and oxygen, allowing the cells to grow also in the inner parts of the scaffold. Such important details were better seen with the macromolecular contrast agent.

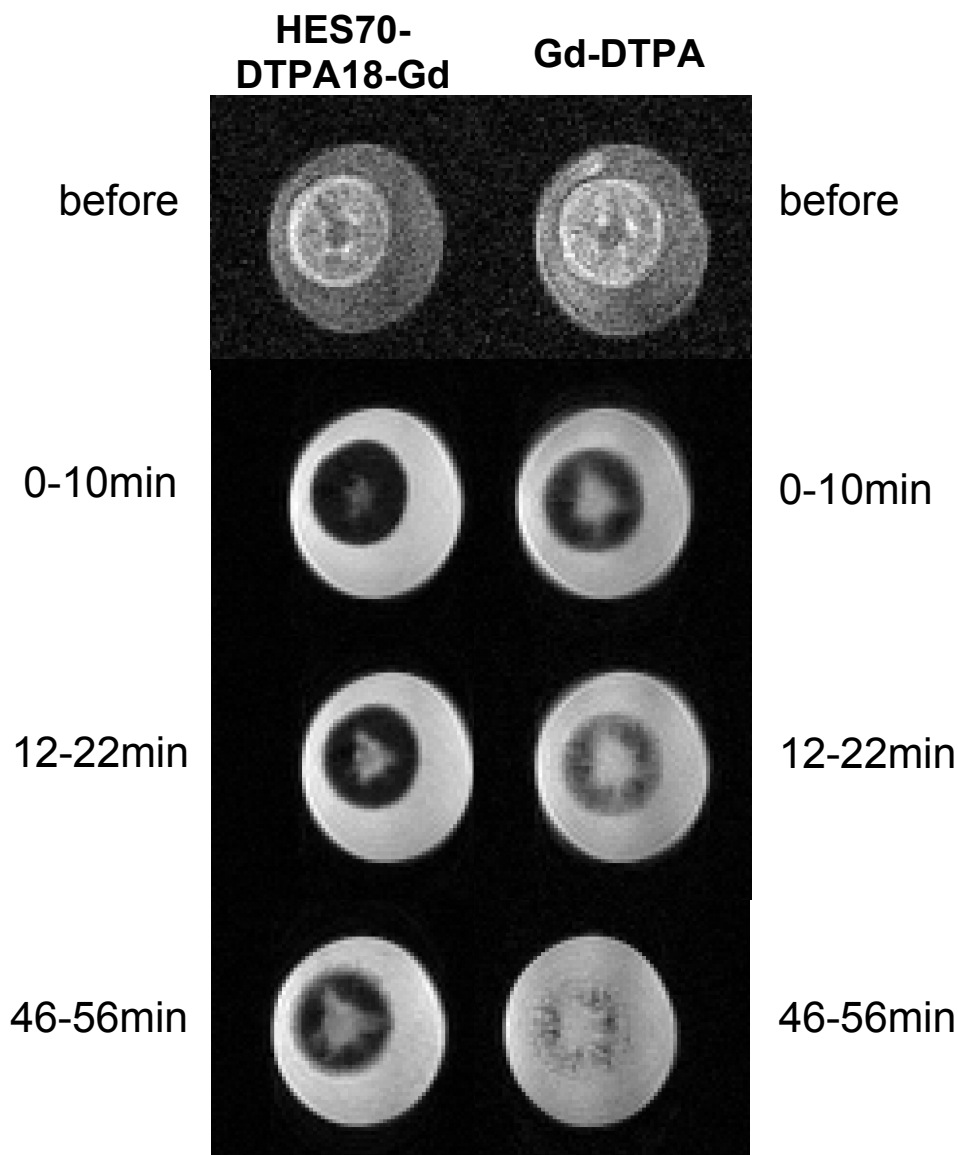


Figure 5.15. In vitro images of chitosan-collagen scaffolds after addition of the MRI contrast agents to the external buffer medium (HES70-DTPA18-Gd to the left, and GD-DTPA to the right).

5.3.5 *In vivo* imaging

Gd chelates are often used as MRI contrast agents for the detection of solid tumors. Although the morphology of contrast-enhanced tumors depends on many factors, such as the tumor type, histological subtype, size, and aggressiveness, it is possible to observe that the tumor rim usually enhances more strongly than the core. This has been observed in human breast cancer [24-26], gliomas, [27], hepatic metastases [28] and musculoskeletal tumors [29, 30]. Using dynamic MRI (i.e. a series of time-dependent images taken rapidly after injection), and after i.v. injection of a low molar mass Gd chelate, an initial rim enhancement is observed, followed by

a washout effect (reduction in the rim enhancement and increase in enhancement of the tumor core). The reason for this peripheral enhancement is because the rim is the advancing front of the tumor, where the process of angiogenesis is actively taking place, leading to better vascularization. By contrast, the core can become hypoxic, leading to fibrosis or necrosis. Furthermore, the core of the tumor is known to have a higher interstitial pressure, and thus any convection-driven transport would actually take place from the core (high pressure) to the periphery of the tumor (lower pressure) [31]. The following washout effect is due to diffusion of the low-molar-mass contrast agents into the core, since they can easily leave the blood pool and permeate into the interstitial tissues.

It is worth noting that such an MRI morphological pattern (the rim enhancement) is so characteristic for solid tumors, that it can be used for the differentiation between malignant and benign masses, where in the latter case, a rather homogenous contrast enhancement is observed all over the benign mass [29]. It has also been suggested to give a rough estimate for the aggressiveness of breast cancer [24].

Macromolecular MRI contrast agents are expected to have a long circulation time and be confined to the blood pool. This should give a longer time window for imaging and pathology-revealing images, since they normally have a limited tissue perfusion. For instance, Daldrup *et al.* [32] have shown that, the macromolecular contrast agent, in this case an albumin-(Gd-DTPA) conjugate, is more specific in differentiating between benign and malignant masses, and in staging of a mammary tumor model in rats than the gadopentate dimeglumine. These effects were related to the macromolecular hyperpermeability of the microvessels in malignancies. The latter are disorganized and perforated, with the degree of disorganization increasing with increasing malignant tumor grade [32]. Meanwhile, a comparison between albumin-(Gd-DTPA) and a cascade polymer developed by Schering AG, Berlin, Germany was carried out to test their ability to identify moderately leaky vasculature (subcutaneously planted adenocarcinoma) and severely compromised vasculature (reperfused infarcted myocardium) [33]. The cascade polymer being smaller than 30,000 g/mole and having a globular shape was not as effective as the albumin conjugate in identifying the case of mildly increased vascular permeability, as it is not exclusively confined to the blood pool and may leak through normal vasculature [33].

Figures 5.16a & b shows the MRI images of the nude mice carrying subcutaneously implanted coloncarcinoma cell lines (DLD-1 (left side) and HT29 (right side)) before and after i.v. injection of 150 μ l of 8 % w/v HES70-DTPA18-Gd. Panels a-c in Figure 5.16a show the transaxial images for the kidneys. Due to the use of a short TR, the images are considered to be T1-weighted. Before injection of the contrast agent, it is possible to identify a dark renal sinus and a brighter renal cortex. The former usually contains urine, which, being a liquid, has a long T1 and thus appears dark. After injection of Gd-HES, an inversion of the contrast could be seen, where the renal sinus looks much brighter than the cortex (See Figure 5.16a). The signal enhancement of the renal sinus is 4-5 times that before Gd-HES injection and extends over nearly 5 h. After 8 h, the enhancement of the renal sinus returns back close to the state before injection. Meanwhile, the increase in signal enhancement for the cortex is lower, where it reaches twice as much as the original state and also goes back to normal after 8 h. These results point to long circulation time of Gd-HES. It also points to the elimination of Gd-HES through the kidneys, although a detailed study for the amount eliminated through the kidneys and other pathways is necessary. However, these results show that an application of Gd-HES to image the urinary tract seems quite feasible.

Panels a-c in Figure 5.16b show the 2 subcutaneous tumors before and after injection of Gd-HES. After injection, a clear and persistent rim enhancement can be observed in the HT29 tumor for more than 3 hours. Moreover, a central accumulation of the contrast agent in tumor HT29 can be seen in panel c, which is quite evident after 8 h. Although the contrast enhancement of the rim of DLD-1 tumor is not as strong as HT29, it is still possible to discern the tumor rim. In panel c, it is even possible to identify 3 lobes inside the DLD-1 tumor. The latter is not possible to identify after 8 h, probably due to the diffusion of the contrast agent to the tumor center. Tozera *et al.* used multi-photon fluorescence microscopy to investigate the vascular network of some tumors including HT29 [34]. They could show that the latter has a highly vascularized periphery, with vessels that extend to the center (see Figure 5.17). This explains the strong peripheral enhancement observed in the MRI measurements. To the best of the author's knowledge, no similar investigation for the vascular network of DLD-1 tumors is available in the literature for comparison.

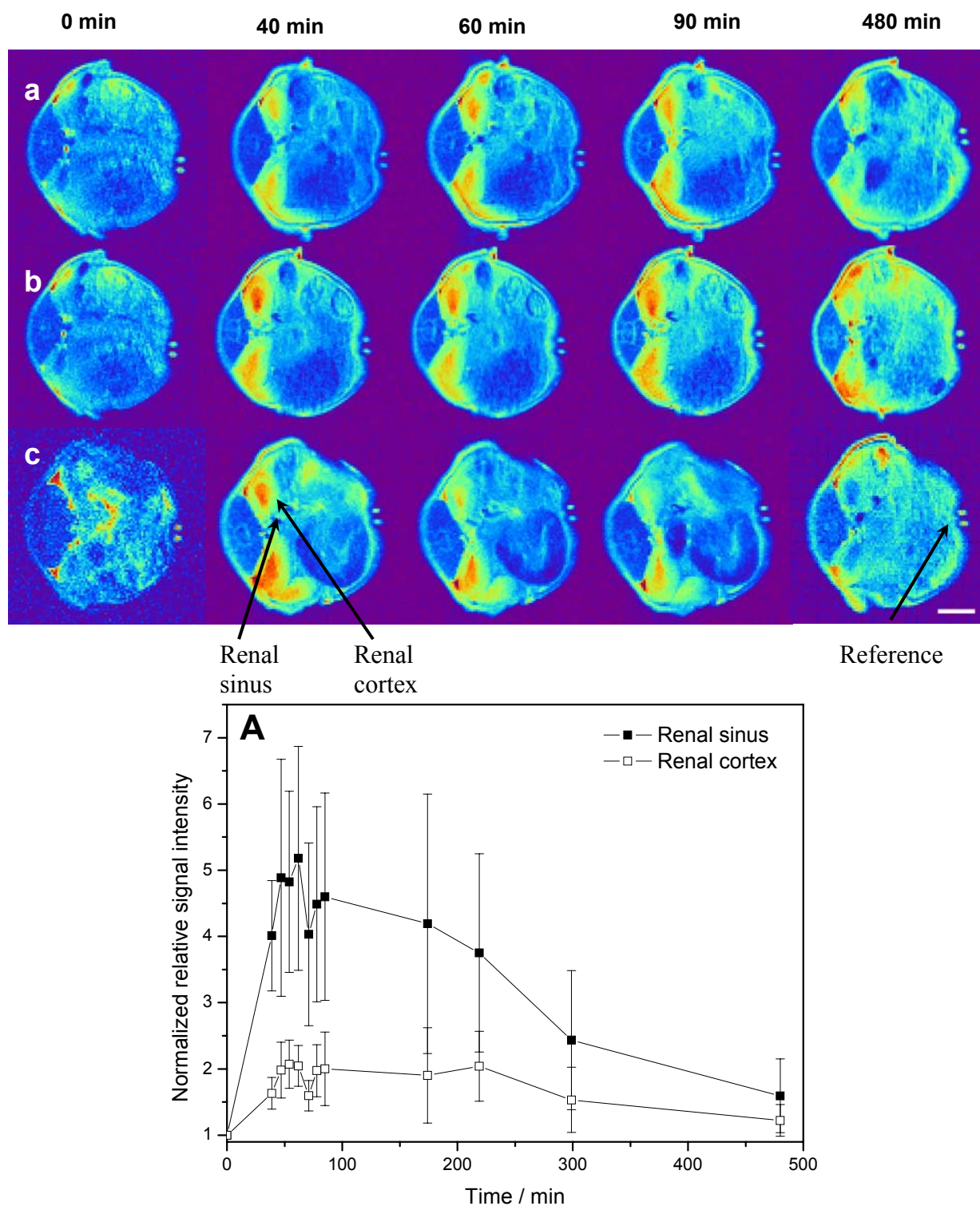


Figure 5.16a. Axial MRI sections (3 mm thick) in nude mice 30 days after s.c. injection of 2 human colon carcinoma cell lines; DLD-1 (down) and HT29 (up). The animals were injected with 150 μ l of HES 70-DTPA 18-Gd solution (polymer conc. 8 % w/v, ca. 0.03 mmol Gd/Kg). Panels a-c show images of the kidneys in 3 different mice (scale bar equals 0.5 cm). Graph A shows the normalized relative signal intensity in the renal sinus and cortex after Gd-HES injection.

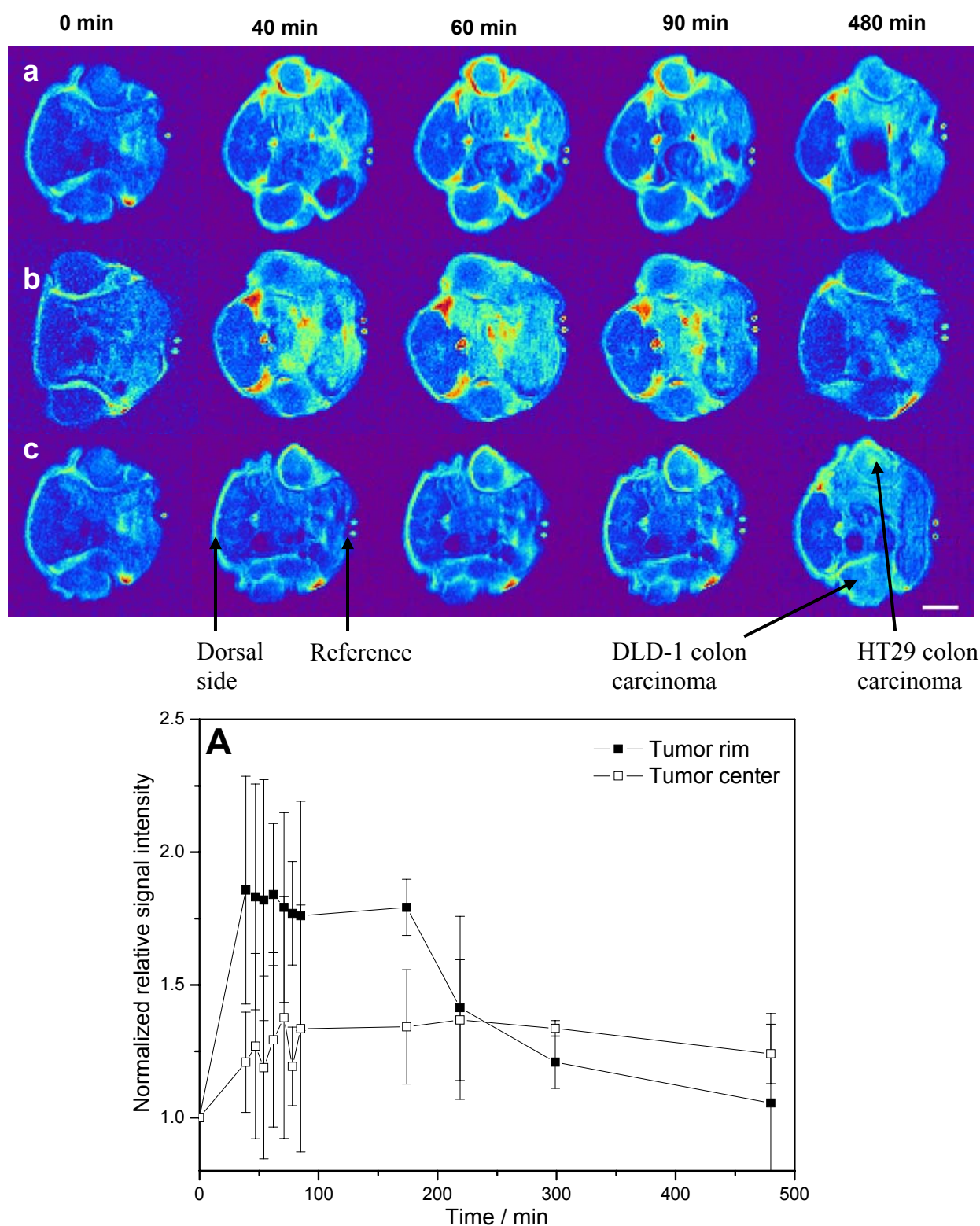


Figure 5.16b. Axial MRI sections (3 mm thick) in nude mice 30 days after s.c. injection of 2 human colon carcinoma cell lines; DLD-1 (down) and HT29 (up). The animals were injected with 150 μ l of HES 70-DTPA 18-Gd solution (polymer conc. 8 % w/v, ca. 0.03 mmol Gd/Kg). Panels a-c show images of the tumor area in 3 different mice (scale bar equals 0.5 cm). Graph A shows the normalized relative signal intensity in the rim and center of the HT29 tumor.

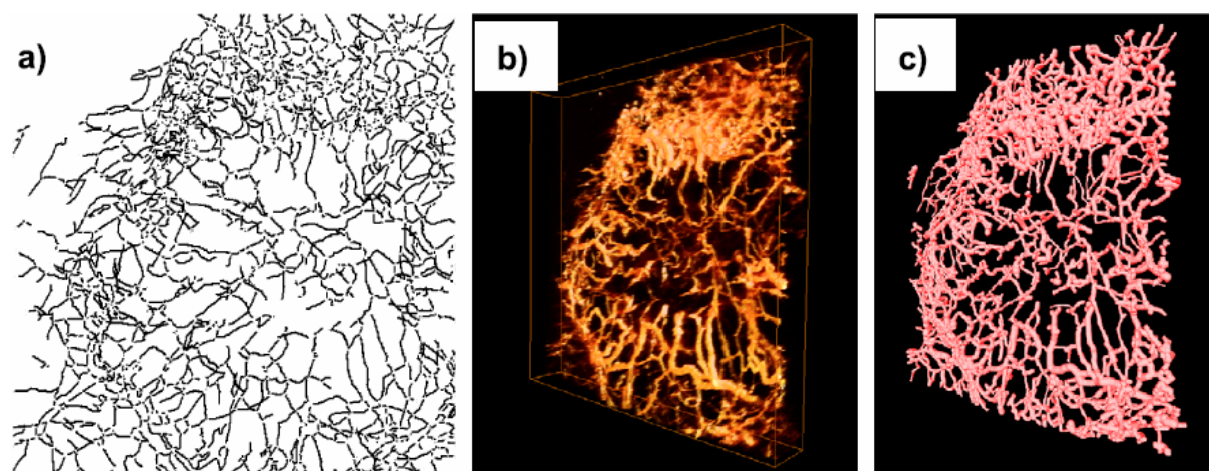


Figure 5.17. 3D image reconstructions for HT29 tumor. Image (a) shows all vascular traces projected onto the 2D x–y plane. The maximum and the orthogonal tumor diameter in the x-y plane is 1.4 x 1.3 mm. Image (b) shows the original volume-rendered data, and image (c) shows the surface-rendered images of vascular networks following vascular tracing and diameter measurements (from reference [34]).

By contrast, the signal enhancement of Gd-BOPTA is very much less and is over a much shorter time interval as seen in Figure 5.18 a and b. The enhancement of the renal sinus, as seen in panel a-c in Figure 5.18a, is quite limited and the signal enhancement is back to the original state in less than 40 min. Additionally, no significant tumor-rim enhancement could be seen in panels a-c in Figure 5.18b. The possible reason for this is the rapid elimination of Gd-BOPTA, and the necessity to obtain the images within the first 2 min after injection of the contrast agent [35], while in this case, the first image was taken 20 minutes after injection.

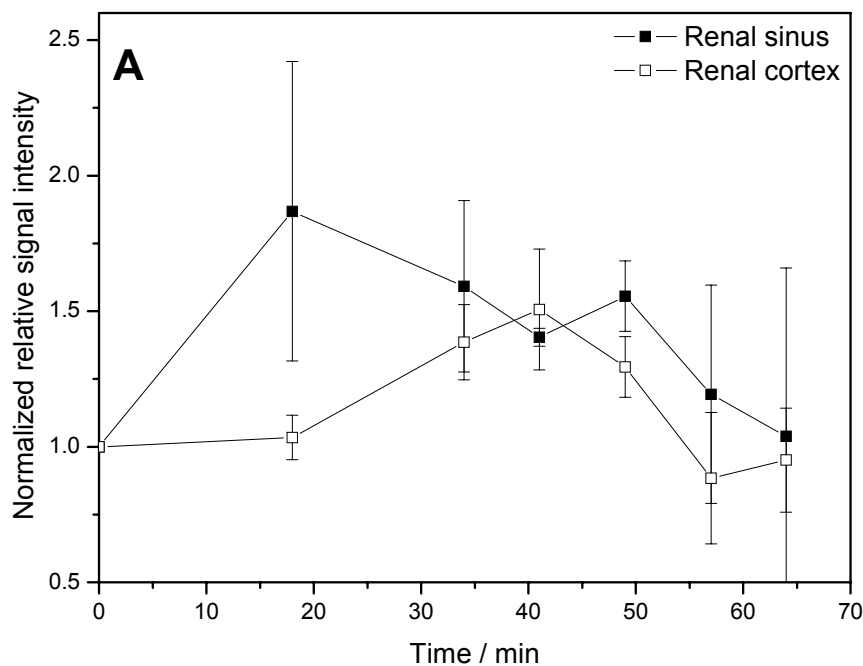
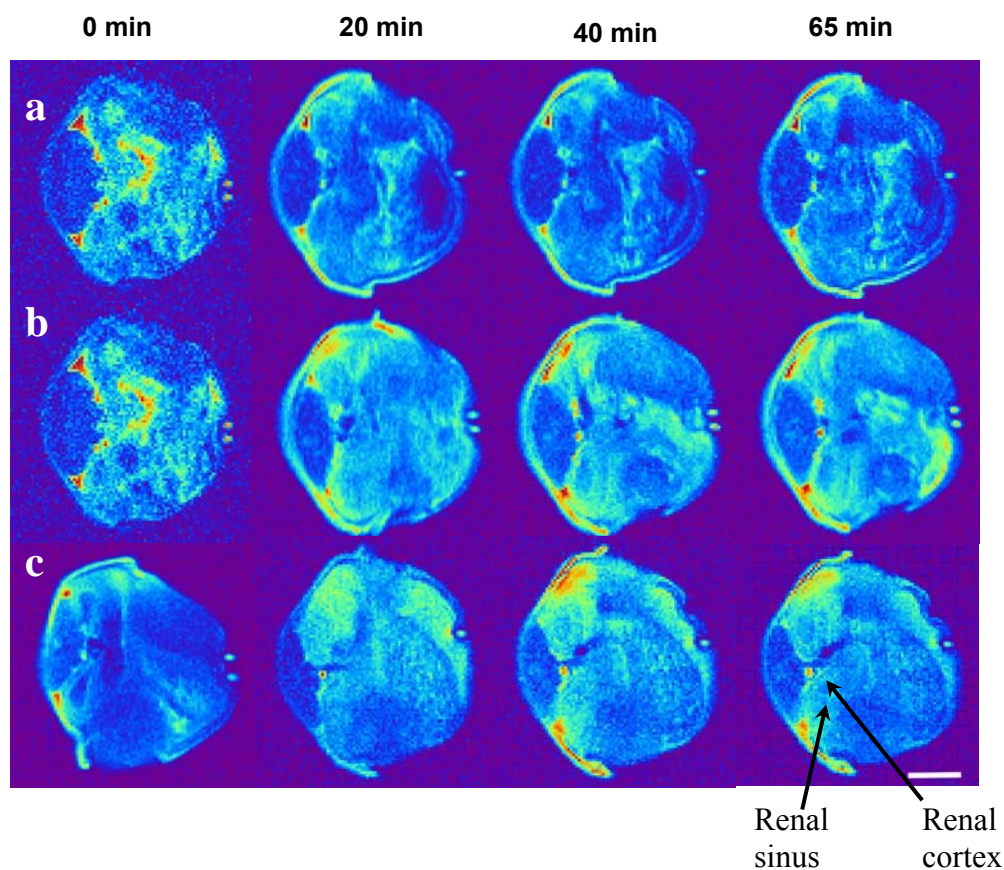


Figure 5.18a. Axial MRI sections (3 mm thick) in nude mice 30 days after subcutaneous injection of human colon carcinoma cell lines; namely DLD-1 (down) and HT29 (up). The animals were injected with 150 μ l of 5 mMol/l Multihance[®] (0.03 mmol Gd/Kg). Panels a-c show images of the kidneys in 3 different mice (scale bar equals 0.5 cm). Graph A shows the normalized relative signal intensity in the renal sinus and cortex after Multihance[®] injection.

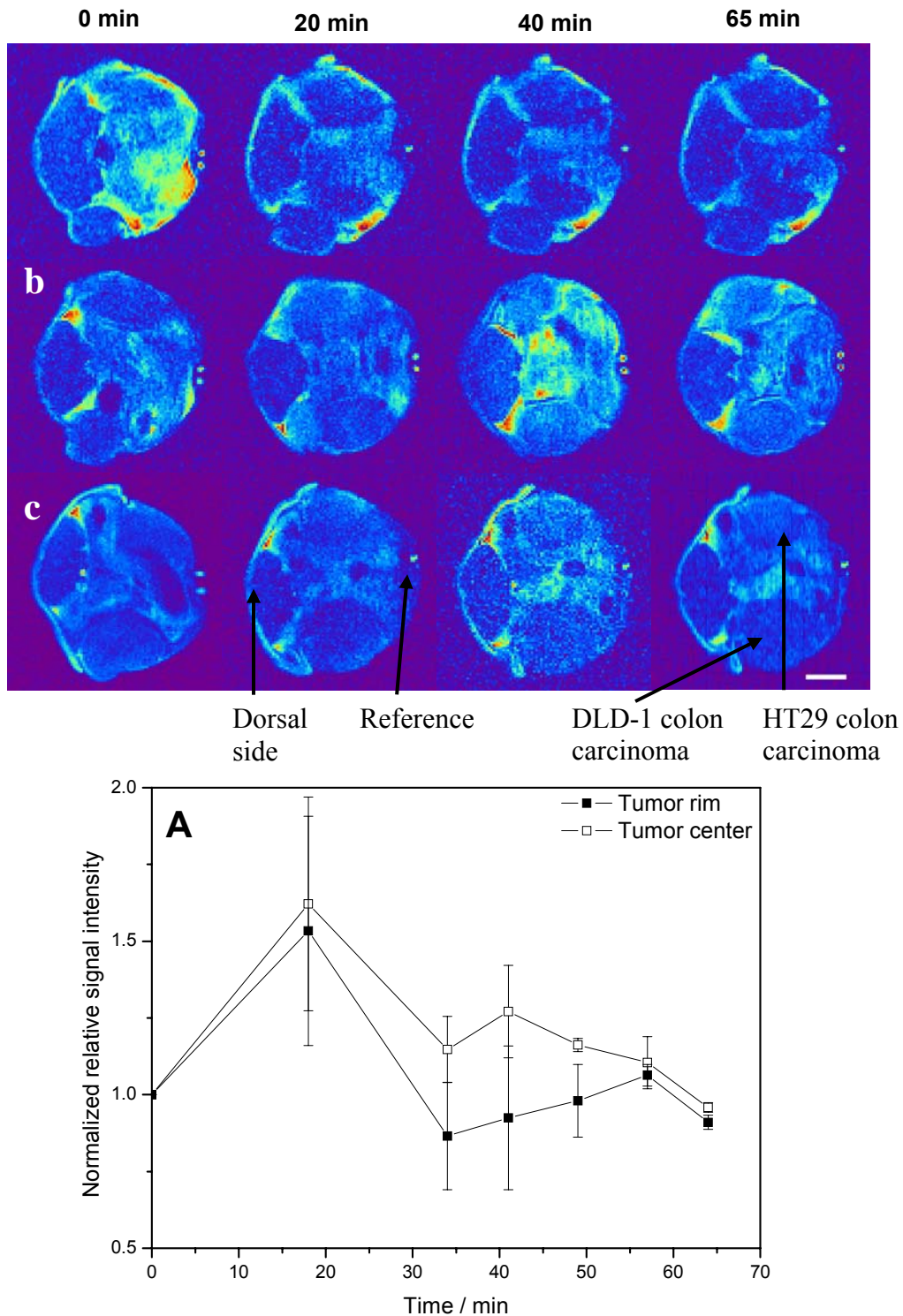


Figure 5.18b. Axial MRI sections (3 mm thick) in nude mice 30 days after subcutaneous injection of human colon carcinoma cell lines; namely DLD-1 (down) and HT29 (up). The animals were injected with 150 μ l of 5 mMol/l Multihance[®] (0.03 mmol Gd/Kg). Panels a-c show images of the tumor area in 3 different mice (scale bar equals 0.5 cm). Graph A shows the normalized relative signal intensity in the rim and center of the HT29 tumor.

Figure 5.19 shows the results of using Gd-HES as a blood pool contrast agent as compared to the low molar mass Gd-BOPTA. While the Gd-HES contrast agent produced a clearly strong contrast allowing the visualization of the heart as well as the carotid artery and the jugular vein (see the insert in Figure 5.19, Gd-BOPTA did not. Moreover, Gd-HES clearly circulated in the blood for an extended period of time, and could be detected in the circulation even after more than 2.5 h from injection.

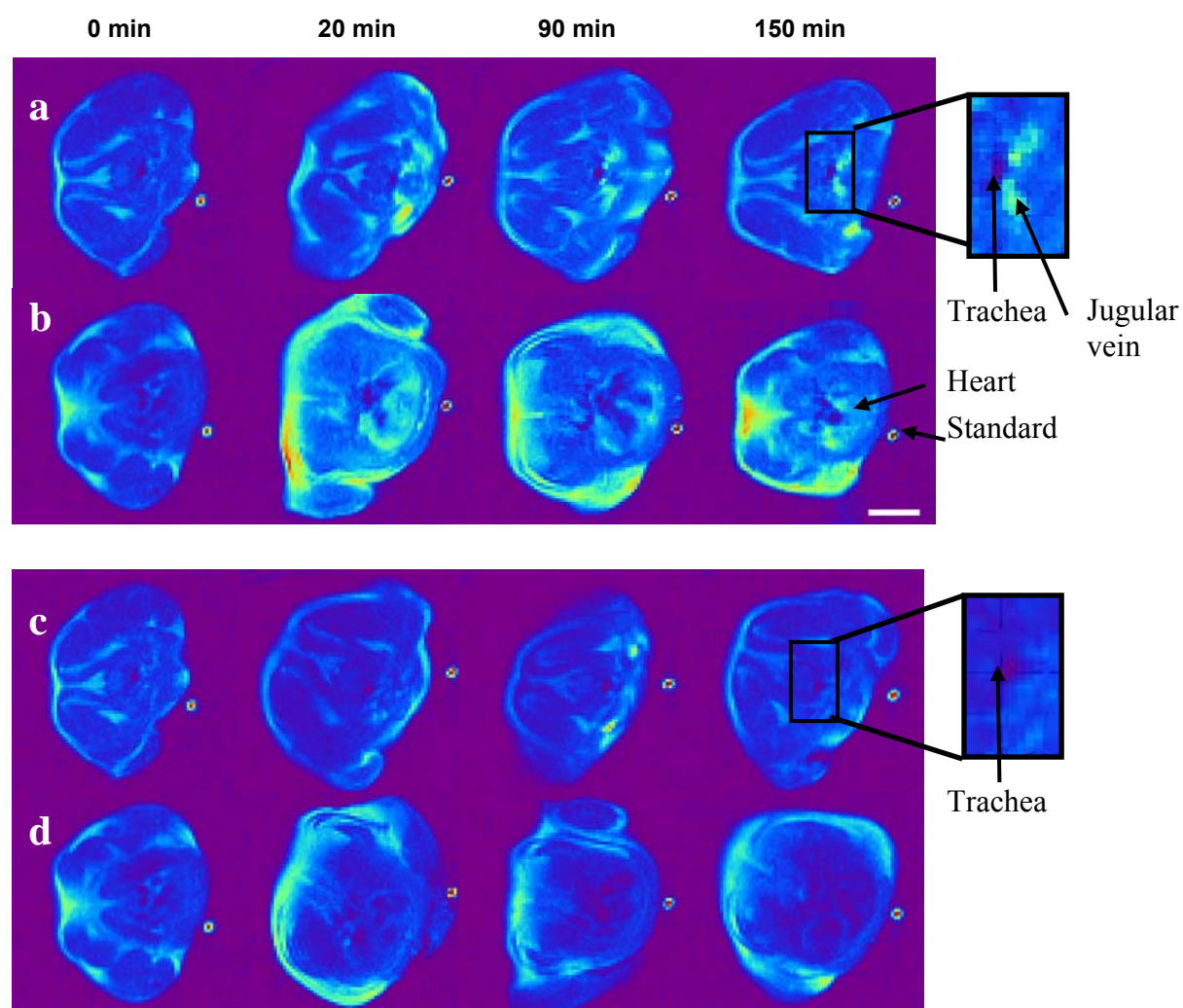


Figure 5.19. MRI images of Balb/c mice after injection of HES 70-DTPA 18-Gd (panels a and b) or Gd-BOPTA (panels c and d). Panel a and c show the neck region, where the insert show a magnification for the trachea, the jugular vein and the carotid arteries. Panel b and d are for the thorax showing the heart (scal bar equals 0.5 cm).

5.4 Conclusions and outlook

HES was esterified with DTPA using DCC, DTPA and NHS, to get samples with different molar masses and different degrees of modification. Using $^1\text{H-NMR}$ and conductometric titration, the molar substitution of DTPA was found to be between 18-24 mol%. The average molar mass M_w , and the distribution were analysed using AF4 coupled to MALS. Results show that the molar mass and polydispersity of HES-DTPA conjugate increased considerably compared to the original HES. This is attributed to the intermolecular repulsion between the charged groups, as well as possible crosslinking due to polyactivation of the multifunctional DTPA. Upon complexation with Gd, both the molar mass and polydispersity decreased, due to the disappearance of the electrostatic repulsion, and a possible slow metal catalysed hydrolysis of the ester bond. Relaxivity of the macromolecular Gd conjugate was compared with that of Gd-DTPA, and was found to be 2-2.5 times that of the latter, pointing to a better efficiency in signal enhancement. *In vitro* imaging of a tissue engineering scaffold using GD-HES produced higher quality images as compared to Gd-DTPA. The slow diffusion of the macromolecular contrast agent allowed a clear identification of the internal structure of the scaffold. *In vivo* experiments concentrated on applying Gd-HES for angiography and tumor localization. The large molar mass of GD-HES allowed its confinement to the blood pool, thus giving very good images for carotid arteries and jugular veins as well as the heart for longer than 2.5 h. In case of solid tumors, a clear rim enhancement of the human colon carcinoma cells injected subcutaneously in nude mice could be observed, even after nearly 5 h from injection. In general, the low molar mass counterpart (Gd-BOPTA) was eliminated within 40 min after injection, and was not suitable for angiography. Moreover, the animals seemed to tolerate the Gd-HES better than Gd-BOPTA, since the animals lost weight upon repeated administration of the latter but not the former. In brief, these results suggest that Gd-HES is a novel biodegradable macromolecular contrast agent with possible applications in the clinical settings.

5.5 References

- [1] P.C. Lauterbur, Image formation by induced local interactions: Examples employing nuclear magnetic resonance. *Nature* 242 (1973) 190-191.
 - [2] P.V. Prasad, *Magnetic resonance imaging - Methods and biological applications*, Humana Press, New Jersey, USA, 2006.
 - [3] V. Kuperman, *Magnetic Resonance Imaging - Physical Principles and Applications*, Academic Press, New York, 2000.
 - [4] T. Barrett, H. Kobayashi, M. Brechbiel, P.L. Choyke, Macromolecular MRI contrast agents for imaging tumor angiogenesis. *European Journal of Radiology* 60 (2006) 353–366.
 - [5] D. Weishaupt, V.D. Köchli, B. Marincek, *How does MRI work?- An introduction to the physics and function of magnetic resonance imaging.*, Springer Verlag, Germany, 2006.
 - [6] P. Storey, in: P. V. Prasad (Ed.), *Magnetic resonance imaging - Methods and biological applications*, Humana Press, New Jersey, USA, 2006, pp. 3-57.
 - [7] M.H. Levitt, *Spin dynamics: Basics of nuclear magnetic resonance*, John Wiley and Sons, New York, USA, 2001.
 - [8] P. Caravan, J.J. Ellison, T.J. McMurry, R.B. Lauffer, Gadolinium(III) Chelates as MRI Contrast Agents: Structure, Dynamics, and Applications. *Chemical Reviews* 99(9) (1999) 2293-2352.
 - [9] H.J. Weinmann, R.C. Brasch, W.R. Press, G.E. Wesbey, Characteristics of gadolinium-DTPA: a potential NMR contrast agent. *American Journal of Roentgenology* 142 (1984) 619.
 - [10] J.-H. Kim, K. Park, H.Y. Nam, Seulki Lee, K. Kim, I.C. Kwon, Polymers for Bioimaging. *Progress in Polymer Science* 32 (2007) 1031–1053.
 - [11] W.J.M. Mulder, G.J. Strijkers, G.A.F.v. Tilborg, A.W. Griffioen, K. Nicolay, Lipid-based nanoparticles for contrast-enhanced MRI and molecular imaging. *NMR in Biomedicine* 19 (2006) 142–164.
 - [12] H.C. Schwickert, T.P.L. Roberts, A. Mühler, M. Stiskal, F. Demsar, R.C. Brasch, Angiographic properties of Gd-DTPA-24-cascade-polymer -- a new macromolecular MR contrast agent. *European Journal of Radiology* 20 (1995) 144-150.
-

-
- [13] M.D. Ogan, U. Schmiedl, M.E. Moseley, W. Grodd, H. PaaJanen, R.C. Brasch, An intravascular contrast-enhancing agent for magnetic resonance blood pool imaging: preparation and characterization. *Investigative Radiology* 22 (1987) 665–671.
- [14] L.J. Kroft, J. Doornbos, S. Benderbous, A. de Roos, Equilibrium phase MR angiography of the aortic arch and abdominal vasculature with the blood pool contrast agent CMD-A2-Gd-DOTA in pigs. *Journal of Magnetic Resonance Imaging* 9 (1999) 777-785.
- [15] P. Loubeyre, E. Canet, S. Zhao, S. Benderbous, M. Amiel, D. Revel, Carboxymethyl-dextran-gadolinium-DTPA as a blood-pool contrast agent for magnetic resonance angiography. Experimental study in rabbits. *Investigative Radiology* 31 (1996) 288-293.
- [16] H. Kobayashi, M.W. Brechbiel, Nano-sized MRI contrast agents with dendrimer cores. *Advanced Drug Delivery Reviews* 57 (2005) 2271– 2286.
- [17] K.C.P. Li, L.R. Pelc, S.A. Napel, M.L. Goris, David T. Lin, C.K. Song, A.N. Leung, G.D. Rubin, M.D. Hollett, D.P. Harris, MRI of Pulmonary Embolism using Gd-DTPA-Polyethylene glycol polymer enhanced 3d fast gradient echo technique in a canine model. *Magnetic Resonance Imaging* 15(5) (1997) 543-550.
- [18] X.X. Wen, E.F. Jackson, R.E. Price, E.E. Kim, Q.P. Wu, S. Wallace, C. Charnsangavej, J.G. Gelovani, C. Li, Synthesis and characterization of poly(L-glutamic acid) gadolinium chelate: A new biodegradable MRI contrast agent. *Bioconjugate Chemistry* 15(6) (2004) 1408-1415.
- [19] W.-M. Kulicke, U. Kaiser, D. Schwengers, R. Lemmes, Measurements of the refractive index increment on hydroxyethyl starch as a basis for absolute molecular weight determinations. *Starch* 43(10) (1991) 392-396.
- [20] D.R. Lide, *CRC Handbook of Chemistry and Physics*, 85th edition, CRC Press, Boca Raton, Florida, 2004.
- [21] R. Rebizak, M. Schaefer, E. Dellacherie, Polymeric Conjugates of Gd³⁺-Diethylenetriaminepentaacetic Acid and Dextran. 1. Synthesis, Characterization, and Paramagnetic Properties. *Bioconjugate Chemistry* 8 (1997) 605-610.
- [22] F.E. Armitage, D.E. Richardson, K.C.P. Lis, Polymeric Contrast Agents for Magnetic Resonance Imaging: Synthesis and Characterization of Gadolinium Diethylenetriaminepentaacetic Acid Conjugated to Polysaccharides. *Bioconjugate Chemistry* 1(6) (1990) 395-374.
-

-
- [23] R. Rebizak, M. Schaefer, E. Dellacherie, Polymeric Conjugates of Gd³⁺-Diethylenetriaminepentaacetic Acid and Dextran. 2. Influence of Spacer Arm Length and Conjugate Molecular Mass on the Paramagnetic Properties and Some Biological Parameters. *Bioconjugate Chemistry* 9 (1998) 94-99.
- [24] C.K. Kuhl, MRI of breast tumors. *European Radiology* 10 (2000) 46-58.
- [25] S. Mussurakis, P. Gibbs, A. Horsman, Peripheral enhancement and spatial contrast uptake heterogeneity of primary breast tumours: Quantitative assessment with dynamic MRI. *Breast Imaging* 22(1) (1998) 35-46.
- [26] L.D. Buadu, J. Murakami, S. Murayama, N. Hashiguchi, S. Sakai, S. Toyoshima, K. Masuda, S. Kuroki, S. Ohno, Patterns of peripheral enhancement in breast masses: Correlation of findings on contrast medium enhanced MRI with histologic features and tumor angiogenesis. *Breast Imaging* 21(3) (1997) 421-430.
- [27] C. Tsien, D. Gomez-Hassan, R.K.T. Haken, D. Tatro, L. Junck, T.L. Chenevert, T. Lawrence, Evaluating changes in tumor volume using magnetic resonance imaging during the course of radiotherapy treatment of high-grade gliomas: Implications for conformal dose-escalation studies. *International Journal of Radiation Oncology Biology and Physics* 62(2) (2005) 328-332.
- [28] D.G. Mitchell, S. Saini, J. Weinreb, E.E.D. Lange, V.M. Runge, J.E. Kuhlman, Y. Parisky, C.D. Johnson, J.J. Brown, M. Schnall, R.J. Herfkens, P.L. Davis, D. Gorczyca, G. Sica, G.S. Foster, M.E. Bernardino, Hepatic metastases and cavernous hemangiomas: Distinction with standard- and triple-dose gadoteridol-enhanced MR imaging. *Radiology* 193 (1994) 49-57.
- [29] L.D. Ma, F.J. Frassica, E.F. McCarthy, D.A. Bluemke, E.A. Zerhouni, Benign and malignant musculoskeletal masses: MR imaging differentiation with rim-to-center differential enhancement ratios. *Radiology* 202(3) (1997) 739-744.
- [30] M.J.A. Geirnaerd, J.L. Bloem, H.-J.v.d. Woude, A.H.M. Taminiau, M.A. Nooy, P.C.W. Hogendoorn, Chondroblastic osteosarcoma: characterisation by gadolinium-enhanced MR imaging correlated with histopathology. *Skeletal Radiology* 27 (1998) 145-153.
- [31] R.K. Jain, Delivery of molecular and cellular medicine to solid tumors. *Advanced Drug Delivery Reviews* 46 (2001) 149-168.
- [32] H. Daldrup, D.M. Shames, M. Wendland, Y. Okuhata, T.M. Link, W. Rosenau, Y. Lu, R.C. Brasch, Correlation of dynamic contrast enhanced MR imaging with histologic
-

- tumor grade: Comparison of macromolecular and small-molecular contrast media. *American Journal of Roentgenology* 171 (1998) 941-949.
- [33] H.C. Roberts, M. Saeed, T.P.L. Roberts, A. Muhler, D.M. Shames, J.S. Mann, M. Stiskal, F. Demsar, R.C. Brasch, Comparison of albumin-(Gd-DTPA)₃₀ and Gd-DTPA-24-cascade-polymer for measurements of normal and abnormal microvascular permeability. *Journal of Magnetic Resonance Imaging* 7(2) (1997) 331-338.
- [34] G.M. Tozera, S.M. Ameer-Begb, J. Bakera, P.R. Barberb, S.A. Hilla, R.J. Hodgkissb, R. Locke, V.E. Prisea, I. Wilsona, B. Vojnovic, Intravital imaging of tumour vascular networks using multi-photon fluorescence microscopy. *Advanced Drug Delivery Reviews* 57 (2005) 135-152.
- [35] E.A. Morris, Breast cancer imaging with MRI *Radiologic Clinics of North America* 40(3) (2002) 443-466.
-

PART IV

Enzymatically-catalyzed

HESylation

Chapter 6

Enzymatically- catalyzed HESylation using microbial transglutaminase: Proof of feasibility

6.1 Introduction

Polymer-protein conjugation is one of the successful approaches for the formulation and delivery of therapeutic proteins [1]. The multitude of therapeutic proteins, produced from the current biotech revolution, usually have some limitations, such as short circulation time, poor stability and immunogenicity [2]. The chemical conjugation of these proteins to water soluble polymers leads to a number of advantages, including an increase in the circulation time, protection from digestion by proteolytic enzymes, reduced recognition by antibodies and reduced immunogenicity [3]. The standard polymer for this application is polyethylene glycol (PEG), and the PEGylation of proteins lead to a number of polymer-protein conjugates being currently in the market, such as PEG adenosine deaminase, PEG L-asparaginase and PEG interferon [1]. The success of PEGylation lead many researches to test other polymers including poly (hydroxypropyl methacrylamide), poly(acrylic acid), poly(maleic acid), poly(vinyl alcohol), albumin and dextran [4-6]. Despite the fact that PEG is not biodegradable, no other polymer was found to have a superior performance so far.

In general, there are several chemical approaches to couple proteins to polymers [2, 3]. However, many of them can have deteriorating effects with the very sensitive and fastidious protein molecules [7]. Accordingly, enzymatic procedures were

proposed and tested as a gentle alternative to the chemical coupling. Among these, the microbial transglutaminase-catalyzed reaction has earned a great deal of attention for site specific conjugation [8]. Transglutaminases (TG) catalyze an acyl transfer between the γ -carboxamide group of a glutaminy residue (acyl donors) and a variety of primary amines (acyl acceptors), including the amino group of lysine [9]. In mammals, there are 6 isolated and characterized isoenzymes of TG, including the blood clotting factor XIIIa, keratinocyte TG, and tissue TG [10]. These TGs play an important role in blood clotting, wound healing, epidermal keratinization and stiffening of the erythrocyte membrane [10]. They need Ca^{2+} for their activation at concentrations higher than the normal physiological levels, i.e. they are normally inactive, and are activated only in case of the disruption of the homeostasis. They also show a strict specificity in recognising the glutamine residues, but a poor specificity for the amine group [10].

To be able to commercially use TG for protein cross-linking, a constant supply was needed. Accordingly, 5000 microorganisms were screened for TG activity [9]. A variant of *Streptomyces mobaraensis* was found to secrete an enzyme with high TG activity [9]. This microbial transglutaminase (MTG) is composed of 331 amino acids, with a single Cys residue at the bottom of a deep cleft of the molecule. It is believed that this Cys⁶⁴ residue is an essential part of the active site of the enzyme. Contrary to eukaryotic TG, MTG is rather small, with a molar mass of 38 kDa [9], while the former is between 77-90 kDa [10]. More importantly, MTG shows some advantages over eukaryotic TG, namely; (i) it is calcium-independent and (i) has lower specificity requirements [9]. Accordingly, it has found a number of applications in the food industry for crosslinking meat and fish products [9]. For instance, legume globulins, wheat globulins, egg yolk and albumin proteins, actins, myosins, fibrins, milk caseins, α -lactalbumin and β -lactoglobulin could be crosslinked with MTG [9]. It is thus used to produce restructured meat and fish by binding together small pieces of meat. It can also be used in the production of yogurt by cross-linking milk casein, or tofu, by its action on the soybean proteins [9].

In biomedical applications, MTG was used to immobilize enzymes, or to couple therapeutic proteins to water-soluble polymers [8]. Sato *et al.* provided a clear demonstration for the power of using MTG in protein-polymer conjugation, when they used it to couple aminated PEG selectively to one glutamine residue (Gln74) of the

recombinant human interleukin-2 [11]. Other therapeutic proteins that can act as substrates for MTG include human growth hormone [12], human interleukin 6, and human interferon- α [11]. Fontana *et. al* have recently reviewed the interplay between the catalytic activity of MTG and the substrate structural characteristics that favour such site-specificity [12]. Other enzymes and polypeptides were coupled to aminated polymers (other than PEG) such as aminated dextran [13], gum arabic [14], carboxymethyl cellulose and Ficoll [15].

With the aim of studying the feasibility of using MTG for HESylation, this study reports the modification of HES with hexamethylene diamine (HMDA) as well as N-Carbobenzyloxy glutaminy glycine (Z-QG) to act as a substrate for MTG (both as acyl acceptor and acyl donor, respectively), and the reaction of the modified HES with model compounds. For these reactions, a recently prepared recombinant MTG (rMTG) carrying 6 histidine residues at the C- terminus is used [16, 17]. The histidine tag (His-tag) facilitates the work up and separation of the products, and provides the possibility for immobilization of enzymes without loss of activity [18].

6.2 Experimental

6.2.1 Materials

HES 70 (M_w 70 kDa) was a gift from Serumwerke Bernburg, Germany. Dicyclohexyl carbodiimide (DCC), N-hydroxysuccinimide (NHS), tosyl chloride, hexamethylenediamine (HMDA), N,N-dimethylcasein (DMC), and monodansyl cadaverine (MDC) were purchased from Sigma-Aldrich, Germany. 4-(dimethylamino)pyridine (DMAP) was purchased from Merck, Germany. N-carbobenzyloxy glutaminy glycine (Z-QG) was purchased from Bachem AG, Switzerland. Dithiothreitol (DTT) was purchased from Carl Roth GmbH, Germany. All other solvents and chemicals were reagent grade and were used as received.

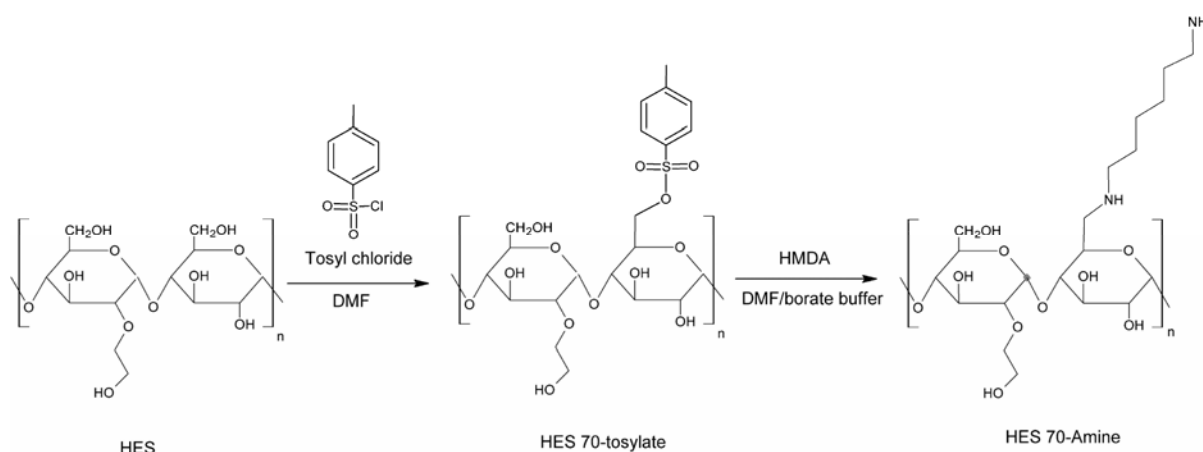
6.2.2 HES carrying a lysine component: Modification of HES with hexamethylenediamine to produce HES 70-Amine

The synthesis of aminated HES was carried out according to the procedure of Ehrenfreund-Kleinman *et al.* with some modifications [19] (Scheme 6.1). 1 gram HES 70 was dried at 105 °C for 2 h. The dried HES was dissolved in 10 ml dry DMF + 1 ml triethylamine at 60 °C. Tosyl chloride (0.5 g) was dissolved in 1 ml dry DMF. Both

solutions were cooled on ice to 0 °C, and protected from light. Tosyl chloride solution was added gradually to the HES solution and stirred at 0 °C. After 1 h, the solution was precipitated in 100 ml cold acetone, filtered and washed with another 100 ml acetone. The precipitate was dissolved in water and dialysed against distilled water for 3 days (MWCO 6-8 kDa, Spectrapor, U.S.A.), then lyophilized.

From the prepared HES tosylate, 200 mg were dissolved in 30 ml DMF/borate buffer pH 10 (1:2), then an excess of HMDA (500 mg) dissolved in 10 ml DMF/borate buffer (1:2) was added to the HES solution and stirred overnight. The solution was precipitated in 200 ml isopropanol/methanol mixture (1:1 by volume), filtered and washed with 100 ml of the precipitating solvent. The precipitate was air dried at room temperature for 2 days.

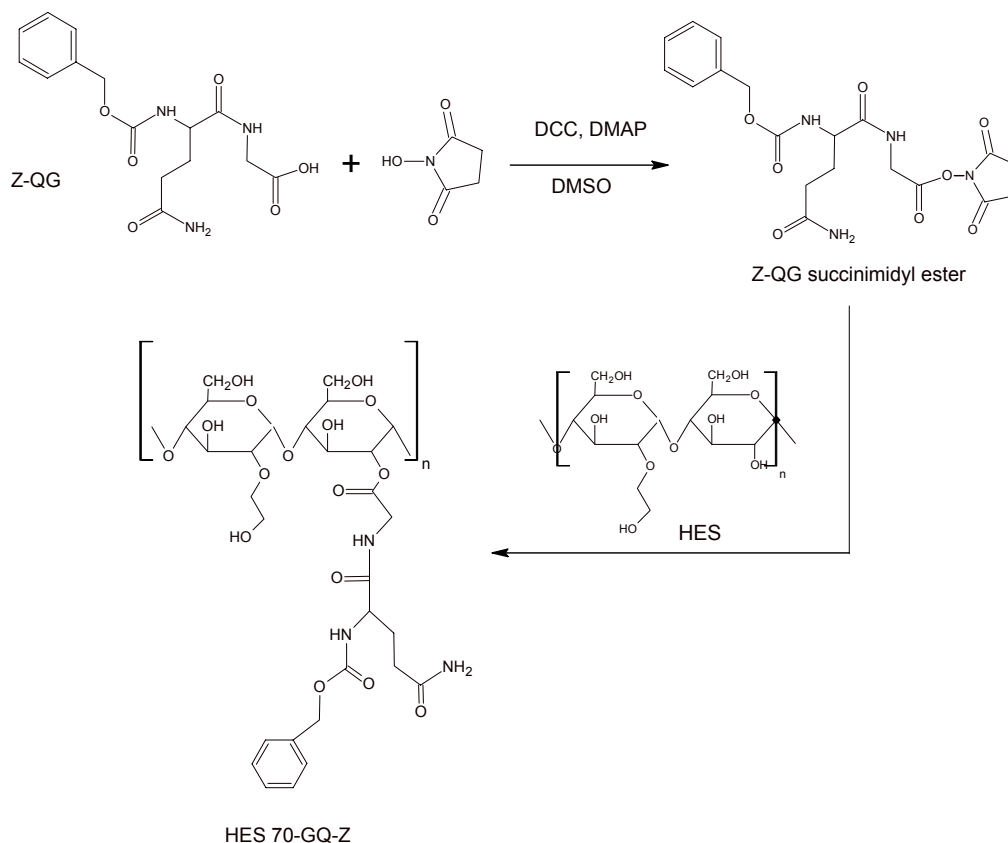
Scheme 6.1. Preparation of HES 70-Amine.



6.2.3 HES carrying a glutaminy component: Modification of HES with N-carbobenzyloxy glutaminy glycine (Z-QG) to produce HES 70-GQ-Z

In 2 ml dry DMSO, 185 mg Z-QG, 114 mg DCC, 66 mg DMAP, and 64 mg NHS were dissolved successively. After stirring at room temperature and 400 rpm for 24 h, the solution was filtered to remove the insoluble by-product of the reaction, dicyclohexylurea (DCU), while the filtrate contained an activated form of Z-QG, namely; its succinimidyl ester. No further purification was needed for the activated dipeptide, since the reaction does not yield interfering side products. The filtrate was directly added to 1 g HES 70 (5.4 mM AGU) dissolved in 10 ml DMSO, and stirred for 6 h. The solution was then dialyzed against distilled water for 3 days (MWCO 6-8 kDa, Spectrapor, U.S.A.), filtered then lyophilized. Scheme 2 shows this 2-step reaction.

Scheme 6.2. Preparation of HES 70-GQ-Z in 2 steps.



6.2.4 ^1H NMR

For ^1H NMR measurements, 50 mg polymer samples were dissolved in 600 μl D_2O and measured at 400 MHz (Gemini 2000, Varian Inc., USA).

6.2.5 Preparation of rMTG

A histidine-tagged pro-MTG is produced by soluble expression in *E. coli* as mentioned elsewhere [17]. The cultivation of *E. coli* BL21(DE3) pDJ1-3 was carried out in a batch process using the auto-induction method. The cells were disintegrated by high pressure homogenization, and then MTG was obtained from pro-MTG by TAMEP, the endogenous protease from *Streptomyces mobaraensis*, and then purified by immobilized metal affinity chromatography (IMAC)

6.2.6 Reaction of HES 70- GQ-Z with monodansyl cadaverine (MDC)

MDC, a fluorescent dye carrying an alkyl amino group, was coupled to HES 70-GQ-Z using rMTG, where 25 μl of 5 mM MDC solution in 0.1 M acetic acid were added to 75 μl of 1 % w/v solution of HES 70-GQ-Z dissolved in 0.1 M Tris buffer pH 8. One hundred μl of rMTG in glycerin (activity 15 U/ml) were added to this mixture and incubated at 37 $^\circ\text{C}$ for 1 h, after which the sample was separated by sodium

dodecylsulfate poly(acrylamide) gel electrophoresis (SDS-PAGE) according to the method of Laemmli [20] using a Mighty Small apparatus from Hoefer (Amersham Biosciences, Germany). The gels were examined under UV light (excitation filter 365 nm, emission filter 520 nm). A number of control experiments were carried out simultaneously, where 0.5 % w/v dimethylcasein (DMC) was allowed to react with MDC in the presence of rMTG as a positive control. Similarly, unmodified HES was tested if it could bind MDC in the presence of rMTG, and HES 70-GQ-Z was tested if it could bind MDC in the absence of rMTG.

6.2.7 Reaction of HES 70- Amine with dimethyl casein (DMC)

One hundred μ l of HES 70-Amine (5 mg/ml) were added to 100 μ l of DMC (5 mg/ml) both dissolved in 0.1 M Tris buffer pH 8. To this mixture, 100 μ l of rMTG were added and the sample incubated at 37 °C for 1 h. Samples were taken at 10, 20, 30 and 60 min, boiled with sample buffer for 3 min, and finally separated by SDS-PAGE (as above) and stained with Coomassie blue. A negative control investigated the possibility of crosslinking DMC with rMTG in the absence of HES 70-Amine. As a positive control, rMTG was used to crosslink 0.2 % w/v human serum albumin (HSA) in 10 mM DTT to prove that rMTG is active.

6.3 Results and discussion

There are more than 20 patents describing the conjugation of HES to different molecules, including low molar mass drugs, polypeptides and polynucleotides [21-33]. These patents describe the use of chemical reactions for the coupling of HES, usually through its reducing end group. For instance, the reducing end group (aldehyde group) is reacted with a protein amino group to form a Schiff's base [34], or is oxidized to a carboxylic group, either chemically [34] or enzymatically [26], and then forms an amide bond with a protein's amino group. These methods may have detrimental effects on sensitive proteins, and may not be sufficiently selective. Accordingly, an enzymatic coupling method using microbial transglutaminase (MTG) was studied and evaluated as reported here.

Several researches have modified macromolecules using different protein tags or functional groups to act as substrates for MTG. The most common is the functionalization with an amine group to act as acyl acceptor. Ohtsuka *et al.* [35]

found that for primary amines to act as MTG substrates, the alkyl chain should contain more than 4 carbon atoms. That is why hexamethylene diamine was chosen for this study. Other routes include the functionalization with a lysine-containing tag [7, 36], N-terminal glycine [37], or a glutamine-containing tag [38, 39].

^1H NMR spectroscopy was used to evaluate the extent of modification of HES as seen in Figure 6.1 and 6.2. To determine the percentage of molar substitution (MS, number of molecules bound to 100 AGUs) for HES 70-Amine, the relation between peak **a**, representing the protons at C1 of the AGU (5.2-5.6 ppm), and peak **c**, representing 2 methylene protons (1.4-1.6 ppm) was used (Figure 6.1). MS for HES 70-Amine was found to be 3.9 mol%. Similarly, in case of HES 70-GQ-Z, the relation between peak **a** (the protons at C1 of the AGU) and peak **c** for the protons of the phenyl ring (7.35 ppm) was used (Figure 6.2). MS for HES 70-GQ-Z was found to be 4.6 mol%. Although Z-QG was not soluble in water, HES 70-Q was completely soluble in water, PBS pH 7.4 and tris buffer pH 8 (up to the maximum concentration tested, which is 1 % w/v). Similarly, HES 70-K was soluble in water, PBS and tris buffer.

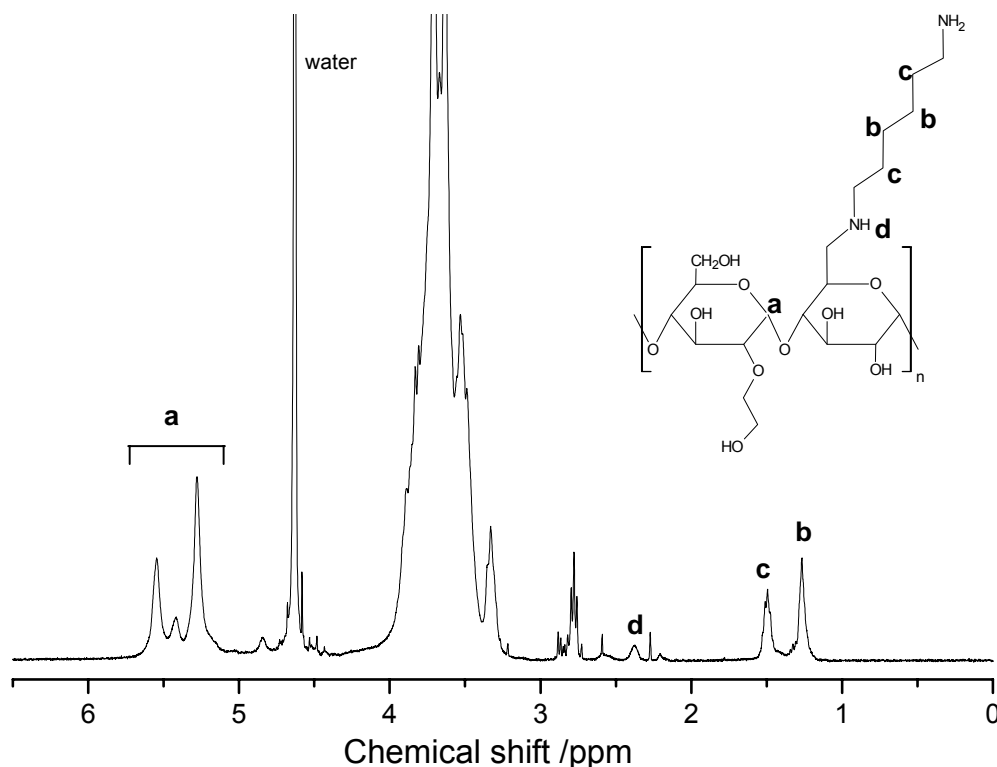


Figure 6.1. ^1H NMR spectrum of HES 70-Amine dissolved in D_2O with peak assignment. The broad peak between 3.3 and 4.1 ppm belongs to the protons of the polymer backbone.

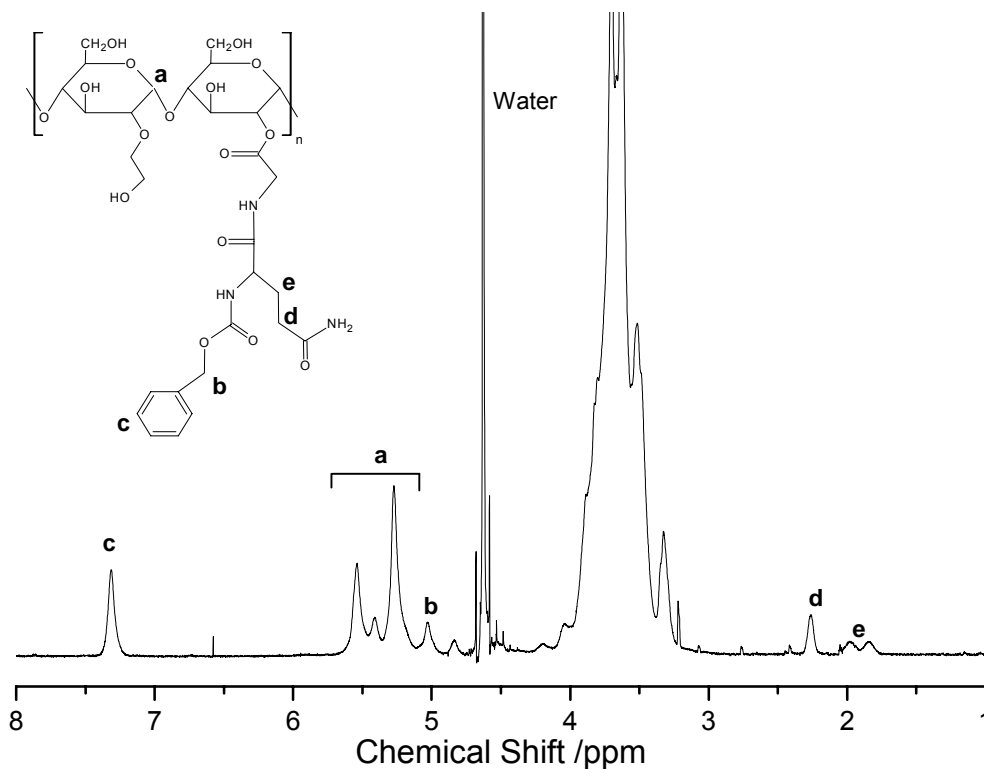


Figure 6.2. ^1H NMR spectrum of HES 70-GQ-Z dissolved in D_2O with peak assignment. The broad peak between 3.3 and 4.1 ppm belongs to the protons of the backbone.

MDC is a known substrate for MTG, acting as acyl acceptor, and is usually used to test whether a protein can act as an acyl donor for MTG [26]. Indeed, the reaction of MDC and HES 70-GQ-Z catalyzed by the rMTG lead to a successful conjugation, as evidenced by the presence of high molar mass fluorescent molecules after gel electrophoresis (see Figure 6.3). It is worth mentioning that, contrary to the positive control trace of DMC which shows a clear band for the protein (lane 4), that for HES extends over a large distance due to its high polydispersity (lane 1). The control experiments show that, neither the unmodified HES can undergo this reaction in the presence of rMTG (lane 2), nor can HES 70-GQ-Z in the absence of rMTG (lane 3), indicating that the modification of HES succeeded in making HES 70-GQ-Z an accepted acyl donor for the rMTG.

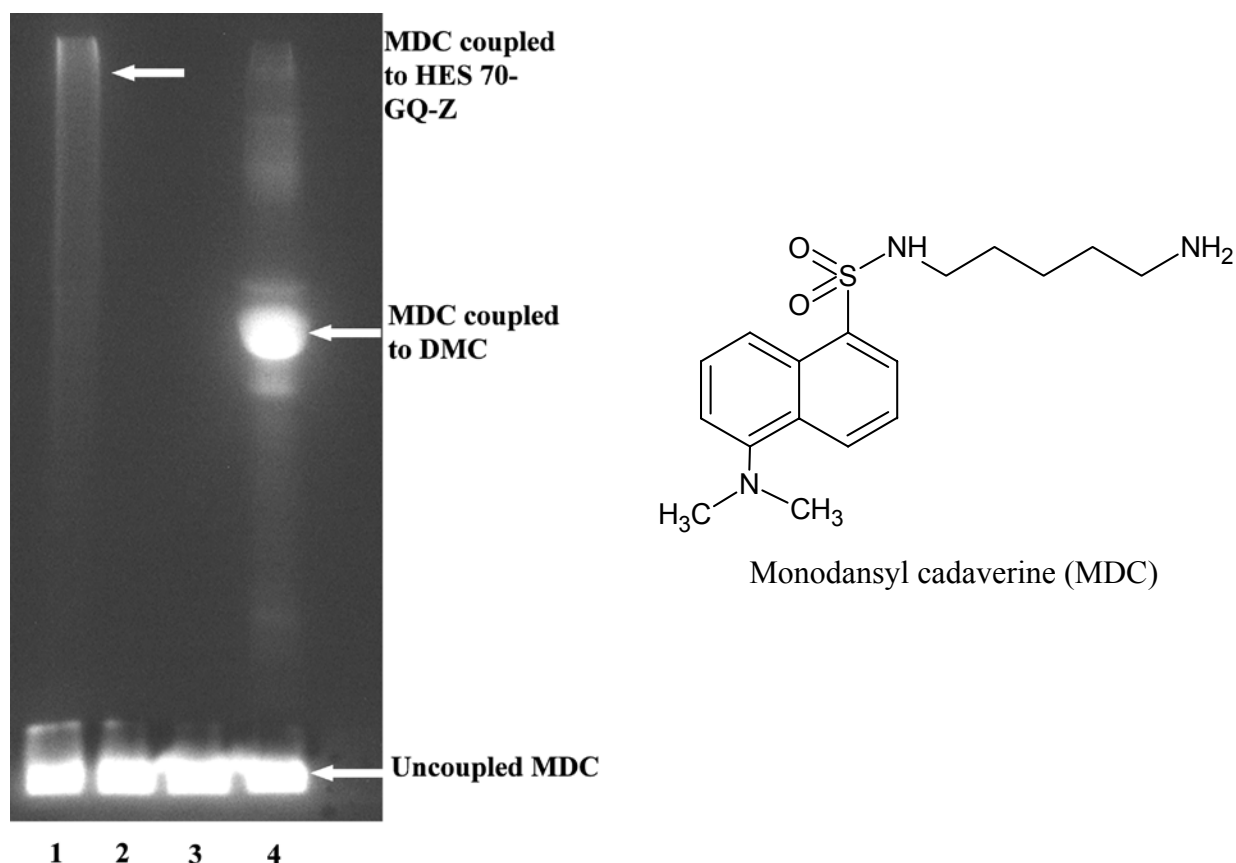


Figure 6.3. Fluorescence image of the SDS PAGE gel for the coupling of HES 70-GQ-Z to MDC using rMTG. Lane (1) HES 70-GQ-Z + rMTG + MDC. Lane (2) HES 70 + rMTG + MDC. Lane (3) HES 70-GQ-Z + MDC (no rMTG). Lane (4) DMC + rMTG +MDC. From top to bottom, the arrows point to MDC coupled to HES70-Q, the band of DMC coupled to MDC and uncoupled MDC. Also the chemical structure of MDC is shown.

DMC is known to act only as acyl donor for MTG, because all the lysine groups are blocked by methylation, thus it is a useful substrate to test the conjugation with acyl acceptors. Results for the reaction of DMC with HES 70-Amine are shown in Figure 6.4. The reaction is rapid, where the band of pure DMC almost disappears after 10 min (lane 2), while another band for the HES-DMC conjugate appears at the interface between the collection and separation gel. With increasing reaction time, another band appears on top of the stacking gel, which increases in intensity with increase in time. This is probably due to the fact that both HES 70-Amine, and DMC are multivalent, thus allowing the formation of cross-linked aggregates with large molar masses. Finally, lane 10 shows the cross-linking of human serum albumin (HSA) by rMTG as a positive control. The intact HSA is not a substrate for rMTG, thus dithiothreitol (DTT) is needed to reduce the sulphur bridges of HSA and unfold the molecule for the reaction with rMTG. In conclusion, the above reaction shows that

the modification of HES with HMDA succeeded in rendering HES 70-Amine a substrate for rMTG. The formation of crosslinked aggregates as seen in this case is due to the fact that both the aminated HES and the model protein, DMC, were multivalent. In case of therapeutic proteins, MTG usually adds selectively to one or two amino acid residues [11, 12]. In some cases, the protein is not a substrate for MTG, and thus it is engineered to carry a peptide tag at one end that is recognized by MTG [7]. As for HES, it is possible to use monovalent HES with lower molar mass. The later can be produced by reductive amination of the reducing end of HES. Using these measures, the cross-linking problem can be alleviated.

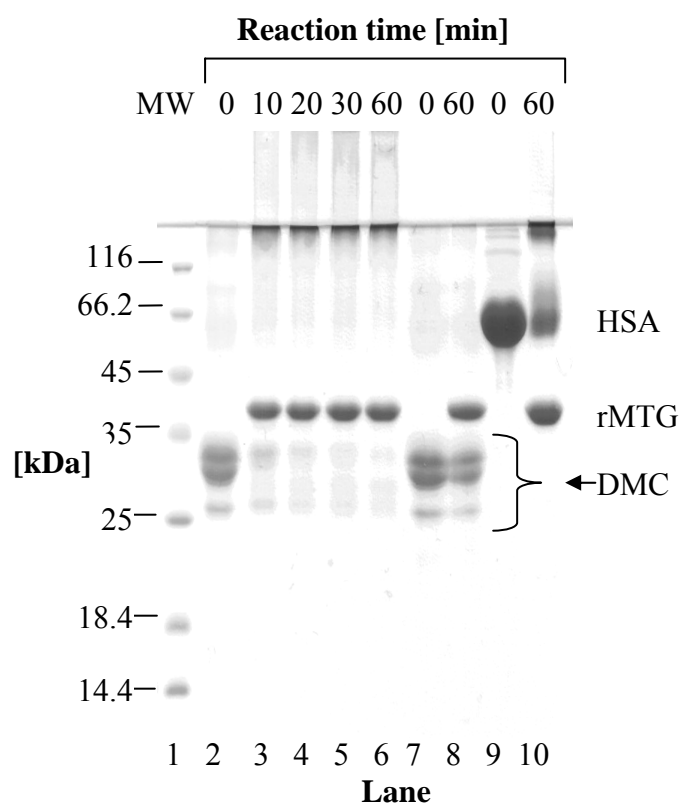


Figure 6.4. Image of the SDS PAGE gel for the coupling of HES 70-Amine to DMC using rMTG.

Lane (1) molar mass marker, (2) HES 70-Amine + DMC (no rMTG), (3) HES 70-Amine + rMTG + DMC after 10 min, (4) 20 min, (5) 30 min, (6) 60 min, (7) DMC alone, (8) DMC + rMTG after 60 min, (9) HSA+DTT, (10) HSA + DTT + rMTG after 60 min. Lanes 3-6 show the product of coupling of DMC to HES 70-Amine at the interface between the stacking and separation gels. At the top of the stacking gel, a crosslinked product with high molar mass could be seen, showing an increase in concentration with time. Lane 8 shows that no change in the molar mass of DMC occurred in the absence of HES 70-Amine. Lane 10 shows the crosslinking of HSA as a positive control.

6.4 Conclusions and outlook

This study was designed as a feasibility study to show whether a biosynthetic approach using MTG for HESylation is possible or not. HES was modified by esterification with Z-QG to give HES 70-GQ-Z (MS 4.6 mol%). The latter acted as acyl donor for the reaction with MDC catalyzed by rMTG. HES was also modified to carry primary amino groups of HMDA in two reaction steps giving HES 70-Amine (MS 4.8 mol%). The reaction of DMC with HES 70-Amine, using rMTG as a biocatalyst, led to a rapid and successful conjugation. Reactions for longer periods of time led to the formation of crosslinked aggregates of high molar mass. This enzymatic procedure is a promising approach for a simple and mild conjugation of proteins and drugs to a fully biodegradable water soluble polymer, in order to alter their pharmacokinetics and biological fate. However, lots of work is still needed to answer important questions, such as the efficiency of the coupling reaction, the range of proteins that could be used, the activity of the HESylated conjugates, and the immunogenicity of the conjugates.

6.5 References

- [1] R. Duncan, The dawning era of polymer therapeutics. *Nature Reviews Drug Discovery* 2 (2003) 347-360.
 - [2] J.M. Harris, R.B. Chess, Effect of PEGylation on Pharmaceuticals. *Nature reviews Drug discovery* 2 (2003) 214-221.
 - [3] G. Pasut, F.M. Veronese, PEGylation of proteins as tailored chemistry for optimized bioconjugates. *Advances in Polymer Science* 192 (2006) 95-134.
 - [4] N.V. Korte, The conjugation of proteins with polyethylene glycol and other polymers: Altering properties of proteins to enhance their therapeutic potential. *Advanced Drug Delivery Reviews* 10 (1993) 91-114.
 - [5] Q. Zhao, V. Tolmachev, J. Carlsson, H. Lundqvist, J. Sundin, J.-C. Janson, A. Sundin, Effects of Dextranation on the Pharmacokinetics of Short Peptides. A PET Study on mEGF. *Bioconjugate Chemistry* 10 (1999) 938-946.
 - [6] R. Satchi-Fainaro, H. Hailu, J.W. Davies, C. Summerford, R. Duncan, PDEPT: Polymer-Directed Enzyme Prodrug Therapy. 2. HEMA Copolymer- β -lactamase and HEMA Copolymer-C-Dox as a Model Combination. *Bioconjugate Chemistry* 14 (2003) 797-804.
 - [7] J. Tominaga, N. Kamiya, S. Doi, H. Ichinose, T. Maruyama, M. Goto, Design of a specific peptide tag that affords covalent and site-specific enzyme immobilization catalyzed by microbial transglutaminase. *Biomacromolecules* 6(4) (2005) 2299-2304.
 - [8] H. Sato, Enzymatic procedure for site-specific pegylation of proteins. *Advanced Drug Delivery Reviews* 54 (2002) 487-504.
 - [9] K. Yokoyama, N. Nio, Y. Kikuchi, Properties and applications of microbial transglutaminase. *Applied Microbiological Biotechnology* 64 (2004) 447-454.
 - [10] M. Griffin, R. Casadio, C.M. Bergamini, Transglutaminases : Nature's biological glues. *Biochemical Journal* 368 (2002) 377-396.
 - [11] H. Sato, E. Hayashi, N. Yamada, M. Yatagai, Y. Takahara, Further studies on the site-specific protein modification by microbial transglutaminase. *Bioconjugate Chemistry* 12(5) (2001) 701-710.
 - [12] A. Fontana, B. Spolaore, A. Mero, F.M. Veronese, Site-specific modification and PEGylation of pharmaceutical proteins mediated by transglutaminase. *Advanced Drug Delivery Reviews* 60 (2008) 13-28.
-

-
- [13] A. Valdivia, R. Villalonga, P. Di Pierro, Y. Perez, L. Mariniello, L. Gomez, R. Porta, Transglutaminase-catalyzed site-specific glycosidation of catalase with aminated dextran. *Journal of Biotechnology* 122(3) (2006) 326-333.
- [14] J. Flanagan, H. Singh, Conjugation of sodium caseinate and gum arabic catalyzed by transglutaminase. *Journal of Agricultural and Food Chemistry* 54(19) (2006) 7305-7310.
- [15] M.L. Villalonga, R. Villalonga, L. Mariniello, L. Gomez, P.D. Pierro, R. Porta, Transglutaminase-catalysed glycosidation of trypsin with aminated polysaccharides. *World Journal of Microbiology and Biotechnology* 22 (2006) 595-602.
- [16] C.K. Marx, T.C. Hertel, M. Pietzsch, Soluble expression of a pro-transglutaminase from *Streptomyces mobaraensis* in *Escherichia coli*. *Enzyme and Microbial Technology* 40 (2007) 1543-1550.
- [17] C.K. Marx, T.C. Hertel, M. Pietzsch, Purification and activation of a recombinant histidine-tagged protransglutaminase after soluble expression in *E. coli* and partial characterization of the active enzyme. *Enzyme and Microbial Technology* (2008) (<http://dx.doi.org/10.1016/j.enzmictec.2008.1003.1003>).
- [18] A.E.G. Cass, J.K. Zhang, A Study of His-Tagged Alkaline Phosphatase Immobilization on a Nanoporous Nickel– Titanium Dioxide Film. *Analytical Biochemistry* 292(2) (2001) 307-310.
- [19] T. Ehrenfreund-Kleinman, J. Golenser, A.J. Domb, Conjugation of amino-containing drugs to polysaccharides by tosylation: amphotericin B–arabinogalactan conjugates. *Biomaterials* 25 (2004) 3049-3057.
- [20] U.K. Laemmli, Cleavage of structural proteins during the assembly of the head of bacteriophage T4. *Nature* 227 (1970) 680-685.
- [21] M. Orlando, J. Hemberger, Coupling low molecular substances to hydroxyalkyl starch WO/2003/074088, 28.02.1003, 2003.
- [22] W. Eichner, H. Knoller, K. Lutterbeck, N. Zander, R. Frank, K. Sommermeyer, H. Conradt, E. Grabenhorst, Conjugates of hydroxyalkyl starch and G-CSF WO/2005/0140502995.
- [23] K. Sommermeyer, R. Frank, N. Zander, Conjugates of a polymer and a protein linked by an oxime linking group WO/2005/0140242005.
- [24] W. Eichner, K. Lutterbeck, N. Zander, R. Frank, H. Knoller, H. Conradt, Conjugates of hydroxyethyl starch and erythropoietin WO/2005/0923692005.
-

-
- [25] J. Hemberger, M. Orlando, Coupling proteins to a modified polysaccharideWO/2003/0740872003.
- [26] J. Hemberger, D. Merkel, A. Mitsch, M. Orlando, J. Delbos-Krampfe, Method for coupling enzymatically activated glycoconjugates to hydroxyalkyl starchWO/2006/0948262006.
- [27] K. Sommermeyer, Water-soluble antibiotic comprising an amino sugar, in the form of a polysaccharide conjugateWO/2003/000738, 19.06.2002, 2003.
- [28] W. Eichner, M. Schimmel, F. Hacket, E. Kraus, N. Zander, R. Frank, H. Conradt, K. Langer, M. Orlando, K. Sommermeyer, Conjugates of hydroxyalkyl starch and a proteinWO/2005/0923902005.
- [29] N. Zander, R. Frank, Conjugates of hydroxyethyl starch and a proteinWO/2005/0923912005.
- [30] K. Sommermeyer, Method for producing conjugates of polysaccharides and polynucleotidesWO/2005/074993, 08.02.2005, 2005.
- [31] N. Zander, W. Eichner, H. Conradt, F. Hacket, K. Langer, M. Orlando, R. Frank, Conjugates of hydroxyalkyl starch and a protein prepared by reductive aminationWO/2005/092928, 11.03.2005, 2005.
- [32] R. Frank, H. Conradt, E. Grabenhorst, N. Zander, Production of bioactive glycoproteins from inactive starting material by conjugation with hydroxyalkyl starchWO/2006/094810 09.03.2006, 2006.
- [33] K. Sommermeyer, W. Eichner, S. Frie, C. Jungheinrich, R. Scharpf, K. Lutterbeck, Conjugate of hydroxyalkyl starch and an active agentWO/2002/080979, 15.03.2002, 2002.
- [34] M. Orlando, Modification of proteins and low molecular weight substances with hydroxyethyl starch (HES). Justus Liebig Universität Giessen, Gießen, 2003.
- [35] T. Ohtsuka, A. Sawa, R. Kawabata, N. Nio, M. Motoki, Substrate Specificities of Microbial Transglutaminase for Primary Amines. *Journal of Agricultural and Food Chemistry* 48 (2000) 6230-6233.
- [36] T. Tanaka, N. Kamiya, T. Nagamune, Peptidyl linkers for protein heterodimerization catalyzed by microbial transglutaminase. *Bioconjugate Chemistry* 15(3) (2004) 491-497.
- [37] T. Tanaka, N. Kamiya, T. Nagamune, N-terminal glycine-specific protein conjugation catalyzed by microbial transglutaminase. *FEBS Letters* 579(10) (2005) 2092-2096.
-

- [38] N. Kamiya, T. Takazawa, T. Tanaka, H. Ueda, T. Nagamune, Site-specific cross-linking of functional proteins by transglutamination. *Enzyme and Microbial Technology* 33 (2003) 492-496.
- [39] J. Tominaga, Y. Kemori, Y. Tanaka, T. Maruyama, N. Kamiya, M. Goto, An enzymatic method for site-specific labeling of recombinant proteins with oligonucleotides. *Chemical Communications*(4) (2007) 401-403.
-

PART V

Summary

Chapter 7

Summary

7.1 English version

The current thesis describes 3 projects for the modification of hydroxyethyl starch (HES) to produce nanomedicines. The latter are nanosized drug and contrast agent delivery systems for the treatment, monitoring and diagnosis of humans. In the first project, HES was esterified with fatty acids to produce a hydrophobically-modified amphiphilic polymer (HM-HES). HM-HES was characterized using ^1H NMR, Raman spectroscopy and asymmetric flow field flow fractionation (AF4). HM-HES self assembled into polymersomes as confirmed by freeze-fracture TEM and cryoTEM. HM-HES was used to modify the surface of PLGA nanospheres and compared to the well-known amphiphilic polymers, Pluronics. HM-HES was found to reduce the adsorption of human serum albumin and fibrinogen, and to reduce phagocytosis by monocytic macrophages as good as Pluronic F127 and better than F68. These results suggest that HM-HES might be a suitable substitute for Pluronics in stabilizing nanoparticles, and are encouraging to test these polymers *in vivo*.

The second project involved the modification of HES with diethylenetriaminepentaacetic acid (DTPA) to chelate Gd^{3+} ions and act as a macromolecular MRI contrast agent. The macromolecular chelate was characterized by ^1H NMR and conductometric titration. It showed 2-3 times higher relaxivity than Gd-DTPA , indicating a better performance as an MRI contrast agent. Moreover, *in vivo* results showed a prolonged circulation time (more than 2.5 h), and proved to be

a good contrast agent for angiography, urography as well as in the diagnosis of solid tumors.

The third project described the use of the enzyme microbial transglutaminase (MTG) for the coupling of HES to model proteins and small molecules. To act as substrates for MTG, HES was modified with N-carbobenzyloxy glutaminyl glycine (Z-QG) and hexamethylenediamine (HMDA) to act as acyl donor and acyl acceptor, respectively. Using SDS-PAGE, it was possible to show that the modified HES successfully coupled to dimethyl casein (DMC), a model protein, and monodansyl cadaverine (MDC), a fluorescent probe, proving that the modified HES was accepted as a substrate by MTG. This process is a simple and mild approach to produce fully biodegradable polymer-drug and polymer-protein conjugates.

7.2 German version

Die vorliegende Dissertation beschreibt 3 Projekte zur Modifikation von Hydroxyethylstärke (HES). Diese soll zur Produktion nanoskaliger Arzneistofffreigabesysteme und Kontrastmittel für die Behandlung, Überwachung und Diagnose von Krankheiten beim Menschen dienen.

Im ersten Projekt wurde HES mit Fettsäuren verestert, um ein hydrophob modifiziertes amphiphiles Polymer (HM-HES) zu produzieren. HM-HES wurde mittels ^1H -NMR-Spektroskopie, Raman-Spektroskopie und asymmetrischer Fluss-Feld-Fluss-Fraktionierung (AF4) charakterisiert. Die Bildung von Polymersomen durch HM-HES wurde mittels Gefrierbruch-TEM und CryoTEM bewiesen. HM-HES wurde verwendet, um die Oberfläche von PLGA-Nanosphärulen zu modifizieren, und mit der Modifikation durch bekannte amphiphile Polymere, Poloxamere, verglichen. HM-HES reduzierte die Adsorption von menschlichem Serumalbumin und Fibrinogen, sowie die Phagozytose der Nanosphärulen durch Makrophagen so gut wie Pluronic F127 und besser als Pluronic F68. Diese Ergebnisse zeigen, dass HM-HES ein geeigneter Ersatz für Poloxamere beim Stabilisieren von Nanopartikeln sein kann, und legen eine *in vivo*-Untersuchung dieser Polymere nahe.

Das zweite Projekt umfasste die Veränderung von HES mit Hilfe von Diethylentriaminpentaessigsäure (DTPA), um Gd^{3+} -Ionen zu komplexieren und ein makromolekulares MRT-Kontrastmittel zu gewinnen. Der makromolekulare Komplex wurde mittels 1H -NMR-Spektroskopie und konduktometrischer Titration charakterisiert. Er zeigte zwei- bis dreifach höhere Relaxivität als Gd-DTPA, was seine Eignung als MRT-Kontrastmittel untermauert. Außerdem zeigten *in vivo* -Ergebnisse eine verlängerte Zirkulationszeit (mehr als 2,5 h) und erwiesen, dass Gd-HES ein gutes Kontrastmittel sowohl für Angiographie, Urographie als auch in der Diagnose von festen Tumoren ist.

Das dritte Projekt beschäftigte sich mit der Verwendung des mikrobiellen Enzyms Transglutaminase (MTG) für die Verbindung von HES mit Mustereiweißen und kleinen Molekülen. Um HES für die Enzymreaktion zugänglich zu machen, wurde sie mit N-carbobenzyloxyglutaminyglycin (Z-QG) oder Hexamethyldiamin (HMDA) modifiziert, um als Acylspender, beziehungsweise Acylakzeptor, zu reagieren. Mit Hilfe der SDS-PAGE war es möglich zu zeigen, dass sich die modifizierte HES erfolgreich an Dimethylcasein (DMC), ein Mustereiweiß, und Monodansylcadaverin (MDC), eine Fluoreszenzsonde koppeln ließ. Durch die Bindung an MDC konnte nachgewiesen werden, dass die modifizierte HES als Substrat von MTG akzeptiert wurde. Dieser Prozess ist ein einfacher und schonender Ansatz, um vollständig bioabbaubare Konjugate von HES mit Proteinen oder anderen Molekülen zu produzieren.

Erklärung

Hiermit erkläre ich, dass ich mich mit der vorliegenden Arbeit erstmals um die Erlangung eines Doktorgrades bewerbe.

Ferner erkläre ich, dass ich die vorliegende Arbeit selbstständig und ohne fremde Hilfe angefertigt, andere als die von mir angegebenen Quellen und Hilfsmittel nicht benutzt und die den verwendeten Werken wörtlich oder inhaltlich entnommenen Stellen als solche kenntlich gemacht habe.

Halle (Saale), September 2008

Ahmed Besheer

Ahmed Besheer

Institute of Pharmaceutical Technology and Biopharmacy
Martin Luther University, Halle-Wittenberg
Wolfgang-Langenbeck-Str. 4
06120 Halle/Saale
Germany
Phone: Office + 49 345 5525218
Home + 49 345 7792923
e-mail: ahmed.besheer@pharmazie.uni-halle.de



Education

- Jul 2005 – Sep 2008 Ph.D. student under the supervision of Prof. Karsten Mäder (Dep. of Pharmaceutical Technology) and Prof. Jörg Kressler (Dep. of Physical Chemistry), Martin Luther University, Halle, Germany.
- Project theme: “Nanomedicines based on modified Hydroxyethyl starch: from synthesis to *in vivo* evaluation.”
- Oct 2003 – Jun 2005 M.Sc. “Applied Polymer science”, Martin Luther University, Halle, Germany.
- Thesis: “ESR investigations of polymeric drug delivery systems using spin labeling technique”.
 - Final total grade: 1.1
- Sep 1995- May 2000 B.Sc. of Pharmaceutical Sciences, Ain Shams University, Cairo, Egypt. (a 5 years pharmacist-education degree)
- Final grade: Excellent with Honour
 - Ranking 7th among 241 students, (top 3%)

Awards and honours

- Oct 2005 Anton-Wilhelm-Amo prize for the best Diploma/Master’s thesis in Martin-Luther-University, Halle for the year 2005.
- Feb 2007 Best poster award (3rd place) in the 6th International Symposium for Polymer Therapeutics, Berlin, Germany.

Work Experience

- Oct 2005 – Apr 2008 Teaching assistant, department of pharmaceutical technology and biopharmaceutics, Martin Luther University, Halle, Germany.
- Teaching “Arzneiformenlehre I, Suppositorien” and “Arzneiformenlehre II, Halbfeste Arzneiformen”
- Sep 2000 - Sep 2003 Teaching assistant, department of pharmaceutics, faculty of pharmacy, Ain Shams Uni., Cairo, Egypt.
- Teaching “pharmaceutical formulation course” for fourth year students and “physical pharmacy course” for first year students
- June 2000- Sep 2003 Practicing pharmacist in a community pharmacy, Cairo, Egypt.

Memberships

Member of the “Arbeitsgemeinschaft für Pharmazeutische Verfahrenstechnik” (APV)
Member of the “Egyptian Syndicate of Pharmacists”

Personal Info

Date, place of birth 14th October, 1976 ; Cairo

PUBLICATIONS

Research papers

1. C. Lemarchand, R. Gref, S. Lesieur, H. Hommel, B. Vacher, M. Besnard, A. Besheer, K. Mäder, P. Couvreur, Physicochemical characterization of polysaccharide coated nanoparticles, *J. Contr. Rel* 108, 97-111 (2005).
2. A. Besheer, K. Wood, N. Peppas, K. Mäder, Loading and mobility of spin labelled insulin in responsive complexation hydrogels intended for oral administration, *J. Contr. Rel.* 111, 73-80 (2006).
3. A. Besheer, G. Hause, J. Kressler, K. Mäder, Hydrophobically modified Hydroxyethyl starch: synthesis, characterization and aqueous self-assembly into nanosized polymeric micelles and vesicles, *Biomacromol.* 8, 359-367(2007)
4. A. Besheer, K. Mäder, S. Kaiser, J. Kressler, C. Weis, E. K. Odermatt, Tracking the urinary excretion of High molar mass poly(vinyl alcohol), *J. Biomed. Mater. Res. B Appl. Biomat.* 82, 383-9 (2007).
5. A. Besheer, K. Mäder, J. Kressler, Nanosized drug delivery systems based on hydrophobically modified Hydroxyethyl starch, *Polymer preprints*, 48(2), 948-949 (2007).
6. A. Besheer, T. Hertel, J. Kressler, K. Mäder, M. Pietzsch, Enzymatically-catalyzed HESylation using microbial transglutaminase – a proof of feasibility, *J. Pharm. Sci.*, In Press.
7. A. Besheer, J. Vogel, T. Groth, J. Kressler, K. Mäder, Physicochemical characterization and phagocytosis of PLGA nanospheres stabilized with different amphiphilic polymers – A comparison of hydrophobically-modified hydroxyethyl starch vs. Pluronics, *Mol. Pharm.*, In Press.

Book Chapters

1. A. Besheer, J. Kressler, K. Mäder, Nanosized polymers in drug delivery in, H. Nalwa (Ed.) Polymeric nanostructures and their applications, Part II, American Scientific Publishers, CA, USA, 2007.

Oral presentations

1. A. Besheer, Enzymatic modification of hydroxyethyl starch (HES) to produce nano-sized drug carriers, *1. Mitteldeutsches Doktorandentreffen Pharmazeutische Technologie, Jena 2005.*

Posters

1. J. Kuntsche, A. Besheer, K. Mäder, Investigations of hydrophobically-modified hydroxyethyl starches (HM-HE) by asymmetrical flow field flow fractionation, *7th International symposium on polymer therapeutics, Valencia, Spain (May 2008)*
2. A. Besheer, J. Vogel, T. Groth, J. Kressler, K. Mäder, Comparison of hydrophobically-modified Hydroxyethyl starch vs. Pluronic as stabilizers for PLGA Nanospheres, *CRS German chapter meeting, Braunschweig, Germany, (March 2008)*
3. A. Besheer, G. Hause, J. Kressler, K. Mäder, Hydrophobically-modified Hydroxyethyl starch: synthesis, characterization and self-assembly into polymeric micelles and vesicles, *6th International symposium on polymer therapeutics, Berlin, Germany (February 2007)*
4. A. Besheer, A. Rube, K. Mäder, ESR Investigations of the microenvironment of nanostructured drug delivery systems using spin probes and spin labels, *ESF conference Nanomedicine: a new opportunity for improving diagnosis, prevention and treatment for disease, Sant Feliu de Guixols, Spain, (September 2006).*
5. A. Besheer, K. M. Wood, N. A. Peppas, K. Mäder, Loading and mobility of spin labeled insulin in responsive complexation hydrogels - An ESR study, *The 33rd annual meeting of the controlled release society, Vienna, Austria (July 2006).*
6. A. Rube, A. Besheer, H. Metz, V. V. Khramtsov, K. Mäder, Microencapsulation for the protection of spin labels, *The international conference/workshop on electron paramagnetic resonance spectroscopy and imaging of biological systems, Ohio, USA.(September 2005)*
7. R. Androsch, A. Besheer, J. Radusch, Super-molecular structure of isotactic polypropylene as a function of thermal treatment, *21st annual meeting of the polymer processing society, Leipzig, Germany. (June 2005)*
8. A. Besheer, J. Xu, R. Androsch, J. Radusch, Imaging of the super-molecular structure of semi-crystalline polymers using Atomic Force Microscopy, *the international conference on polymeric materials 2004, Martin Luther University in Halle/Saale, Germany. (September 2004)*